VILNIUS UNIVERSITY

Andrius Džiaugys

Influence of impurities on dielectric properties of ferroelectric and superionic crystals

Doctoral dissertation
Physical science, Physics (02 P)

Vilnius, 2011

The thesis was prepared at Vilnius university in 2007 – 2011.

Scientific head:

prof. habil. dr. Jūras Banys (Vilnius university, physical sciences, physics – 02 P)

Aknowledgements

Sincerely grateful:

To the Head prof. Jūras Banys for the excellent supervision;
Dr. Jan Macutkevič for the valuable advices;
Dr. Robertas Grigalaitis and PhD student Maksim Ivanov for the collaboration in experimental work;
PhD students Simonas Greičius, Andrius Mikonis, Tadas Ramoška, Povilas Keburis, Saulius Rudys and Šarūnas Bagdzevičius for the friendly atmosphere in the laboratory;
Prof. Yu Vysocianskii, prof. I. Studenyak, Dr. I. Pritz and Dr. M. Trubicyn for the crystals grown in their laboratories;
Prof. W. Kleeman for the valuable advices analyzing experimental data and introduction with SQUID technique;
to all employees of the Deparment of Radiophysics;
to my wife for the understanding and moral support.

CONTENT

1. INTRODUCTION

Today widely used ferroelectrics are investigated since the discovery of the ferroelectricity in Rochelle salt in 1920. The main property of ferroelectrics is appearance of spontaneous polarization at certain temperature, which direction can be changed by an external electric field. Nowadays the ferroelectrics containing of several feroically active sublattices are very attractive, because interactions between these sublattices can caused novel phenomena. Antiferroelectrics, ferrielectrics and multiferoics belong to these materials. In this work new crystalline materials MNP_2X_6 (M = Cu, Ag; N=In, Cr, Bi; X=S, Se) were investigated, which have ferrielectric and multiferroic properties. It was also demonstrated that electric and dielectric properties of these materials can be effectively changed by doping. Well known ferroelectric $Pb_6Ge_{11}O_3$ crystal was investigated by dopping it with a very little amount of copper (0.1 % and 0.5%). Even a small amount of impurities is enough to the change of phase transition temperature and emergence of the dipole glass state at the low temperatures. In addition the mixed superionic crystals $Cu_6PS_5(I_xBr_{1-x})$ were also investigated.

The dielectric and electric properties of above mentioned materials have been investigated by broadband dielectric spectroscopy methods, which allow to analyze the collective processes related to order – disorder and displacive phase transitions, ions migration and freezing of dipoles (glassy state) in the wide temperature (25 K iki 500 K) and frequency (10^{-5} iki 3 GHz) ranges. Other investigation methods such as X ray scattering and electron microscopy can reveal the static structure of materials, but do not say anything about microscopic movements in the crystal. The advantage of other dynamic investigation methods, such as nuclear magnetic resonance and neutron scattering, is selectivity, but the broadband dielectric spectroscopy allows

investigation of dynamic phenomena in a wide range of relaxation times from ps to a few years, which is not available with other methods.

By substitution or doping it becomes possible to tailor the ferroelectric materials to different properties. In this work it is determined that the substitution of 10% Cu ions by Ag ions shifts the phase transition temperature of $CuInP_2S_6$ crystal toward lower temperatures while the addition of In ions shifts the phase transitions temperature toward the higher ones. The phase transition temperature difference is about 50 K for mentioned crystals. If the ferroelectric crystal $CuInP_2S_6$ is mixed with the antiferroelectric $CuCrP_2S_6$ the dipole glass phase occupies the middle of the phase diagram. The distribution of relaxation times has been calculated from the broadband dielectric spectra of dipolar glasses. The double potential well model for the distribution of relaxation times reveals the relation between the macroscopic and microscopic parameters of the dipolar glasses. Also the contribution of domain walls dynamics was separated from the dipole glass freezing in PGO and $CuBiP_2Se_6$ crystals.

The aim and tasks of the work

The aim of the dissertation is investigations of impurities influence on dielectric properties of ferroelectric and superionic crystals.

The tasks of the dissertation are:

1. Investigate the influence of small amount of paraelectric $AgInP_2S_6$, antiferroelectric $CuCrP_2S_6$ and In to the phase transition and conductivity properties of $CuInP_2S_6$ crystal;
2. Investigate the ionic conductivity and its relaxation in $CuInP_2S_6$ and $AgInP_2(S_xSe_{1-x})_6$ crystals;
3. Analyze of the antiferrielectric phase transitions of $CuCrP_2S_6$ and $CuBiP_2Se_6$ crystals;

4. Investigate the dielectric dispersion of dipole glasses of mixed $CuIn_xCr_{1-x}P_2S_6$ crystals in middle part of a phase diagram;
5. Investigate the dielectric properties of mixed superionic $Cu_6PS_5(I_xBr_{1-x})$ crystals;
6. Analyze the influence of small amount of off-center Cu ions to the dielectric properties of PGO crystal;
7. Investigate the magnetic properties of mixed $CuIn_xCr_{1-x}P_2S_6$ crystals.

Scientific novelty

1. For the first time dielectric properties of the mixed $CuIn_xCr_{1-x}P_2S_6$ crystals were investigated in the wide frequency range 20 Hz – 3 GHz and a phase diagram of this crystal family was obtained. The dipole glass phase was observed and microscopic parameters were extracted from dielectric properties.
2. For the first time it was measured complex dielectric permittivity dependence on temperature (30K – 300 K) for the $CuBiP_2Se_6$. The antiferroelectric phase transition temperature was determined. At low temperatures a dipole glass phase is observed in these crystals.
3. The dielectric and electric properties of newly synthesized $AgInP_2(S_xSe_{1-x})_6$ crystals in the wide temperature range (110 K –350 K) are presented.
4. From the distribution function of relaxation times of PGO crystals the domain wall motion dynamics were separated from the dipole glass freezing.
5. For the first time the dielectric properties in the frequency range 20 Hz – 1 MHz of newly synthesized $Cu_6PS_5(I_x,Br_{1-x})$ mixed crystals were investigated in wide temperature range .

Statements presented for defence

1. The first-order ferrielectric phase transition in nominally pure $CuInP_2S_6$ is accompanied by coexistence of dipolar glass phase and ferrielectric phase at low temperatures.
2. In mixed $CuIn_xCr_{1-x}P_2S_6$ crystals the antiferromagnetic and the antiferroelectric phase transition temperatures decrease with the increase of In^+ ions concentration. Both phase transitions disappear below critical concentration x=0.3. Weak third order magneto-electric activity was observed in $CuIn_xCr_{1-x}P_2S_6$ below critical indium concentration x=0.3. Local order parameter distribution clearly shows dipolar glass state existence.
3. The ferroelectric phase transition in PGO crystals is mixed "order-disoder" and displacive. The doping of PGO crystals by off-center Cu ions causes the appearance of dipole glass dispersion at low temperatures.

1.1. List of Publications on the theme of the thesis

1. A. Dziaugys, J. Banys, V. Samulionis and Y. Vysochanskii, *Dielectric and ultrasonic studies of new $Ag_{0.1}Cu_{0.9}InP_2S_6$ layered ferroelectric compound,* ISSN 1392-2114 ULTRAGARSAS (ULTRASOUND), **63** (2008) 3.
2. A. Dziaugys, J. Banys, A. Kezionis, V. Samulionis, I. Studenyak , C*onductivity investigations of Cu_7GeS_5I family fast-ion conductors*, Solid State Ionics **179** (2008) 168–171.
3. A. Dziaugys, J. Banys, J. Macutkevic, and Y. Vysochanskii, *Conductivity Spectroscopy of New $AgInP_2S_6$ Crystals,* Integrated Ferroelectrics, **103** (2009) 52–59.
4. A. Dziaugys, J. Banys, J. Macutkevic, and Yu. Vysochanskii, *Dielectric Properties of New $AgInP_2Se_6$ Crystals,* Ferroelectrics, **391** (2009) 151–157.

5. A. Dziaugys, J. Banys, J. Macutkevic, R. Sobiestianskas and Yu. Vysochanskii, *Dipolar glass phase in ferrielectrics: $CuInP_2S_6$ and $Ag_{0.1}Cu_{0.9}InP_2S_6$ crystals,* Phys. Status Solidi A, **207** (2010) 1960–1967.
6. A. Dziaugys, J. Banys, J. Macutkevic, V. Samulionis, Yu. Vysochanskii, *Dielectric spectroscopy of $CuBiP_2S_6$ crystals*. Physica Status Solidi (c), **6** (2009) 2734 – 2736.
7. A. Dziaugys, J. Banys, V. Samulionis, and I. Studenyak, *Dielectric Properties of Cu_6PS_5I Single Crystals,* Integrated Ferroelectrics, **109** (2009) 18–26.
8. A. Dziaugys, J. Banys, Yu. Vysochanskii, *Broadband dielectric investigations of indium rich $CuInP_2S_6$ layered crystals*, Zeitschrift für Kristallographie, 226 (2011) 171-176.
9. A. Dziaugys, J. Banys, V. Samulionis, Yu. Vysochanskii. *Investigation of $CuInP_2S_6$ family layered crystals for ultrasonic transducers* // ISAF: 2009 18th IEEE international symposium on the applications of ferroelectrics. - Book Series: IEEE international symposium on applications of ferroelectrics. New-York: IEEE, (2009) 116-120.
10. A. Dziaugys, J. Banys, J. Macutkevic, Yu. Vysochanskii, I. Pritz and M. Gurzan, *Phase transitions in $CuBiP_2Se_6$ crystals*, Phase transitions, **84** (2011), 147-156.
11. A. Dziaugys, J. Banys, V. Samulionis, J. Macutkevic, Yu. Vysochanskii, V. Shvartsman, W. Kleemann, “Ferroelectrics / Book 3", ISBN 978-953-307-455-9, Intech 2011.
12. A. Dziaugys, J. Banys, I. Studenyak, “*Dielectric investigations of superionic Cu_6PS_5Br single crystal”*, Solid State Ionics, 2011 in press. doi:10.1016/j.ssi.2011.04.011

1.2 Theses of papers at international scientific conferences

1. A. Džiaugys, J. Banys, V. Samulionis, J. Macutkevič, Y. Vysochanskii, *Dielectric studies of mixed $CuIn_{0.4}Cr_{06}P_2S_6$ and $CuIn_{0.5}Cr_{0.5}P_2S_6$ crystals* // 37-th Lithuanian national physics conference, Vilnius, 2007 June 11-13. Vilnius, 2007, p. 68.
2. A. Džiaugys, J. Banys, V. Samulionis, Y. Vysochanskii. *Dielectric and ultrasonic investigation of new piezoelectric crystals $CuIn_xCr_{1-x}P_2S_6$* // Smart materials and structures: 2nd international workshop, Kiel, 2007, 29-31 August. Kiel, 2007, p. 128.
3. A. Džiaugys, J. Banys, V. Samulionis, Y. Vysochanskii, *Dielectric studies of mixed $CuIn_{0.4}Cr_{0.6}P_2S_6$ and $CuIn_{0.8}Cr_{0.2}P_2S_6$ crystals* // Functional materials and nanotechnologies (FM&NT-2007): international Baltic Sea region conference, Riga, April 24, 2007: book of abstracts. Riga, 2007, p. 33.
4. A. Džiaugys, J. Banys, A. Kežionis, V. Samulionis, I. Studenyak. *Conductivity investigations of Cu7GeS5I family fast-ion conductors* // 8th international symposium on systems with fast ionic transport: book of abstracts, Vilnius, 23-27 May, 2007. Vilnius, 2007, p. 108.
5. A. Džiaugys, J. Banys, J. Macutkevič, Y. Vysochanskii. *Dielectric investigation of new ferroelectric crystals $CuIn_xCr_{1-x}P_2S_6$* // Seminar properties of ferroelectric and superionic systems, Ukraine, 12-13 November, 2007. Uzhgorod, 2007, p. 20.
6. J. Banys, R. Grigalaitis, P. Keburis, A. Džiaugys, A. Mikonis. *Dielectric relaxation in ferroelectrics, relaxors and dipolar glasses* // Seminar properties of ferroelectric and superionic systems, Ukraine, 12-13 November, 2007. Uzhgorod, 2007, p. 16.
7. A. Džiaugys, J. Banys, V. Samulionis, Y. Vysochanskii. *Dipolar glass behaviour of $CuIn_{1-x}Cr_xP_2S_6$ crystals* // EMF-2007: 11th European meeting on ferroelectricity, Slovenia, 3-7 September 2007 : programme and book of abstracts. Bled, 2007, p. 77.

8. A. Džiaugys, J. Banys, V. Samulionis, I. Studenyak. *Dielectric properties of Cu_6PS_5I single crystal* // Lithuanian-French-Ukrainian workshop on materials for functional elements of solid state ionics: programme and book of abstracts, 13 october, 2008, Vilnius. Vilnius: Vilniaus universiteto leidykla, 2008, p. 18.
9. A. Džiaugys, J. Banys, Yu. Vysochanskii. *Dielectric investigation of new inhomogeneous ferroelectric $CuIn_xCr_{1-x}P_2S_6$ crystals with ferroelectric and dipolar glass coexistence* // RCBJSF-9: the 9th Russian-CIS-Baltic-Japan Symposium on Ferroelectricity, Vilnius, Lithuania, June 15-19, 2008: abstract book. Vilnius, 2008, p. 164.
10. A. Mikonis, A. Džiaugys, J. Banys. *Two dimensional relaxation times distribution obtained from dielectric spectroscopy measurements of $CuIn_xCr_{1-x}P_2S_6$ crystals* // RCBJSF-9: the 9th Russian-CIS-Baltic-Japan Symposium on Ferroelectricity, Vilnius, Lithuania, June 15-19, 2008 : abstract book. Vilnius, 2008, p. 166.
11. A. Džiaugys, J. Banys, Yu. Vysochanskii. *Conductivity investigations of new functional material $AgInP_2S_6$* // Functional materials and nanotechnologies (FM&NT-2008): international Baltic Sea region conference, Riga, April 1-4: book of abstracts. Riga, 2008, p. 131.
12. A. Džiaugys, J. Banys, Yu. Vysochanskii. *Dielectric investigation of new layered $AgInP_2(S_xSe_{1-x})_6$ crystals* // ECAPD'9 : 9th European conference on applications of polar dielectrics, Roma, Italy, August 25-29, 2008 : abstract book. Roma, 2008, p. 228.
13. A. Džiaugys, J. Banys, J. Macutkevič, V. Samulionis, Yu. Vysochanskii. *Conductivity investigations of new $CuBiP_2S_6$ crystal* // 15th semiconducting and insulating materials conference, June 15-19, Vilnius, Lithuania: programme and abstracts. Vilnius, 2009, p. 111.
14. A. Džiaugys, J. Banys, M. Trubitsyn, *Broadband dielectric spectroscopy of $Pb_5Ge_3O_{11}$ ferroelectric crystal* // IMF -ISAF 2009 :

12th international meeting on feroelectricity and 18th IEEE international symposium on the applications of ferroelectric : program abstracts book, August 23-27, Xi'an, China. Xi'an, 2009, p. 18.

15. A. Džiaugys, J. Banys, V. Samulionis, I. Studenyak, *Dielectric investigations of phase transitions in $Cu_6PS_5(I,Br)$ crystals* // 2nd seminar : Properties of ferroelectric and superionic systems, Ukraine, Uzhgorod, 19-20.X.2009. Uzhgorod, 2009, p. 29.
16. A. Džiaugys, J. Banys, V. Samulionis, I. Studenyak, *Dielectric properties of $Cu_6PS_5(I,Br)$ single crystals* // Functional materials and nanotechnologies (FM&NT-2009) : international Baltic Sea region conference, Riga, March 31- April 3: book of abstracts. Riga, 2009, p. 153.
17. A. Džiaugys, J. Banys, J. Macutkevič, V. Samulionis, Yu. Vysochanskii, *Electrical conductivity in $CuBiP_2S_6$ crystal* // 2nd seminar : Properties of ferroelectric and superionic systems, Ukraine, Uzhgorod, 19-20.X.2009. Uzhgorod, 2009, p. 30.
18. A. Džiaugys, J. Banys, J. Macutkevič, Yu. Vysochanskii, *Origin of dipolar glass phase in ferrielectrics: $CuInP_2S_6$ and $Ag_{0.1}Cu_{0.9}InP_2S_6$* // 2nd seminar : Properties of ferroelectric and superionic systems, Ukraine, Uzhgorod, 19-20.X.2009. Uzhgorod, 2009, p. 8.
19. Džiaugys Andrius, Banys Jūras, Studenyak Ihor P. Conductivity investigation of Cu_6PS_5Br crystal // 9th international symposium on systems with fast ionic transport: book of abstracts, Riga, June 1-4, 2010. Riga, 2010, p. 83.
20. Džiaugys Andrius, Banys Jūras, Vysochanskii Yulian. High conductivity of $AgInP_2(S_xSe_{1-x})_6$ mixed crystals // 9th international symposium on systems with fast ionic transport: book of abstracts, Riga, June 1-4, 2010. Riga, 2010, p. 82.
21. Džiaugys Andrius, Banys Jūras, Macutkevič Jan, Samulionis Vytautas, Vysochanskii Yulian. Broadband dielectric spectroscopy of

indium rich $CuInP_2S_6$ layered crystals // RCBJSF-10: the 10th Russian-CIS-Baltic-Japan Symposium on Ferroelectricity, Yokohama, Japan, June 20-24, 2010: abstract book. Yokohama, 2010, p. 127.

22. Džiaugys Andrius, Banys Jūras, Trubitsyn M. P. Phase transition dynamics in Pb5Ge3O11 crystals // Functional materials and nanotechnologies (FM&NT-2010): international conference, Riga, March 16-19 : book of abstracts. Riga : Latgales druka, 2010, p. 102.
23. V.Samulionis, A.Dziaugys, J.Banys, Yu.Vysochanskii, „Ultrasonic and electroacoustic investigation of phase transitions in layered $CuBiP_2Se_6$ and $CuBiP_2S_6$ crystals," 10^{th} Symposium on Ferroelectricity Russia/CIS/Baltic/Japan, Yokohama, Japan, p.79, 20 – 24 June (2010).
24. A. Dziaugys, J. Banys, V. Samulionis and I.Studenyak, „Dielectric investigations of phase transitions in $Cu_6PS_5(I_x,Br_{1-x})$ mixed crystals," in ECAPD-10, Edinburgh, Great Britain, p. 107, 9-12 August (2010).
25. A. Dziaugys, J. Banys, Yu. Vysochanskii, W. Kleemann, V. Shvartsman, „Dielectric spectroscopy of the mixed $CuIn_xCr_{1-x}P_2S_6$ crystals," 1st Lithuanian Ukrainian Polish conference, LUP 1, Taujenai, Lithuania, p. 67, 12 – 16 September (2010).

2. OVERVIEW

2.1 Introduction

In the 19th century, several studies [1],[2] were carried out to understand pyroelectricity, the phenomenon known since ancient times [3]. Such investigations lead eventually to the discovery of piezoelectricity by J. Curie and P. Curie [4]. However, the history of ferroelectricity started around 1665 when Elie Seignet of La Rochelle, France, created sodium potassium tartrate tetrahydrate, $NaKC_4H_4O_6.4H_2O$, later known as Rochelle salt. E. Schrodinger was the first to use the term "ferroelectricity" in 1912 [5], although it was not until 1920 when J. Valsek [6] demonstrated that the direction of the spontaneous polarization of Rochelle salt could be reversed by application of an electric field. More than a decade was to pass before a whole series of new ferroelectrics, phosphates and arsenates of potassium were produced [5]. The best known member of this family is KH_2PO_4 (KDP) [7]. After the 40's ferroelectricity stopped to be a rarity, because the $BaTiO_3$ was found to be ferroelectric [8]. During the same decade, several other members of this structural family as $KNbO_3$ [9], $LiNbO_3$ and $LiTaO_3$, $PbTiO_3$ [10] were shown also to be ferroelectrics. From then on the ferroelectrics field has been greatly growing, especially for their interest as ferroelectric random access memories, and more inorganic as well as organic ferroelectric materials have been discovered and studied.

2.2 The structural symmetry

According to Neumann's principle [11], symmetry elements of all physical properties in a crystal should include all symmetry elements of the point group of this crystal. Thus if a physical parameter is subjected to a symmetry operation of the crystal, the value of this physical parameter should remain invariant. In the nature, there are 32

macroscopic symmetry types (point groups or crystal classes) and 11 of them possess a center of symmetry. Of the 21 non-centric crystal classes, all except one produce an electric field when subjected to stress. The effect is linear, and it is called the piezoelectric effect. The reverse effect is always present: the crystal contracts or expands when subjected to an external field. Applying a mechanical stress or an electric field can polarize piezoelectric materials. Of the 20 piezoelectric crystal classes 10 are characterized by the fact that they have a unique polar axis. Crystals belonging to these classes are called polar because they possess spontaneous polarization or electric moment per unit volume. The spontaneous polarization is in general temperature dependent and it can be detected by observing the flow of charge to and from the surfaces on change of temperature. This is the pyroelectric effect and the 10 polar classes are often referred to as the pyroelectric classes. All ferroelectric materials are a subset of pyroelectric materials in which the direction of the spontaneous polarization can be changed between two or more orientation states by an applied electric field. The orientation states have the same crystal structure, but differ in the direction of the spontaneous polarization at zero applied electric field.

2.3 Ferroelectric crystals

A ferroelectric crystal exhibits an electric dipole moment even in the absence of an external electric field. In the ferroelectric state the centre of positive charge of the crystal does not coincide with the centre of negative charge. The plot of polarizations versus electric field for the ferroelectric state shows a hysteresis loop. A crystal in a normal dielectric state usually does not show significant hysteresis when the electric field is increased and then reversed, both slowly. The ferroelectricity usually disappears above a certain temperature called the transition temperature, or the Curie temperature. The state above this temperature is called paraelectric state. In paraelectric phase the

ferroelectric order is destroyed. Some ferroelectric crystals have no Curie temperature because they melt before leaving the ferroelectric phase. The ferroelectric crystals may be classified into two main groups, order – disorder or displacive. For the displacive ferroelectrics, below the phase transition a spontaneous polarization appears due a concerted displacement of ions in one or more sublattices. For the order-disorder ferroelectrics, below the phase transition a spontaneous polarization appears due an orientation of dipoles in one direction.

There has been a tendency recently to define the character of the transition in terms of the dynamics of the lowest frequency ("soft") optical phonon modes. If a soft mode can propagate in the crystal at the transition, then the transition is displacive. If the soft mode is only diffusive (non-propagating) there is really not a phonon at all, but only a large amplitude hopping motion between the wells of the order-disorder system.

2.4 Soft optical phonons

The atoms of a crystal vibrate around their equilibrium position at finite temperatures. There are lattice waves propagating with certain wavelengths and frequencies through the crystal [12]. The characteristic wave vector $\vec{q}$ can be reduced to the first Brillouin zone of the reciprocal lattice, $0 \leq q \leq \pi/a$, where a is the lattice constant.

In every lattice there are three modes with the different frequencies belonging to one longitudinal and two transverse branches of the acoustic phonons. A vibration of the atoms perpendicular to the propagation corresponds to a transverse wave, a vibration in the direction of the propagation corresponds to a longitudinal wave. The acoustic phonons have an elastic nature. All atoms vibrate as a linear chain independent of the number of different atoms per lattice cell. The sound velocity v_s gives the wavelengths of the acoustic phonons; therefore, no coupling of acoustic phonons with electromagnetic waves exists ($v_s << v_{Light}$).

In case of the non-primitive lattices with the different atoms in the elementary cell, the sub-lattices can vibrate against each other. A vibration with a frequency $\omega \neq 0$ becomes possible even for the wave vector $q=0$. The opposite movement of neighbouring atoms evokes large dipole moments allowing a coupling to electromagnetic waves.

In general, each mode of the phonon dispersion spectra is collectively characterized by the relating energy, i.e. the frequency and wave vector, and is associated with a specific distortion of the structure.

The local electric field in ionic crystals leads to a splitting of the optical vibration modes. The longitudinal mode frequency is shifted to higher frequencies while the transverse mode frequency is shifted to lower frequencies. The softening of the transverse modes is caused by a partial compensation of the short-range lattice (elastic) forces on the one hand and the long-range electric fields on the other hand. This effect is strongest at the zone center [12]. If the compensation is complete, the transverse optic mode frequency becomes zero when the temperature is decreased, ω_{TO} $(T \rightarrow T_c) \rightarrow 0$, and the soft phonon condenses out so that at T_c a phase transition to a state with spontaneous polarization takes place (ferroelectric phase transition). At the zone center (wave vector is 0) the wavelength of the TO mode is infinite ($\lambda_0 \rightarrow \infty$), i.e. the region of homogeneous polarization becomes infinite. In the case of the softening of the TO mode the transverse frequency becomes zero and no vibration exists anymore (“frozen in”).

A linear relation (Cochran law) between ω^2_{TO} and T at the zone centre is found suggesting that the temperature dependence of the optic mode frequency relates to the phase transition [13]:

$$\omega_{TO}^2 = A_{cr}\left|T - T_C\right| \tag{2.4.1}$$

in accordance with the Lyddane-Sachs-Teller relation:

$$\frac{\varepsilon(T,0)}{\varepsilon_{\infty f}} = \frac{\omega_{LO}^2}{\omega_{TO}^2(T)}. \tag{2.4.2}$$

where $\varepsilon_{\infty f}$ is the contribution of the all higher modes and electronic polarization, ω_{LO} is the longitudinal optic mode frequency, and ε (T, 0) is contribution of presented mode.

2.5 Antiferroelectric crystals

In the ferroelectric state the crystal exhibits the spontaneous electric polarization. The antiferroelectric crystal is defined as a crystal whose structure can be considered as being composed of two sublattices polarized spontaneously in antiparallel directions. But the spontaneous macroscopic polarization of the crystal as a whole is zero.

2.5.1 Thermodynamic description of second order antiferroelectric phase transition

At this point our interest in the effects of varying temperature makes it expedient to alter our approach to the problem and introduce a phenomenological expansion for the Helmholtz free energy per unit volume:

$$A(P_a, P_b, T) = A_0 + f(P_a^2 + P_b^2) = gP_aP_b + h(P_a^4 + P_b^4)\,. \qquad (2.5.1.1)$$

In this approximation the transition will be second order, as is known from the ferroelectric case. The term in P_a^4 and P_b^4 is introduced to restrict the catastrophe to a finite polarization. The quantities *f, g, h* are functions of the temperature and are, if we were to neglect entropy changes, simply related to the polarizability and local constants. We have

$$\partial A / \partial P_a = E = 2fP_a + gP_b + 4hP_a^3\,. \qquad (2.5.1.2)$$

So that the spontaneous polarization ($E=0$) in the antiferroelectric state ($P_{sa}=-P_{sb}$) is given by

$$P_{sa}^2 = (g - 2f)/4h\,. \qquad (2.5.1.3)$$

If in the antiferroelectric state we apply a small electric field *ΔE* the macroscopic polarization $\Delta P = P_a + P_b$ is given by, taking $P_a \cong -P_b$,

$$2\Delta E = 2f\Delta P + g\Delta P + 12hP_{sa}^2\Delta P$$

or

$$\chi = \Delta P / \Delta E = 1/2(g - f)\,. \qquad (2.5.1.4)$$

At the Curie point *g=2f*, so that

$$\chi(T = T_c) = 1/g\,. \qquad (2.5.1.5)$$

on the antiferroelectric side. In the unpolarized state we neglect the fourth - power term in Eq. (2.5.1.1) and find

$$\chi = 2/(2f + g)\,. \qquad (2.5.1.6)$$

This reduces at the Curie point to

$$\chi(T = T_c) = 1/g\,. \qquad (2.5.1.7)$$

on the unpolarized side. A comparison of Eqs. (2.5.1.5) and (2.5.1.7) shows that the dielectric permittivity is continuous across the Curie point, and it does not necessarily have a high value. We suppose that *f*, which is related to the atomic polarizabilities, varies with temperature near the Curie point as

$$f = \frac{1}{2}g + \lambda(T - T_c)\,. \qquad (2.5.1.8)$$

where λ is a constant. This expression has as consequences

$$(T<T_c)\quad P_{sa}^2 = P_{sb}^2 = \lambda(T - T_c)/2h\,, \qquad (2.5.1.9)$$

$$(T<T_c)\quad \chi = 1/[g - 2\lambda(T - T_c)]\,, \qquad (2.5.1.10)$$

$$(T>T_c)\quad \chi = 1/[g + 2\lambda(T - T_c)]\,. \qquad (2.5.1.11)$$

If λ is positive, the antiferroelectric region lies on the low-temperature side of the Curie point and the dielectric permittivity changes slope slightly and goes through a maximum (which may not always be discernible) at the transition point. If λ is negative the antiferroelectric state lies on the high-temperature side of the Curie point and the dielectric permittivity will be a minimum there.

2.5.2 First order antiferroelectric phase transition

We develop now a first – order transition theory for antiferroelectrics and write the free energy

$$A = A_0 + f(P_a^2 + P_b^2) + gP_aP_b + h(P_a^4 + P_b^4) + j(P_a^6 + P_b^6). \quad (2.5.2.1)$$

We have

$$\partial A / \partial P_a = E = 2fP_a + gP_b + 4hP_a^3 + 6jP_a^5. \quad (2.5.2.2)$$

So that the spontaneous polarization in the antiferroelectric state (P_{sa}=-P_{sb}) is given by

$$6jP_{sa}^4 + 4hP_{sa}^2 + (2f - g) = 0. \quad (2.5.2.3)$$

At the Curie point the free energy for this solution is equal to that for the unpolarized solution P_a=P_b=*0* when

$$(2f - g) + 2hP_{sa}^2 + 2jP_{sa}^4 = 0. \quad (2.5.2.4)$$

The solution of the two Eqs. (2.5.2.3) and (2.5.2.4) gives us

$$(T=T_c) \quad P_{sa}^2 = (g - 2f)/h, \quad (2.5.2.5)$$

$$(T=T_c) \quad P_{sa}^4 = (2f - g)/2j \ . \quad (2.5.2.6)$$

We find that in the antiferroelectric state just below the transition we have

$$\chi^{(-)} = 1/(4f - g). \quad (2.5.2.7)$$

While just above the transition in the unpolarized state we have

$$\chi^{(+)} = 2/(2f + g). \quad (2.5.2.8)$$

Thus, if the antiferroelectric transition is of the first order, there will be a discontinuity in the dielectric permittivity at the Curie point. The condition for the Curie point is found from Eqs. (2.5.2.8) and (2.5.2.9):

$$2j(2f - g) = h^2. \quad (2.5.2.9)$$

If the transition is of the second order, a ferroelectric crystal will have a very high dielectric permittivity at the Curie point, whereas if the transition is of the first order, the dielectric permittivity need not necessarily be very high. An antiferroelectric crystal need not have a high dielectric permittivity for either first, or second – order phase

transitions. The character of the transition is determined largely by the sign of *h* in Eq. (2.5.2.4), a negative sign tending to make the transition first order.

From the considerations given above we may suggest, within the limits of the approximations made, the following conclusion:

The dielectric permittivity at the antiferroelectric Curie point will not in general be particularly large; if the transition is second order, the dielectric permittivity will be continuous and nearly constant with temperature close to the Curie point, with a small discontinuity in the temperature coefficient. In a first – order transition there will be a discontinuity in the dielectric permittivity. In ferroelectrics the dielectric permittivity is very large at the Curie point if the transition is second order. The antiferroelectric dielectric permittivity need not be isotropic.

2.6 Dipole glasses

The ordering of dipole particles is a subject having a very long history, dating back to the studies of Langevin and Debey [14], and is important up to the present. This is particularly true of those systems containing impurities, which are highly sensitive to the effect of spatial "disorder", the random or irregular arrangement of impurities. Thus, according to the Langevin and Debey theory [14], in which interaction between particles is described within the framework of an effective self consistent field (the Lorentz field for dipole systems), a "polarization catastrophe" i.e., an unlimited increase in the polarizability, should be expected as the temperature is decreased.

However, even the earliest experiments [15-17] with alkali halide crystals containing dipole impurities showed that nothing of this kind actually occurred – no ferroelectric phase transition was taking place. The explanation lies in the specificity of the dipole-dipole interaction potential: not only the magnitude, but also the sign of the interaction is

strongly dependent on the relative orientations and positions of the dipoles.

Due to a great spread of local fields at various crystal points, dipole moments at low temperatures get frozen into random orientations, with a total absence of ferroelectric long-range order. Such crystals with dipole impurities can therefore be considered as electrical analogy of spin glasses [18] and generally are called dipole glasses.

The highly polarisable dielectrics containing dipole impurities are quite sensitive to the change of these impurities because of the spatial dispersion of permittivity. The existence of spatial dispersion, characterized by the polarization correlation radius r_c, changes the effective interaction potential between dipoles so that the interaction between impurities separated by distance $r<r_c$ turns out to be predominantly ferroelectric and more complicated than is the usual dipole – dipole interaction; hence the interaction is not specifically a dipole one. Because of the specific nature of the interaction, configurationally fluctuations of local fields (which prevent the ferroelectric phase transition in weakly polarisable alkali halide crystals) decline, and a long-range order can appear in the system at high enough impurity concentrations. It can be stated by now that the situation in highly polarisable crystals is radically different from that in traditional dipole glasses, and quite a number of experiments show convincing evidence for the occurrence of dipole impurity – induced ferroelectric phase transitions [19].

The most typical representative of dipole impurities exhibiting cooperative properties are off-center ions, the so called substitutional impurity ions, whose equilibrium positions are displaced from a lattice site. It is clear that an off-center impurity/vacancy (due to an absent site atom) set in an ionic crystal has effective electric dipole moments. The direction of such dipoles, i.e., the position of an ion, which may have several positions, is not random, but is determined by the crystal

symmetry. Thermal or tunnel jumps between various positions may occur. Therefore the dipoles are not frozen and, like dipole molecules, such as OH^-, can be oriented by both external and internal electric field, which is the prerequisite for the appearance of temperature – dependent cooperative effects.

In particular, no experimental data for dipole glasses give evidence of the occurrence of an equilibrium phase transition to the state of dipole glass. This was most clearly shown by measurements of nonlinear dielectric susceptibility [20]. The experiment detected no critical growth of the susceptibility, as is the case in spin glasses such as CuMn and others [21]; hence the situation in dipole glasses differs radically from that occurring in classical spin glasses. The observed [17] hysteresis loop and residual polarization are direct evidence that interacting impurity dipoles can orient one another. The hysteresis loop shape is quite different from that observed at ferroelectrics. Moreover the residual polarization ($P_r=10\%nd^*$, n – impurity concentration and d^* - effective dipole moment) as well as coercive field are very small comparing with such in ferroelectrics.

The study of low-temperature disordered phases in orientational glasses and particularly in dipole glasses has drawn heavily from the theoretical development that has taken place in the past two decades in the field of spin glasses. Both dipole and spin glasses are characterized by competing interactions and disordered low-temperature phases. Nevertheless an important additional feature has to be considered when dealing with dipole glasses. Substitutional disorder leads to lattice distortions that inevitably give rise to local quenched random electric fields, in addition to the usual random bond interactions. Lattice distortions can not give rise to random magnetic fields unless time-reversal symmetry is broken. The existence of these random fields introduces some modifications of the properties of dipole glasses relative to conventional magnetic spin glasses [22].

Because of the variable – sign nature of the dipole-dipole interaction potential and the random spatial distribution of dipoles, local fields at the impurities have different directions, and therefore, at low temperatures and no external actions, dipoles are frozen in random orientations. Such a low – temperature state of dipole moments randomly oriented in internal fields is commonly referred to as a dipole glass state. There is so far no answer to the question of whether the dipole glass state occurs in real physical systems as a thermodynamic equilibrium one or whether it differs from the paraelectric state only by the presence of long-time relaxation modes. Therefore, when speaking of an analogy between the dipole-glass and spin-glass state, we mean simply an analogy between systems of randomly distributed spins and dipoles, whose interaction potential can change its sign.

It is already known, that the mixture of two different ordered structures gives the condition to form the disordered state at low temperatures. Reasonable examples are mixtures of ferroelectric and antiferroelectric compounds such as rubidium ammonium dihydrogen phosphate (RADP) [23] and mixed crystals $BP_{1-x}BPI_x$ [24] of antiferroelectric betaine phosphate and ferroelectric betaine phosphite show an interesting phase diagram with phase transitions to long-range ordered ferroelastic, ferroelectric, and antiferroelectric phases or to glassy states in dependence on the ratio x of the two compounds [26-30]. In RADP, a frustrated ground state is believed to occur via the competing electric interactions. In the mixed $BP_{1-x}BPI_x$ crystals the competing ferroelectric and antiferroelectric interactions cause a glass-like order behaviour of the protons in the system of hydrogen bonds. The proton glasses are of special interest in so far as they can contribute to the basic understanding of the glassy behaviour of matter as model systems. Theoretical descriptions have been developed for them, which allow comparisons with the experimental results [31-34].

2.7 Domains and domain walls

Domains and domain walls play a very important role in uniaxial materials. Above the transition temperature T_C, a ferroelectric substance has no polarization. Below T_C, the crystal undergoes a spontaneous symmetry breaking in which the equilibrium atomic positions shift to produce a new structure with dipole moment in each unit cell. In uniaxial ferroelectrics the polarization *P* lies parallel to a unique crystallographic axis z. The free energy of the domains with polarization $\pm P$ is the same in the absence of external fields, *E*. Generally, the crystal is divided into regions or domains of opposite polarization with the "up" domains separated from the "down" domains by domain walls. The actual domain structure and geometry in a particular crystal in equilibrium is determined by the condition that the total free energy of the sample is a minimum. However, the domain structure in a given crystal depends crucially on the preparation and history of that crystal; the sample has a particular domain configuration corresponding to a long – lived metastable state, and it is this nonequilibrium configuration which is probed in a given experiment.

On the basis of macroscopic arguments pertaining to equilibrium, the polarization can not vary along the ferroelectric axis: domain walls must be parallel to this axis, since the component of the electric displacement field *D* normal to the wall must be continuous. For the same reason states with domain walls perpendicular to *z* are short lived. Such states can be created by frequent switching of high electric fields, if the samples are large in the z [25] direction. By applying sufficiently large electric fields in the *z* direction (larger than the coercive field E_c) one can produce a monodomain crystal. On removing the applied field the polarization of the sample decreases to a value P_s [26], the spontaneous polarization. Application of an opposite field causes the crystal to reverse its polarization.

Any experiment which probes the local structure of domains in a plane perpendicular to the *z* axis along a particular axis x sees many planes of domain walls orientated at different angles. For a random distribution of circular domains the average apparent domain – wall width d_a is related to *d*, the width normal to the surface by $d_a = \frac{1}{2}\pi d$. Also the average wall velocity υ_a is $\upsilon_a = \frac{1}{2}\pi\upsilon$, where υ is the radial velocity. If the real domain structure is not exactly circular, then the multiplying factor *d* and υ changes slightly.

Another manifestation of domains in polarization switching experiments is that of the Barkhausen pulses. These are due to abrupt changes in polarization, mostly ascribed to the formation and annihilation of whole domains [27]. The lateral growth of domains most likely does not occur as a completely coherent process, but rather by polarization reversal in individual chains along the *z* axis. Each chain switches as a result of large fluctuations of opposite polarization expanding rapidly along the *z* direction. This multistep mechanism lowers considerably the barrier against lateral domain - wall motion.

Domains formation, nucleation and growth are ubiquitous phenomena in ferroelectrics. However, in the absence of an electric field large energies are required to form domains (except near T_c). Thus at lower temperatures domain walls are neither created nor destroyed thermally. Changes in temperature below T_c do not affect the density of domain walls [28],[29]. One is thus forced to treat the crystal as a metastable system rather than one in true equilibrium.

3. MEASUREMENT AND CALCULATION METHODS

3.1 Low - frequency measurements

In the low-frequency (20 Hz – 1 MHz) range, capacitance C_c and tangent of losses tgδ = ε″/ε′ of the sample was measured with the LCR meter HP4284. For all measurements the silver paste has been used for contacts. Complex dielectric permittivity was calculated from the plane capacitor formulas [30]:

$$\varepsilon' = \frac{(C'_{css} - C_{c0})d}{\varepsilon_0 S_s} + 1. \qquad (3.1.1a)$$

$$tg\delta = \frac{C'_{css} tg\delta_{ss} - C_{c0} tg\delta_0}{C'_{css} - C_{c0}}. \qquad (3.1.1b)$$

where C'_{css} and $tg\delta_{ss}$ are capacitance and tangent of losses of the systems with the sample, C_{c0} and $tg\delta_0$ are capacitance and tangent of losses of the systems without the sample, d is height of the sample, S_s is the area of the sample, ε_0 is the dielectric permittivity of vacuum. The area of the sample was much larger as quadrate of height d^2 so that the fringing field effects were in all performed experiments insignificant. The temperature was measured with copper-constantan thermocouple, which one stub was at the sample and another put into ice and water mixture. Measurements were performed during continuous temperature variation with typical rate of 0.5 K/min. All measurements were performed on cooling and heating but most of presented results are on cooling. For heating in all experiments was used home made furnace, for cooling in most experiments was used liquid nitrogen or closed cycle cryostat.

3.2 High - frequency measurements

The coaxial technique is the most convenient for the dielectric spectroscopy of solids in the 1 MHz – 3 GHz frequency range. In this frequency range complex reflectivity coefficient was measured with

Agilient 8714 ET (1 MHz – 3 GHz). The specimen was placed at the end of the coaxial line between the inner conductor and the short piston and formed a capacitor. Such a configuration allowed us to easily place the capacitor into temperature-control device. Coaxial lines are broadband lines. From the low-frequency end they can be used at any frequency. From the superhigh-frequency end the condition of propagation of the main TEM-wave limits application of the coaxial lines. This condition is given by [30]:

$$\lambda_{00} > \pi(r_3 + r_4). \tag{3.2.1}$$

where r_3 and r_4 are the radii of the inner and outward conductors of the coaxial line, λ_{00} is the length of electromagnetic waves.

3.2.1 Complex dielectric permittivity estimation

Complex reflection coefficient R^* is related with the impedance of measuring capacitor Z^*_{ss} and the systems impedance Z_0:

$$R^* = \frac{Z^*_{ss} - Z_0}{Z^*_{ss} + Z_0}. \tag{3.2.1.1}$$

For complex capacitance C_c^* = C_c '- iC_c" of the planar capacitor the relation (2.1a) can be generalized in such a form:

$$\varepsilon' - i\varepsilon'' = \frac{d}{\varepsilon_0 S_s}(C'_c - iC''_c) + 1. \tag{3.2.1.2}$$

Between the complex impedance Z_{ss} and the complex capacitance C_c^* is a well known relation:

$$Z_{ss} = \frac{1}{\omega(C'_{css} + iC''_{css})}. \tag{3.2.1.3}$$

From Eqs. (3.2.1.1), (3.2.1.2) and (3.2.1.3) we obtain the formulas for the real and imaginary parts of the complex dielectric permittivity ε^*:

$$\varepsilon' = \frac{d}{\varepsilon_0 S_s}\left(\frac{-2R\sin\varphi}{\omega Z_0(1 + 2R\cos\varphi + R^2)} - C_{c0}\right) + 1, \tag{3.2.1.4a}$$

$$\varepsilon'' = \frac{d}{\varepsilon_0 S_s}\frac{1 - R^2}{\omega Z_0(1 + 2R\cos\varphi + R^2)} \tag{3.2.1.4b}$$

Before-cited equations are for a quasistatic capacitor in which capacitance is independent of frequency and the electric field is homogeneous in the sample, just as it is when the dimensions of the capacitors are much smaller in comparison to a wavelength λ_{00} of the exciting electric field

3.3 Superconducting quantum interference device setup for magnetoelectric measurements

In the last decade, a tremendous growth of the interest in magnetoelectric (ME) materials has been observed [31]. Possible future applications in data storage technology [32-35] on one hand and new methods and ideas for materials engineering [36] on the other hand have triggered this remarkable trend. The ME effect in its original sense refers to the intrinsic property of some materials to react on an electric field by establishing a magnetic moment, and vice versa, to produce electric polarization by applying a magnetic field [31]. The best investigated, so-called classical material showing the linear ME effect is Cr_2O_3. It has a rhombohedral crystalline and a uniaxial antiferromagnetic (AF) spin structure, with a three-fold easy c axis. The tensor of ME susceptibility α is diagonal, so the maximal magnetization M_z is induced by applying the electric field E_z along the c axis [37]

$$\mu M_z = \alpha E_z . \qquad (3.3.1)$$

Superconducting quantum interference device (SQUID) magnetometry is a widely used method for investigating magnetic properties of various materials. The main part of the SQUID setup consists of one or several Josephson junctions, which are used for sensing an external magnetic flux. For measurements of the magnetic moment, this is converted into a voltage signal by a so-called pickup coil. In the MPMS5S system of Quantum Design being used in this theses, external magnetic fields up

to 5 T can be applied by a superconducting magnetic coil, which surrounds the sample tube with the coaxial pickup coil. Magnetic ac susceptibility is measured as a response to a magnetic ac drive field, being excited by an additional small ac coil, which is wound around the sample. The amplitude of the time dependent response is determined by means of lock-in technique.

In this case, the electric field was applied to the sample via thin copper wires, fixed to silver paste electrodes on the sample surface. The sample itself was placed in a plastic straw between two teflon membranes and put inside the sample tube of a Quantum Design MPMS5S magnetometer. The ME susceptibility value was obtained from the slope of the corresponding electric field dependence on the magnetic dc moment.

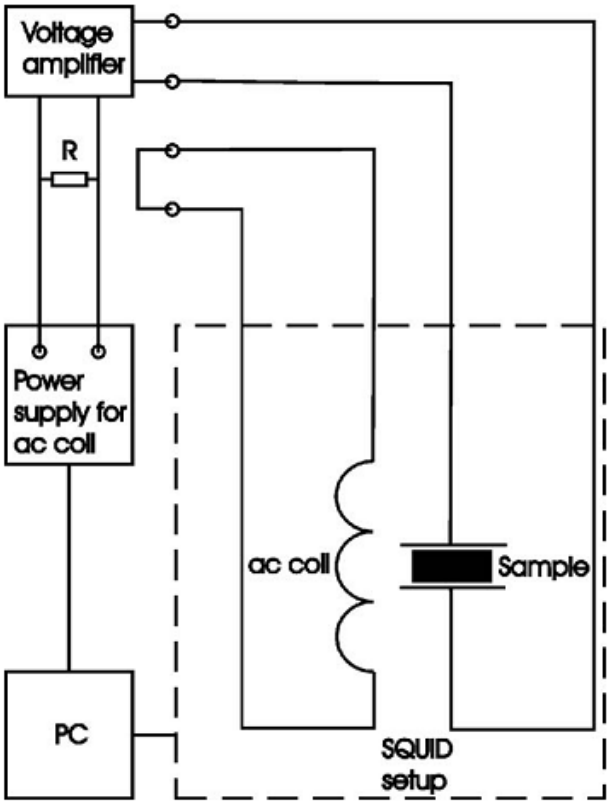

Fig. 3.3.1. Schematic plan of electric connections needed to modify a commercial SQUID magnetometer for ME susceptibility measurements.

The schematic plan is shown in Fig. 3.3.1. The magnetic drive ac field is "switched off" by disconnecting the ac coil from the corresponding power supply (Quantum Design, model 1822). The inputs of the ac coil are short circuited. The power supply delivers a current $I = I_{\max} \cos \varpi t$ via

a new load resistance *R*, whose voltage drop, $U = RI_{\max}\cos\varpi t$, is amplified (or attenuated) by a voltage amplifier and applied to the sample. In the case of a linear ME effect, a magnetic ac moment, $m = m'\cos\varpi t + m''\sin\varpi t$, will then be detected by the SQUID setup at the same frequency ϖ by executing the well-known standard procedure for ac susceptibility measurements.

3.4 Calculations of the relaxation distribution function

In order to get information that is more precise about the real relaxation-time distribution function, a special approach has been developed. We assume that the real and imaginary parts of the dielectric spectrum can be represented as a superposition of independent individual Debye-type relaxation processes [38-40]

$$\varepsilon'(\nu) = \varepsilon_\infty + \Delta\varepsilon \int_{-\infty}^{\infty} \frac{f(\tau)d\lg\tau}{1+(\omega\tau)^2}, \qquad (3.4.1.a)$$

$$\varepsilon''(\nu) = \Delta\varepsilon \int_{-\infty}^{\infty} \omega\tau \frac{f(\tau)d\lg\tau}{1+(\omega\tau)^2}. \qquad (3.4.1.b)$$

Actually, these two expressions are the first kind Fredholm integral equations for the definition of the relaxation-time distribution function $f(\tau)$. Such integral equations are known to be an ill-posed problem. The most general method of considering them is the Tikhonov regularization [41]. Numerical treatment of the integral equations (3.4.1) requires a discretization, which leads to a set of linear nonhomogeneous algebraic equations. In the matrix notation it can be represented as

$$\mathbf{AX = T}. \qquad (3.4.2)$$

Here the components T_n (1<n<N) of the vector **T** represent the dielectric spectrum ($\varepsilon_i', \varepsilon_i''$), (*1<i<N/2*) recorded at some frequencies ω_i. We used

equidistant frequency intervals in the logarithmic scale $\Delta \ln \nu_m = const$. The components X_m (*1<m<M*) of the vector **X** stand for the relaxation time distribution $f(\tau)$ that we are looking for. The symbol **A** stands for the kernel of the above matrix equation. It represents the matrix with elements obtained by the direct substitution of ω_i and τ values into the kernels of the integral equations (3.4.1). Usually the number of data points N exceeds the number of spectrum points M. Due to the fact that Eq. (3.4.2) cannot be solved directly, it is replaced by the minimization of the following function:

$$\Phi_0 = \|T - AX\|^2 = \min . \qquad (3.4.3)$$

Here and further we shall use the following vector norm notation $\|V\|^2 = V^T V$, where the superscript T indicates the transposed vector or matrix. Due to the ill-posed nature of the integral Fredholm equations, the above minimization problem is ill-posed as well, and consequently, cannot be treated without some additional means. Thus, following the Tikhonov regularization procedure the functional Φ_0 is replaced by the expression

$$\Phi(\alpha) = \|T - AX\| + \alpha^2 \|PX\|^2 = \min . \qquad (3.4.4)$$

modified by an additional regularization term. The symbol *P* stands for the regularization matrix. The regularization parameter plays the same role as a filter bandwidth when smoothing noisy data. Usually there are many solutions satisfying Eq. (3.4.4) within the limit given by the experimentally recorded dielectric spectrum errors. Thus, it is necessary to take into consideration as many additional conditions as possible. First, we know that all relaxation-time distribution components have to be positive (X_n>0). Next, sometimes one knows that rather reliable values of the static permittivity $\varepsilon(0)$ or of the limit high-frequency

dielectric permittivity ε_∞. In this case, it is worthwhile to restrict the above minimization problem by fixing either of those values or both. Usually the minimization problem of Eq. (3.4.4) is solved numerically by means of the least squares problem technique [42]. Following the algorithm described by Provencher [43] a program was developed which provides numerical solutions of the restricted minimization problem of Eq. (3.4.4) and extracts the relaxation-time distribution $f(\tau)$ (for details, see [44]). The regularization parameter is crucial for the shape of the distribution function of the relaxation times. Very small values of result in artificial physically meaningless structures in $f(\tau)$, while very large tends to over smooth the shape of $f(\tau)$ and suppress information.

4. RESULTS AND DISCUSION

4.1 PHASE TRANSITIONS IN FERRIELECTRICS

Overview

$CuInP_2S_6$ crystals represent an unusual example of an anticollinear uncompensated two-sublattice ferroelectric system [45]. They exhibit a first-order phase transition of the order–disorder type from the paraelectric to the ferrielectric phase (T_c = 315 K). The

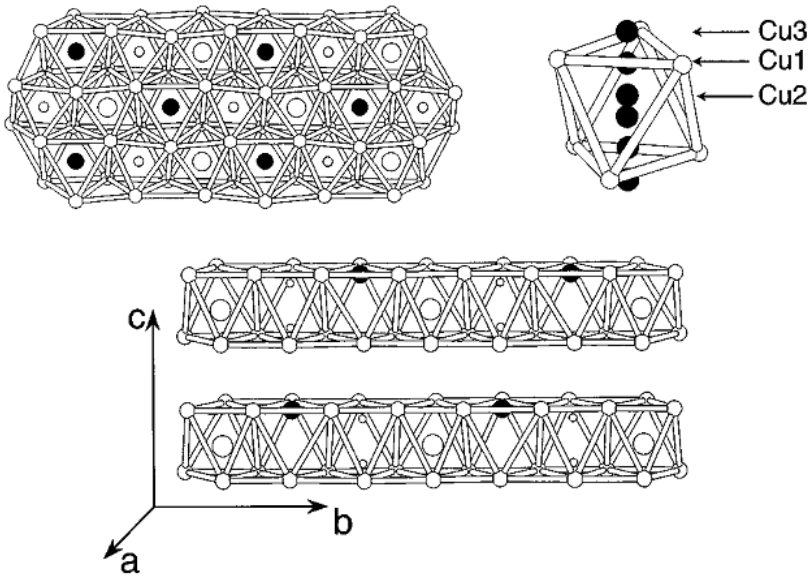

Fig. 4.1.1 Top left: Projection onto the *a*-*b* plane of the $CuInP_2S_6$ structure showing the triangular sublattices formed by the copper and indium cations and the P-P pairs. Top right: A sulfur octahedral cage showing the various types of copper sites: the off-center Cu^1, the almost central Cu^2, and Cu^3 in the interlayer space. At T>315, a twofold axis through the center doubles the number of sites per CuS_6; two off-center sites become inequivalent when unequally occupied at T<315 K. Bottom: Two layers of $CuInP_2S_6$ shown in the ferroelectric phase (T<315 K). The up (down) shifted Cu^I (In^{III}) ions are represented by the larger black (white) circles in the octahedra; the smaller white circles are the *P*.

symmetry reduction at the phase transition (C2/c to Cc) occurs due to the ordering in the copper sublattice and the displacement of cations from the centrosymmetric positions in the indium sublattice. The $CuInP_2S_6$ consists of lamellae defined by a sulphur framework in which the Cu, In cations and P–P pairs fill the octahedral voids and form triangular patterns within a layer [46] (Fig. 4.1.1).

The spontaneous polarization arising at the phase transition to the ferrielectric phase is perpendicular to the layer planes. X-ray investigations have showed that Cu ion can occupy three types of position: (1) Cu^1 - quasitrigonal, off-centered positions; (2) Cu^2 - octahedral, located in the octahedron centers; (3) Cu^3 - almost tetrahedral, penetrating into the interlayer space [47],[48] The degree of occupation strongly depends on the temperature (Fig. 4.1.2).

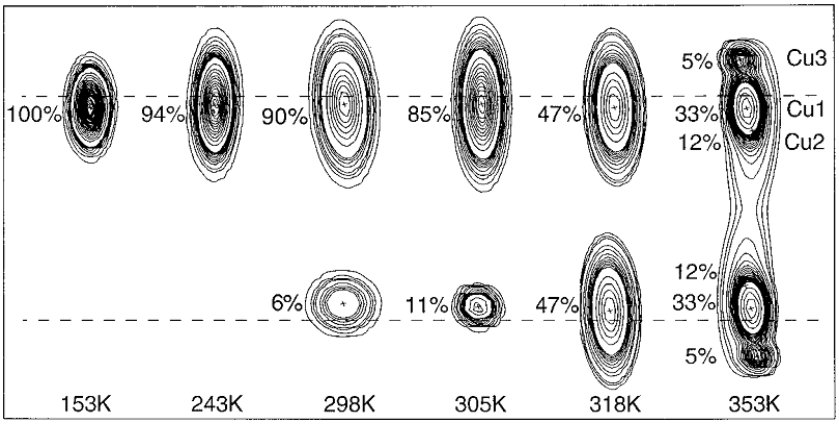

Fig. 4.1.2 Thermal evolution of the different copper site occupancies and the corresponding probability density contours in $CuInP_2S_6$ (see Fig. 4.1.1, top right). The crosses mark the refined positions, and the dashed lines indicate the upper and lower sulfur planes of a single layer. Occupancies not adding up to 100% indicate the presence of diffuse electronic densities between the off-center sites and/or in the interlayer space.

Moreover, two types of position for Cu^1 are distinguished: Cu^{1u} is displaced upwards from the middle of the layer (the centers of the octahedrons) and Cu^{1d} is displaced downwards. The ordering of Cu ions

(hopping between Cu^{1u} and Cu^{1d} positions) in the double minimum potential is the reason for the phase transition dynamics in $CuInP_2S_6$ [58-62]. The electric conductivity of $CuInP_2S_6$ was investigated only in the paraelectric phase [49],[50]. It was found that the DC conductivity in the paraelectric phase follows the Arrhenius law with the activation energy E_A=0.73 eV [50] and more detailed investigations showed E_A=0.63 eV [49] In the both Ref. [49],[50] the electric conductivity of $CuInP_2S_6$ was explained by a Cu ions hopping mechanism. In Ref. [51] was suggested that a coupling between P_2S_6 deformation modes and Cu^1 vibrations enable the copper ion hopping motions that lead to the onset of ionic conductivity in this material at higher temperatures. At low temperatures the dipolar glass phase appears in $CuInP_2S_6$ with small addition of antiferroelectric $CuCrP_2S_6$ or ferroelectric $CuInP_2Se_6$ [52],[53]. However, for mixed ferrielectric-ferroelectric $CuInP_2(S_xSe_{1-x})_6$ only disorder in selenium and sulphur sublattice is evident [54]. It is also very interesting that a nonergodic relaxor phase exist in the mixed $CuInP_2(S_xSe_{1-x})_6$ crystals [53]. Therefore it is very important to insight better into phase transitions dynamics in pure $CuInP_2S_6$ and also to investigate $CuInP_2S_6$ with various impurities.

Similar signatures of disorder might also be expected for the magnetic ground state of $CuCr_{1-x}In_xP_2S_6$, where magnetic Cr^{3+} ions are randomly replaced by diamagnetic In^{3+} ions in the antiferromagnetic (AF) compound $CuCrP_2S_6$ with a Néel temperature $T_N \approx 32$ K [55]. Owing to its competing ferromagnetic (FM) intralayer and AF interlayer exchange interactions [55], randomness and frustration might eventually give rise to spin glass phases in $CuCr_{1-x}In_xP_2S_6$, $x > 0$, similarly as in the related AF compound $Fe_{1-x}Mg_xCl_2$ [56],[57]. The possible coexistence of this spin glass phase with the dipolar glassy one [58] is another timely motivation to study $CuCr_{1-x}In_xP_2S_6$. Indeed, '*multiglass*' behavior was recently discovered in the dilute magnetic perovskite $Sr_{0.98}Mn_{0.02}TiO_3$

[59], paving the way to a new class of materials, '*disordered multiferroics*' [60].

The above mentioned comparison of the two families of dilute antiferromagnets $CuCrP_2S_6$:In and $FeCl_2$:Mg is not fortuitous. Originally, a strong structural analogy had been noticed between the lamellar compounds FeX_2 (*X* = Cl or Br) and transition metal (*M*) thio-phosphate phases, MPS_3, such as $FePS_3$ [55]. Both families are characterized by van der Waals gaps between their crystalline slabs and their ability to act as intercalation host material. The analogy becomes formally apparent when using the notations $Fe_2P_2S_6$ or – stressing the occurrence of P_2 pairs – $[Fe_{2/3}(P_2)_{1/3}]S_2$ [61], and substituting $(Fe^{2+})_2$ by $(Cu^{+}Cr^{3+})$. This transcription discloses, however, that in contrast to the FeX_2 compounds even the undoped $CuCrP_2S_6$ is a 'dilute magnet' from the beginning (*i.e.* in the absence of non-magnetic In^{3+}), since it always hosts two diamagnetic cation sublattices occupied by Cu and P ions. This 'extra' dilution must be taken into account for understanding the magnetic and magnetoelectric properties discussed below.

In this paragraph we present the results of broadband dielectric spectroscopy of $CuInP_2S_6$, $Ag_{0.1}Cu_{0.9}InP_2S_6$ and $CuIn_{1+\delta}P_2S_6$ (Indium enriched $CuInP_2S_6$ crystal) down to the very low temperatures (25K). Crystals of $CuInP_2S_6$, $Ag_{0.1}Cu_{0.9}InP_2S_6$ and $CuIn_{1+\delta}P_2S_6$ were grown by Bridgman method. For the dielectric spectroscopy the layered plate like crystals were used. All measurements were performed in the direction perpendicular to the layers. The sample was placed in the cryostat between the two copper conductors (contacts), the conductors where fresh polished for each measurement for a better electrical contact. The sample was covered by a silver paste for better contacting. Typical dimensions of the samples were ≈ 10 mm^2 area and ≈ 0.2 mm thickness. We demonstrate that the dynamic disorder in Cu sublattice do not vanish in the ferrielectric phase of $CuInP_2S_6$, $Ag_{0.1}Cu_{0.9}InP_2S_6$ and $CuIn_{1+\delta}P_2S_6$. Cu ions hopping in these crystals freeze at very low

temperatures. The broadband spectroscopy and SQUID techniques helped to complement the list of already known properties of the investigated crystals and reveal new features such as dipole glass behaviour and magneto-electric coupling.

4.1.1 Electrical conductivity investigations in $CuInP_2S_6$, $Ag_{0.1}Cu_{0.9}InP_2S_6$ and $CuIn_{1+\delta}P_2S_6$ crystals

Results of the low-frequency dielectric measurements of $Ag_{0.1}Cu_{0.9}InP_2S_6$ are presented in Fig. 4.1.1.1. At low frequencies the dielectric losses increase with increasing temperature and cause an increase of the real part of the dielectric permittivity. Such an effect is caused by the high conductivity.

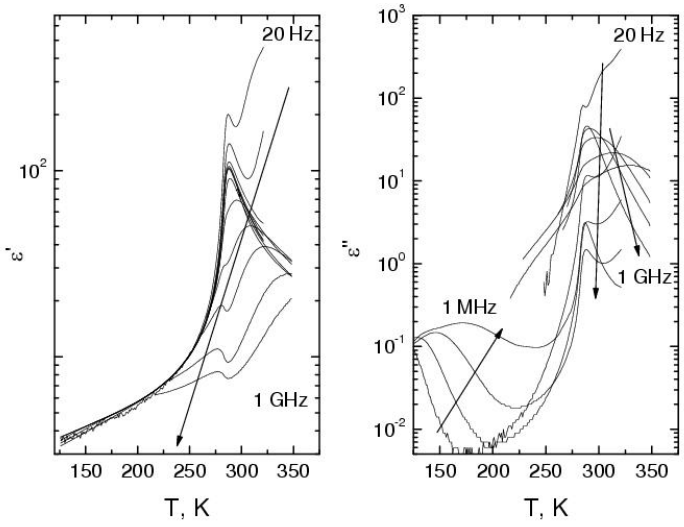

Fig. 4.1.1.1 Temperature dependence of complex dielectric permittivity of $Ag_{0.1}Cu_{0.9}InP_2S_6$.

Fig. 4.1.1.1 shows, that the real part of the dielectric permittivity already corresponds to the static one caused by the critical relaxation at 1 MHz because at that frequency ε'' is already much smaller than ε' (please see also discussion about it in [62].

It was found, that impurity of Ag ions ($Ag_{0.1}Cu_{0.9}InP_2S_6$ single crystal), or addition of extra In ions ($CuIn_{1+\delta}P_2S_6$ single crystal, where δ=0.1 corresponds to 10% of In_2S_3) added in the synthesis mixture during the growing process) drastically changes the dielectric anomaly temperature. The phase transition (PT) temperatures for different crystals are written in the Table 4.1.1.1.

Table 4.1.1.1: Phase transition temperatures got from the dielectric measurements.

Crystal	PT temperature, K
$CuInP_2S_6$	313 [63]
$CuIn_{1+\delta}P_2S_6$	330 [64]
$Ag_{0.1}Cu_{0.9}InP_2S_6$	285 [63]

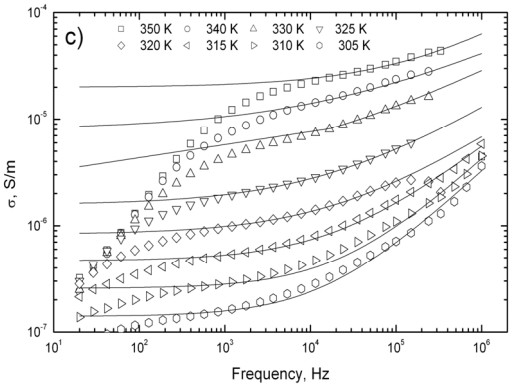

Fig. 4.1.1.2. Frequency dependence of conductivity for $CuIn_{1+\delta}P_2S_6$.

The electric conductivity σ has been calculated according to the equation:

$$\sigma = \varepsilon_0 \varepsilon'' \omega . \qquad (4.1.1.1)$$

The obtained results are presented in Fig. 4.1.1.2. The frequency behaviour of σ has been fitted according to the fundamental equation

$$\sigma = \sigma_{DC} + A\omega^S . \qquad (4.1.1.2)$$

where σ_{DC} is the DC conductivity and $A\omega^S$ is the σ_{AC} conductivity. Such fit describes well dynamic properties of conductivity of presented crystals, however, at frequencies below 1 kHz and at higher temperatures (above ferroelectric PT temperature) the discrepancies appear due the blocking contact effects. To distinguish the volume conductivity from the contact effects the procedure described in Ref. [49] was applied. For $Ag_{0.1}Cu_{0.9}InP_2S_6$ the discrepancies appear also in ferrielectric phase at frequencies above 100 kHz due to the relaxational

soft mode. The DC conductivity close to the ferrielectric phase transition T_c occurs considerably below our low frequency limit, therefore here we could not perform the Almond–West fit. The value of S is of 0.63 ± 0.01 in paraelectric phase and of 0.69 ± 0.05 in ferrielectric phase for $Ag_{0.1}Cu_{0.9}InP_2S_6$. For $CuInP_2S_6$ it is of 0.62 ± 0.02 in paraelectric phase and of 0.65 ± 0.1 in ferrielectric phase. The obtained $\ln(\sigma_{DC}(1/T))$ dependence is presented in Fig. 4.1.1.3. The σ_{DC} conductivity in ferrielectric phase is smaller as in paraelectric phase (Fig. 4.1.1.3). The σ_{DC} conductivity decreases on cooling and exhibit only a weak breaking close to the ferrielectric phase transitions temperature. This is consistent with gradual ordering of Cu ions on cooling [47]. The dependence was fitted with the Arrhenius law:

$$\sigma = \sigma_0 \exp\left(\frac{-E_A}{kT}\right), \tag{4.1.1.3}$$

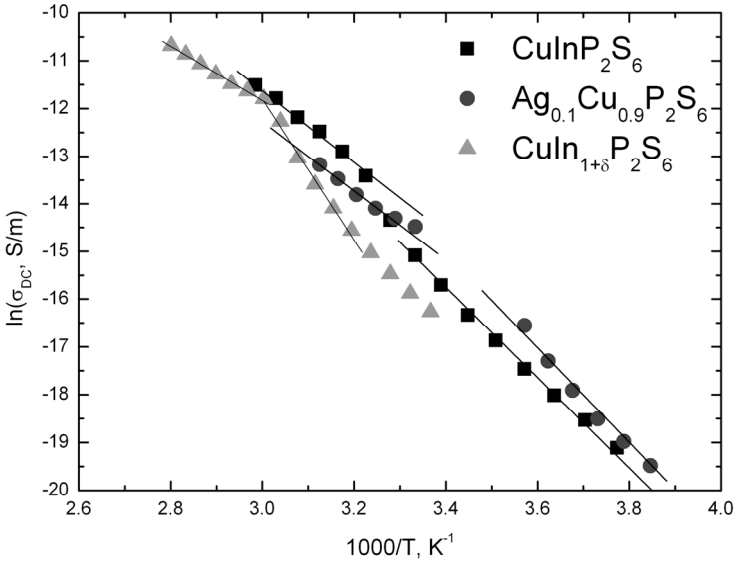

Fig. 4.1.1.3. 1/T dependence of σ_{DC} for $CuInP_2S_6$, $Ag_{0.1}Cu_{0.9}InP_2S_6$ and $CuIn_{1+\delta}P_2S_6$ crystals. Solid lines are the best fit according to (4.1.1.3).

where E_A is the activation energy and k is the Boltzmann constant, separately in the ferroelectric and paraelectric phases. Obtained parameters are presented in Table 4.1.1.2. The values of the activation

Table 4.1.1.2. The conductivity σ_0 and activation energy E_A of $CuInP_2S_6$, $Ag_{0.1}Cu_{0.9}InP_2S_6$ and $CuIn_{1+\delta}P_2S_6$ crystals

Compounds	Phase	σ_0 (S/m)	E_A, K (eV)
$CuInP_2S_6$	Paraelectric	1.33×10^4	7796 (0.672)
$CuInP_2S_6$	Ferrielectric	1.32×10^6	9454 (0.815)
$Ag_{0.1}Cu_{0.9}InP_2S_6$	Paraelectric	8.12×10^2	6381 (0.55)
$Ag_{0.1}Cu_{0.9}InP_2S_6$	Ferrielectric	1.07×10^8	10508 (0.906)
$CuIn_{1+\delta}P_2S_6$	Paraelectric	1.85×10^2	5684 (0.490)
$CuIn_{1+\delta}P_2S_6$	Ferrielectric	1.51×10^{14}	14817 (1.278)

energy E_A and conductivity σ_0 obtained for $CuInP_2S_6$ in the paraelectric phase are close to the values presented in Ref. [49] ($\sigma_0 = 5.9x10^4 S/m$). Such values of activation energy clearly differ from larger gap semiconductive $CuInP_2S_6$, where in the paraelectric phase $E_g = 3.2$ *eV* and in the ferrielectric $E_g = 2.92$ eV [65]. Moreover, the activation energy E_A and σ_0 conductivity are higher in the ferrielectric phase than in the paraelectric phase for all investigated crystals. Therefore free electrons contribution to the conductivity should by excluded in both phases. The main contribution to the electrical conductivity appears due to copper ions migration through the lattice in $CuInP_2S_6$ [49],[50] and as well in $Ag_{0.1}Cu_{0.9}InP_2S_6$ and $CuIn_{1+\delta}P_2S_6$. Copper ions migration through the lattice is complex, involving double-well motions, passage through the basal triangles of the S_6 octahedral cage and hopping within the interlayer space [66]. The activation energy E_A represents some effective average potential barrier for all types of copper ions migration. The activation energy E_A increases in the ferrielectric phase mainly due to elimination of migration channels with lower barriers, such as copper

ions motion in interlayer space. We cannot compare σ_0 in paraelectric and ferrielectric phases, because σ_0 is the conductivity when T $\rightarrow\infty$. Certainly only σ_0 from the paraelectric phase corresponds to the conductivity at very high temperatures. In the paraelectric phase σ_0 is much smaller for $Ag_{0.1}Cu_{0.9}InP_2S_6$ as compared to pure $CuInP_2S_6$ (Table 4.1.1.2). It can be explained by carrier concentration decrease in $CuInP_2S_6$ due to addition of $AgInP_2S_6$. A similar decrease of σ_0 is already observed in $CuInP_2S_6$ with small addition of $CuInP_2Se_6$ [67].

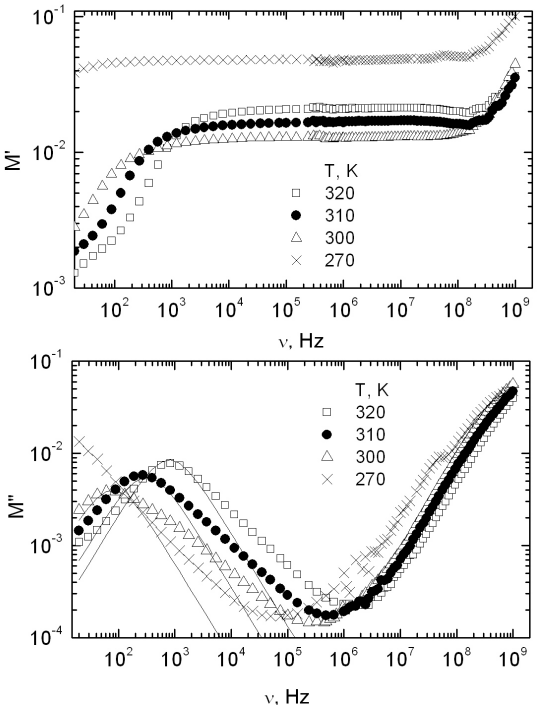

Fig. 4.1.1.4. Plots of the frequency spectra of *M'* and *M"* of $Ag_{0.1}Cu_{0.9}InP_2S_6$ crystals. Solid lines are the best fit according to Ref. [49], with $\varphi(t)$ single exponential decay function.

The DC conductivity is also significantly lower in $CuIn_{1+\delta}P_2S_6$ in comparison with both $CuInP_2S_6$ and $Ag_{0.1}Cu_{0.9}InP_2S_6$ crystals (Fig. 4.1.1.3). This can be explained by significant increase of In^+ ions related defects concentration and decrease of Cu^+ mobile ions concentration in $CuIn_{1+\delta}P_2S_6$.

The conductivity phenomena can be also investigated in terms of electrical modulus $M^*(\omega)$, which is defined as reciprocal complex dielectric permittivity:

$$M^*(\omega)=\frac{1}{\varepsilon^*(\omega)}=\frac{\varepsilon'-i\varepsilon''}{|\varepsilon|^2}=M'+iM''. \qquad (4.1.1.4)$$

Frequency dependence of complex electrical modulus can be described by the integral equation:

$$M^*(\omega) = M_\infty\left(1 - \int_0^\infty e^{-i\omega t}\frac{d\varphi}{dt}dt\right). \qquad (4.1.1.5)$$

The function $\varphi(t)$ gives the time evolution of the electric field within the material. If $\varphi(t)$ is a single exponential decay $e^{-t/\tau}$, then Eq. (4.1.1.5) becomes the Debye like formula. The frequency spectra of *M'* and *M"* of $Ag_{0.1}Cu_{0.9}InP_2S_6$ are presented in Fig. 4.1.1.4. Two dispersion regions can be separated in the spectra: one at low frequencies (20Hz–1MHz) is caused by the conductivity and other at higher frequencies (1MHz–3GHz) is caused by the relaxational soft mode. The low-frequency value of M_0 is almost 0 and represents a lack of the restoring force for the electric field induced by mobile copper ions. The dispersion of M_∞ is not Debye like. The broadening in the modulus spectra at low frequencies indicates a cooperative motion of mobile ions.

4.1.2 Ferrielectric phase transition in $Ag_{0.1}Cu_{0.9}InP_2S_6$ and $CuIn_{1+\delta}P_2S_6$

The $Ag_{0.1}Cu_{0.9}InP_2S_6$ and $CuIn_{1+\delta}P_2S_6$ crystals undergo the phase transition (Fig. 4.1.1.1 and Fig. 4.1.2.1). The nature of such phase transition, similar to the $CuInP_2S_6$, is ferrielectric one ordering in the copper sublattice and displacement of cations from the centrosymmetric positions in the indium sublattice. The temperature of the complex dielectric permittivity maximum is frequency dependent only at higher frequencies (above 50 MHz). The ferrielectric phase transition temperature T_c can be defined by maximum temperature of the real part of complex dielectric permittivity at low frequencies (below 50 MHz). The phase transition temperature T_c in the studied In-rich crystals is substantially higher in comparison to the pure $CuInP_2S_6$ [47]. The

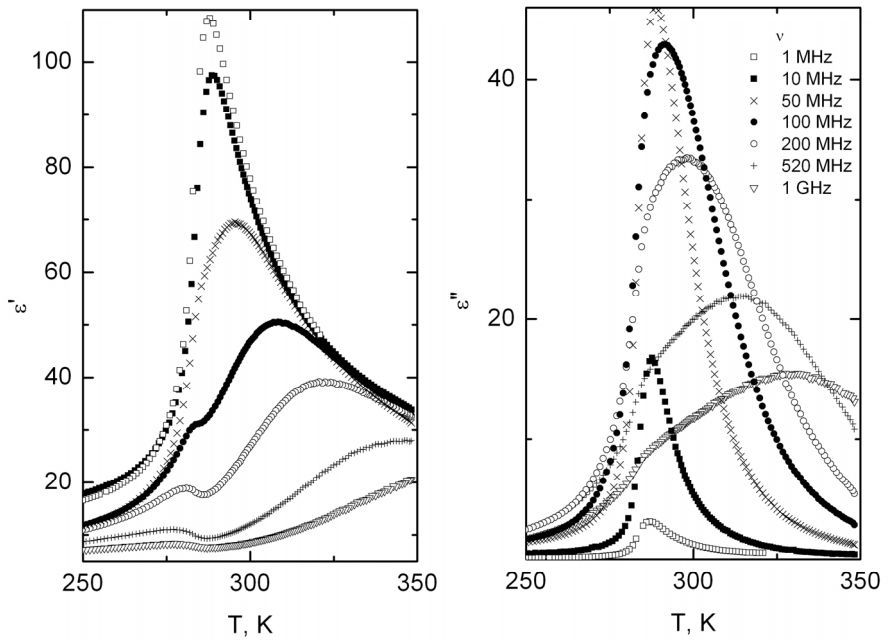

Fig. 4.1.2.1. Temperature dependence of complex dielectric permittivity of $Ag_{0.1}Cu_{0.9}InP_2S_6$ crystal measured at higher frequencies.

ferrielectric dispersion in the vicinity of T_c begins at about 10 MHz for $Ag_{0.1}Cu_{0.9}InP_2S_6$ and 1 kHz for $CuIn_{1+\delta}P_2S_6$ and ranges up to the GHz region (Fig. 4.1.2.2). A characteristic minimum of ε' appears above 100 MHz at T = 285 K for $Ag_{0.1}Cu_{0.9}InP_2S_6$ and 500 MHz at T = 330 K for $CuIn_{1+\delta}P_2S_6$ indicating a critical slowing down typical for the order–disorder phase transitions, for example H-bonded ferroelectrics [68]. The critical slowing down is also expressed as weak breaking in the temperature dependence of ε'' at higher frequencies. More information about the dynamics of ferrielectric phase transition can be obtained by analysis of frequency plot of the complex permittivity at various representative temperatures (Fig. 4.1.2.2) with Cole–Cole formula:

$$\varepsilon^*(\omega) = \varepsilon_\infty + \frac{\Delta\varepsilon}{1+(i\omega\tau)^\alpha} \qquad (4.1.2.1)$$

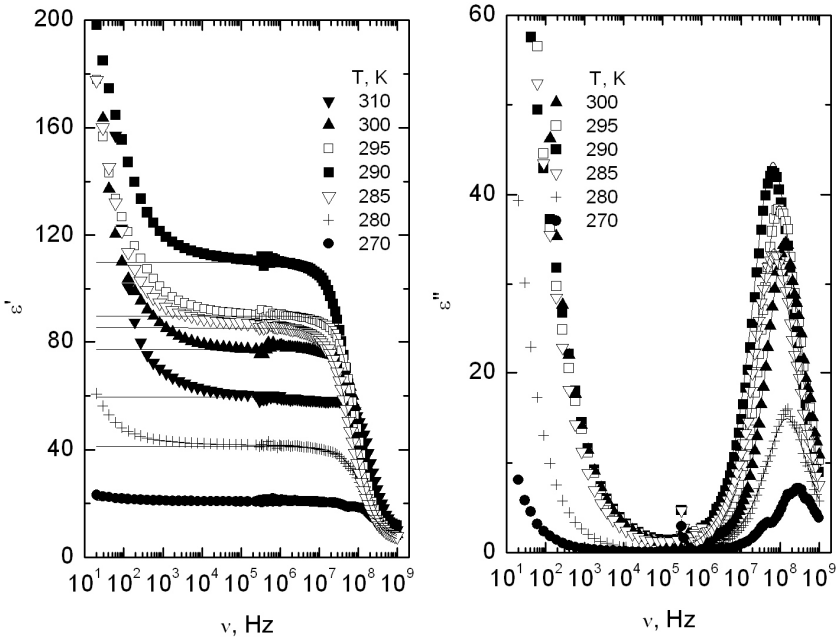

Fig. 4.1.2.2. Frequency dependence of complex dielectric permittivity of $Ag_{0.1}Cu_{0.9}InP_2S_6$ crystals measured at different temperatures. Solid lines are the best fit according to (4.1.2.1).

where $\Delta\varepsilon$ represents dielectric strength of the relaxation, τ is the mean Cole–Cole relaxation time, ε_∞ represents the contribution of all polar phonons and electronic polarization to the dielectric permittivity and α is the Cole–Cole relaxation time distribution parameter; Equation (4.1.2.1) reduces to the Debye formula when $\alpha = 0$. Obtained parameters are presented in Fig. 4.1.2.3. At higher temperatures the α parameter is very small and indicates Debye type dielectric dispersion. On cooling the α parameter increases up to 0.133 for $Ag_{0.1}Cu_{0.9}InP_2S_6$ and 0.22 for $CuIn_{1+\delta}P_2S_6$ substantially below ferrielectric phase transition temperature T_c. The distribution of the relaxation times is much broader in the ferrielectric phase than in the paraelectric one. The temperature dependence of the dielectric strength $\Delta\varepsilon$ was fitted with the Curie–

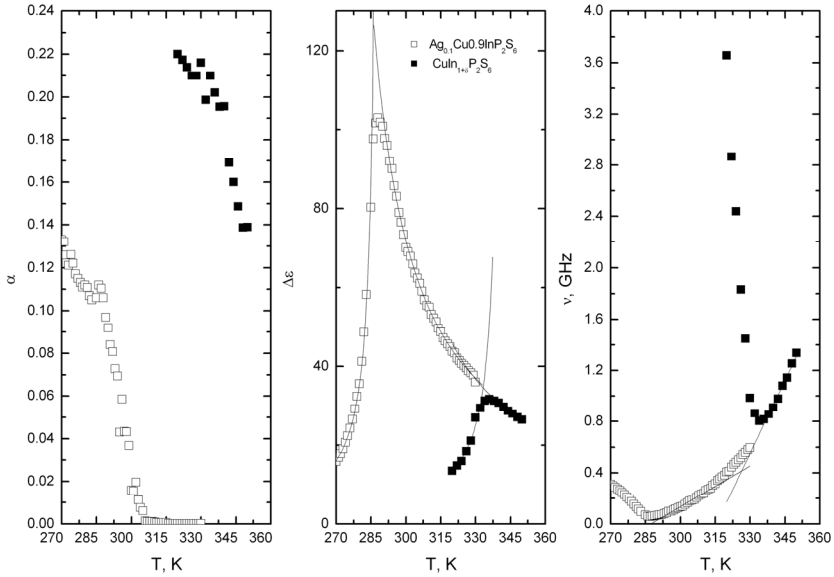

Fig. 4.1.2.3. Cole–Cole parameters of $Ag_{0.1}Cu_{0.9}InP_2S_6$ and $CuIn_{1+\delta}P_2S_6$ crystals.

Weiss law:

$$\Delta\varepsilon = \frac{C_{p,f}}{\left|T - T_{Cp,Cf}\right|} \qquad (4.1.2.2)$$

where $C_{p,f}$ is the Curie–Weiss constant and $T_{Cp,Cf}$ is the Curie–Weiss temperature obtained from the fitting correspondingly in the paraelectric and ferrielectric phases. Obtained parameters for $Ag_{0.1}Cu_{0.9}InP_2S_6$ are C_p = 2294 K, T_{Cp}= 268 K, C_f = 295K, T_{Cf} = 288K and for $CuIn_{1+\delta}P_2S_6$: C_p=1871 K, T_{Cp}=279 K, C_f=290 K, T_{Cf}=341 K. The ratios C_p/C_f = 7.8 (6.45 for $CuIn_{1+\delta}P_2S_6$) and mismatch T_{Cf}–T_{Cp} = 20 K (62 K for $CuIn_{1+\delta}P_2S_6$) show the first order ferroelectric phase transition. The ratio C_p/T_{Cp} = 8.5 (6.7 for $CuIn_{1+\delta}P_2S_6$) and C_f/T_{Cf} = 1 (0.85 for $CuIn_{1+\delta}P_2S_6$) shows that the type of ferroelectric phase transition is mainly of the order–disorder. The temperature dependence of the mean Cole–Cole relaxation time τ in the paraelectric phase was fitted with classical law [68]:

$$\tau = \tau_0 e^{U/kT} \frac{C_p}{T - T_{Cp}}. \qquad (4.1.2.3)$$

where τ_0 is a relaxation time when $T \to \infty$ and exponential factor describes discrepancies from phenomenological Landau–Ginzburg theory close to the phase transition temperature, which appears due to critical fluctuations. Obtained parameters for $Ag_{0.1}Cu_{0.9}InP_2S_6$ are $\tau_0 = 8.1x10^{-16} s$, *U/k* = 2980 K (0.26 eV). Critical fluctuations are negligible for $CuIn_{1+\delta}P_2S_6$ (factor $e^{U/kT}$ =1) and $\tau_0 = 14 ps$.

4.1.3 The ferrielectric and dipolar glass phase's coexistence in $CuInP_2S_6$, $CuIn_{1+\delta}P_2S_6$ and $Ag_{0.1}Cu_{0.9}InP_2S_6$ crystals.

At temperatures below 175 K, the dielectric dispersion effects can be observed at low frequencies for pure $CuInP_2S_6$ (Fig. 4.1.3.1). The similar dielectric dispersion also occurs in $Ag_{0.1}Cu_{0.9}InP_2S_6$ and in $CuIn_{1+\delta}P_2S_6$ at low temperatures. Such dielectric dispersion is typical for

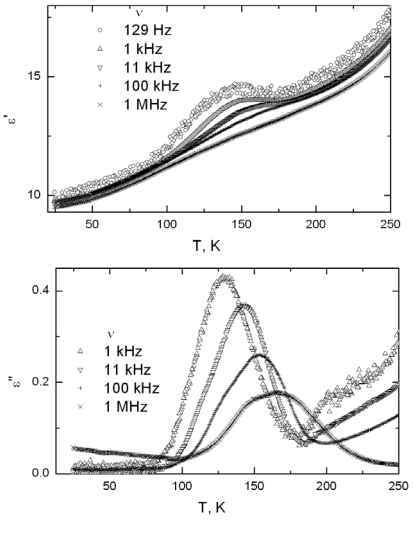

Fig. 4.1.3.1. Temperature dependence of complex dielectric permittivity of $CuInP_2S_6$ crystals. Low-temperature region.

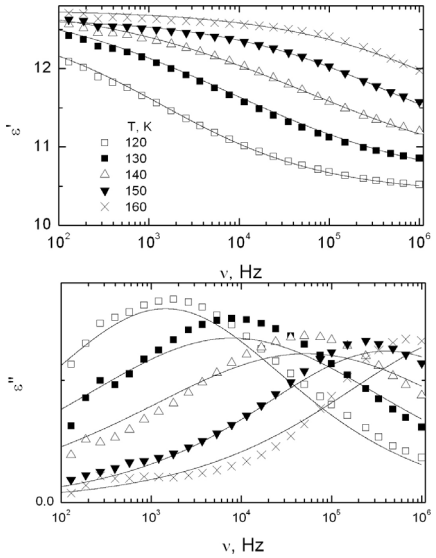

Fig. 4.1.3.2 Frequency dependence of complex dielectric permittivity of $CuInP_2S_6$ crystals measured at different temperatures. Low-temperature region. Solid lines are the best fit according to (4.1.2.1).

dipolar glasses (Figs. 4.1.3.1 and 4.1.3.2) [53],[69]. From dielectric spectra for $CuInP_2S_6$, $CuIn_{1+\delta}P_2S_6$ and $Ag_{0.1}Cu_{0.9}InP_2S_6$ the Cole–Cole parameters were calculated (Fig. 4.1.3.3). The parameter of distribution of relaxation times α is very high and almost temperature independent (average value for $CuInP_2S_6$ is about 0.5 and for $Ag_{0.1}Cu_{0.9}InP_2S_6$ it is about 0.65). That indicates a very wide distribution of relaxation times.

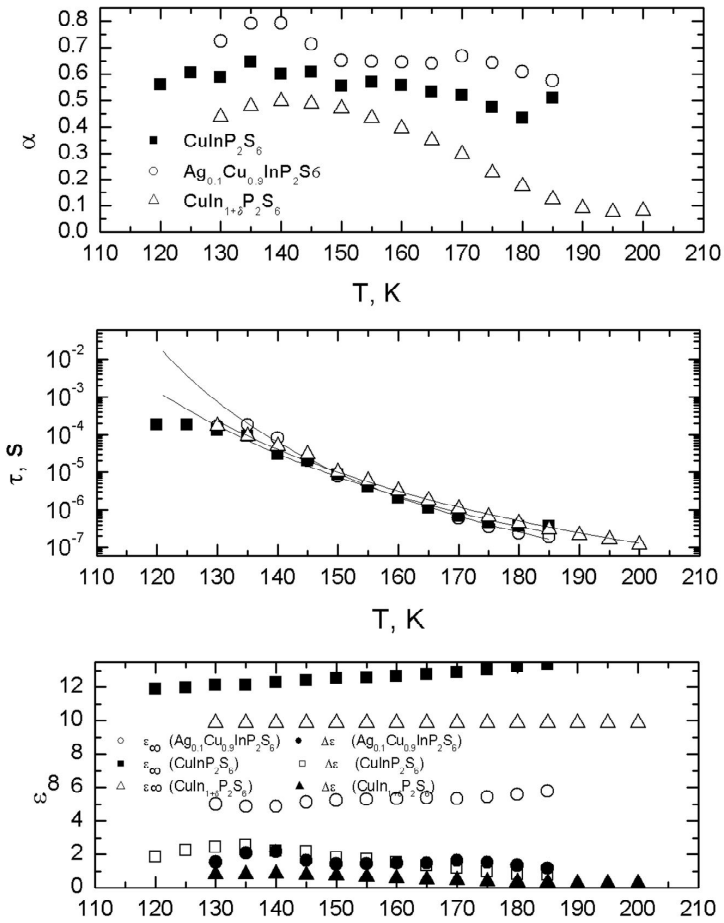

Fig. 4.1.3.3 Cole–Cole parameters of $CuInP_2S_6$ and $Ag_{0.1}Cu_{0.9}InP_2S_6$ crystals. Low-temperature region.

The mean relaxation time increase on cooling according to the Vogel–Fulcher law:

$$\tau = \tau_0 \exp \frac{E_f}{k(T - T_0)} \qquad (4.1.3.2)$$

where E_f is the activation energy, T_0 is the freezing temperature. Obtained parameters are presented in Table 4.1.3.1.

Table 4.1.3.1. The Vogel – Fulcher law parameters of $CuInP_2S_6$, $Ag_{0.1}Cu_{0.9}InP_2S_6$ and $CuIn_{1+\delta}P_2S_6$ crystals.

Compounds	τ_0, s	E_f, K (eV)	T_0, K
$CuInP_2S_6$	3.6×10^{-12}	1645 (0.15)	37
$Ag_{0.1}Cu_{0.9}InP_2S_6$	1.3×10^{-11}	1100 (0.09)	68
$CuIn_{1+\delta}P_2S_6$	1.0×10^{-11}	1483 (0.13)	42

The freezing temperature is higher for $Ag_{0.1}Cu_{0.9}InP_2S_6$ as compared to $CuInP_2S_6$ and $CuIn_{1+\delta}P_2S_6$. For both crystals the dielectric strength $\Delta\varepsilon$ is very weak (about 2) and almost temperature independent which is typical for dipole glasses. What is the nature of dipolar glass phase in pure $CuInP_2S_6$? First of all we must admit that the freezing occurs namely in copper sublattice, because the ferroelectric interaction exist only for copper ions in $CuInP_2S_6$ [47]. Secondly, for dipolar glass phase should exist disorder in copper sublattice and competitive (ferroelectric and antiferroelectric) interactions between copper ions or (and) between copper ions and lattice. Competitive interactions can occur between copper and indium ions. The static disorder in copper sublattice was observed by X-ray investigations [47] mainly at higher temperatures. This disorder is just random distribution of copper ions between more than the three positions (Cu^1, Cu^2, Cu^3). At low temperatures (T=153 K) these investigations showed almost 100% copper ions ordering. However, this is only a static picture of disorder in $CuInP_2S_6$. The dielectric spectroscopy reveals that the dynamic disorder in $CuInP_2S_6$ not vanishes in ferroelectric phase. The dynamic disorder is hopping of Cu ions between several possible static occupation positions. This hopping freezes at very low temperatures. Additional factors, which can

affect the order in Cu sublattice, are various defects, impurities. Very small noncontrollable amount of impurities and defects always exist in pure ferroelectrics. However, usually this factor is only the cause of weak dispersion of dielectric permittivity values and phase transitions temperature of the samples with the same chemical formula. At low temperature, no dipolar glass phase was discovered until now in pure ferroelectrics. Usually to get dipolar glass phase in ferroelectrics at low temperatures, a small amount (several percent) of antiferroelectrics addition is used [70],[71]. The $CuInP_2S_6$ represent another class of ferroelectrics (ferrielectrics) for which dipolar glass phase at low temperatures is observed even in the pure crystals. Therefore $CuInP_2S_6$ with small amount of additions, independent from physical properties of the additions (ferroelectric, antiferroelectric or nonferroelectric) should exhibit the same phase diagram – the ferrielectric phase transition at higher temperatures and the freezing into dipolar glass phase at lower temperatures. In this work, $CuInP_2S_6$ with small addition of nonferroelectric $AgInP_2S_6$ was investigated, however other small additions of antiferroelectric $CuCrP_2S_6$ [52] or ferroelectric $CuInP_2Se_6$ [72] gave the similar result. This is main difference of $CuInP_2S_6$ from other ferroelectrics, which usually exhibits dipole glass behaviour only with the small additions of antiferroelectrics. The phase diagram of ferrielectrics has been studied long time ago in terms of Landau–Ginzburg theory [73]. Following this theory, two order parameters for ferrielectric phase transitions were introduced:

$$Q = \frac{P_a + P_b}{\sqrt{2}}. \qquad \text{(4.1.3.3 a)}$$

$$q = \frac{-P_a + P_b}{\sqrt{2}}. \qquad \text{(4.1.3.3 b)}$$

where P_a and P_b are polarisation of the first and the second sublattice, respectively. Dependent from these parameters four possible phases for ferrielectrics can be described: nonpolar, antipolar, polar or

semipolar. The semipolar phase is defined as a phase with $P_a + P_b \neq 0$ and $P_a - P_b \neq 0$, therefore the ferrielectric phase in $CuInP_2S_6$ is semipolar. However, the dipole glass behaviour can be hardly described in terms of order parameters [74]. Therefore, by such a way we can not identify a possibility of dipole glass phase in ferrielectrics. Another way of considerations of ferroelectric and related phase transitions is random bond random field model [22]. In this model the average coupling constant J and coupling variance ΔJ are introduced. The average coupling constant in ferrielectric can be calculated from the relation $J = T_c/k$. In the ferrielectric coupling variance ΔJ should be also nonzero, because here various interactions exist with different signs between ferrielectric active ions, and only one average coupling constant J can not adequately represent an array of interactions in ferrielectrics. The nonzero coupling variance ΔJ automatically causes a dipole glass phase with freezing temperature $T_0 = \Delta J / k$ [75]. Therefore the semipolar phase in ferroelectric in many aspects is similar to inhomogeneous ferroelectric phase [72]. From it a dipole glass phase follows at the low temperatures. All other ferrielectric phases (nonpolar, antipolar, polar) should not exhibit dipolar glass behaviour.

4.1.4 Magnetic properties of $CuCr_{1-x}In_xP_2S_6$ single crystals.

4.1.4.1 Experimental procedure.

Single crystals of $CuCr_{1-x}In_xP_2S_6$, with x = 0, 0.1, 0.2, 0.4, 0.5, and 0.8 were grown by the Bridgman method and investigated as thin as-cleft rectangular platelets with typical dimensions 4×4×0.1 mm^3. The long edges define the *ab*-plane and the short one the *c*-axis of the monoclinic crystals [55]. While the magnetic easy axis of the x = 0 compound lies in the *ab*-plane [55], the spontaneous electric polarization of the x = 1 compound lies perpendicular to it [76].

Magnetic measurements were performed using a SQUID magnetometer (Quantum Design MPMS-5S) at temperatures from 5 to

300 K and magnetic fields up to 5 T. For magnetoelectric measurements we used a modified SQUID *ac* susceptometer [77], which measures the first harmonic of the *ac* magnetic moment induced by an external *ac* electric field. To address higher order ME effects, additional *dc* electric and/or magnetic bias fields were applied [59]

4.1.4.2 Temperature dependence of the magnetization

The temperature dependence of the magnetization M measured on $CuCr_{1-x}In_xP_2S_6$ samples with x = 0, 0.1, 0.2, 0.4, 0.5 and 0.8 in a magnetic field of $\mu_0 H$ = 0.1 T applied perpendicularly to the *ab*-plane are shown in Fig. 4.1.4.2.1 within $5 \leq T \leq 150$ K. Cusp-like antiferromagnetic (AF) anomalies are observed for x = 0, 0.1, and 0.2, at $T_N \approx 32$, 29, and 23 K, respectively, as displayed in Fig. 4.1.4.2.1. While Curie-Weiss-type hyperbolic behavior, $M \propto (T - \Theta)^{-1}$, dominates above the cusp temperatures [55], near constant values of M are found as $T \rightarrow 0$. They remind of the susceptibility of a uniaxial antiferromagnet perpendicularly to its easy axis, $\chi_\perp \approx const.$, thus confirming its assertion for $CuCrP_2S_6$ [55].

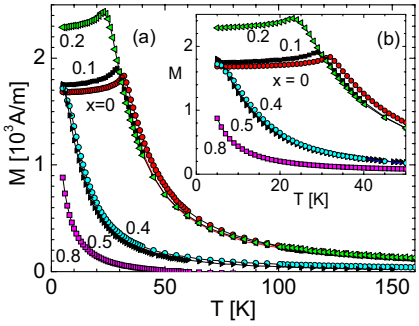

Fig. 4.1.4.2.1 Magnetization M *vs.* temperature T obtained for $CuCr_{1-x}In_xP_2S_6$ with x = 0, 0.1, 0.2, 0.4, 0.5, and 0.8 in $\mu_0 H$ = 0.1 T applied parallel to the *c* axis before (a) and after correction for the diamagnetic underground (b; see text).

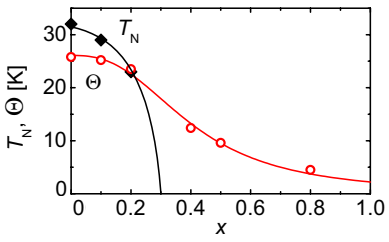

Fig. 4.1.4.2.2 Néel and Curie temperatures, T_N and Θ, *vs.* In^{3+} concentration x, derived from Fig. 4.1.4.2.1 (M) and Fig. 4.1.4.2.3 ($1/M$), and fitted by parabolic and logistic decay curves (solid lines), respectively.

At higher In^{3+} contents, $x \geq 0.4$, no AF cusps appear any more and the monotonic increase of M on cooling extends to the lowest temperatures, $T \approx 5$ K. Obviously the Cr^{3+} concentration falls short of the percolation threshold of the exchange interaction paths between the Cr^{3+} spins, which probably occurs at $x \approx 0.3$.

A peculiarity is observed at the highest In^{3+} concentration, $x = 0.8$ (Fig. 4.1.4.2.1 a). The magnetization assumes negative values at $T >$ 60 K. This is probably a consequence of the diamagnetism of the In^{3+} sublattice, the constant negative magnetization of which becomes dominant at elevated temperatures. For a correct evaluation of the Cr^{3+} driven magnetism we correct the total magnetic moments for the diamagnetic background via the function

$$M = \frac{C}{T - \Theta} + D \,. \qquad (4.1.4.2.1)$$

This model function accounts for pure Curie-Weiss behavior with the constant C at sufficiently high temperature and for the corresponding diamagnetic background D at all compositions. Table 4.1.4.2.1 presents the best-fit obtained parameters. The monotonically decreasing magnitudes of the negative background values $D \approx$ - 53, -31, and -5 A/m for $x = 0.8$, 0.5, and 0.4, respectively, reflect the increasing ratio of paramagnetic Cr^{3+} *vs.* diamagnetic In^{3+} ions. We notice that weak negative background contributions, $D \approx$ - 17 A/m, persist also for the lower concentrations, $x = 0.2$, 0.1 and 0. Presumably the diamagnetism is here dominated by the other diamagnetic unit cell components, *viz.* S_6 and P_2.

Remarkably, the positive, *i. e.* FM Curie-Weiss temperatures, $26 > \Theta > 23$ K, for $0 \leq x \leq 0.2$ decrease only by 8%, while the decrease of T_N is about 28% (Fig. 4.1.4.2.2). This indicates that the two-dimensional (2D) FM interaction within the *ab* layers remains intact, while the interplanar AF coupling becomes strongly disordered and, hence, weakened such T_N decrease markedly. It is noticed that our careful data

treatment revises the previously reported near equality, $\Theta \approx T_N \approx 32$ K for $x = 0$ [55]. Indeed, the secondary interplanar exchange constant, $J_{inter}/k_B = -1$K, whose magnitude is not small compared to the FM one, $J_{intra}/k_B = 2.6$ K [55], is expected to drive the crossover from 2D FM to 3D AF 'critical' behavior far above the potential FM ordering temperature, Θ.

Table 4.1.4.2.1. Best-fit parameters of the data in Fig. 4.1.4.2.1 to *Eq.* (4.1.4.2.1).

x	Θ [K]	C [10^3A/(m·K)]	D [A/m]
0	25.8	20.72	-28.7
0.1	25.2	18.16	-16.4
0.2	23.5	19.53	-16.6
0.4	12.4	6.56	-4.5
0.5	9.6	6.99	-31.4
0.8	4.5	3.19	-54.6

As can be seen from Table 4.1.4.2.1 and from the intercepts with the *T*-axis of the corrected 1/*M vs. T* plots in Fig. 4.1.4.2.3, the Curie-Weiss temperatures attain positive values, $\Theta > 0$, also for high concentrations, $0.4 \leq x \leq 0.8$. This indicates that the prevailing exchange interaction remains FM as in the concentrated antiferromagnet, $x = 0$ [55]. However, severe departures from the straight line behavior at low temperatures, $T < 30$ K, indicate that competing AF interactions favour disordered magnetism rather than pure paramagnetic behavior. Nevertheless, as will be shown in Fig. 4.1.4.2.4 for the $x = 0.5$ compound, glassy freezing with non-ergodic behavior [78] is not perceptible, since the magnetization data are virtually indistinguishable in zero-field cooling/field heating (ZFC-FH) and subsequent field cooling (FC) runs, respectively.

The concentration dependences of the characteristic temperatures, T_N and Θ, in Fig. 4.1.4.2.2 confirm that the system $CuCr_{1-x}In_xP_2S_6$ ceases to become globally AF at low T for dilutions $x > 0.3$, but continues to show preponderant FM interactions even as $x \rightarrow 1$. The tentative percolation limit for the occurrence of AF long-range order as extrapolated in Fig. 4.1.4.2.2 is reached at $x_p \approx 0.3$. This is much lower than the corresponding value of $Fe_{1-x}Mg_xCl_2$, $x_p \approx 0.5$ [79]. Also differenly from this classic dilute antiferromagnet we find a stronger than linear decrease of T_N with x. This is probably a consequence of the

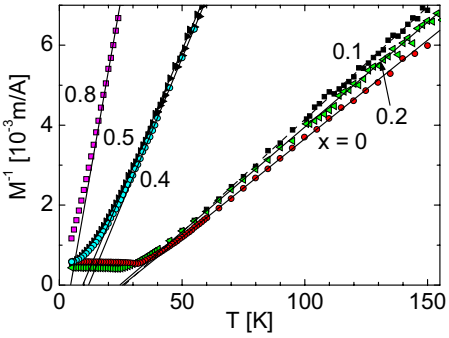

Fig. 4.1.4.2.3. Inverse magnetization M^{-1} corrected for diamagnetic background, *Eq.* (4.1.4.2.1), *vs.* T taken from Fig. 4.1.4.2.1 (inset). The straight lines are best-fitted to corrected Curie-Weiss behavior, *Eq.* (4.1.4.2.1), within individual temperature ranges (Table 4.1.4.2.1). Their abscissa intercepts denote Curie temperatures, Θ (Table 4.1.4.2.1).

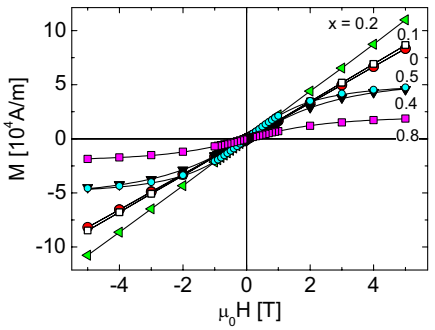

Fig. 4.1.4.2.4. Out-of-plane magnetization of $CuCr_{1-x}In_xP_2S$ with $0 \leq x \leq 0.8$ recorded at $T = 5$ K in magnetic fields $|\mu_0 H| \leq 5$ T. The straight solid lines are compatible with $x = 0$, 0.1, and 0.2, while Langevin-type solid lines, *Eq.* (4.1.4.3.1) and Table 4.1.4.3.1, deliver best-fits for $x = 0.4$, 0.5, and 0.8.

dilute magnetic occupancy of the cation sites in the $CuCrP_2S_6$ lattice [55], which breaks intraplanar percolation at lower x than in the densely packed Fe^{2+} sublattice of $FeCl_2$ [79].

A sigmoid logistic curve describes the decay of the Curie temperature in Fig. 4.1.4.2.2,

$$\Theta = \frac{\Theta_0}{1+(x/x_0)^p}\,, \qquad (4.1.4.2.2)$$

with best-fit parameters Θ_0 = 26.1, x_0 = 0.405 and p = 2.63. It characterizes the decay of the magnetic long-range order into 2D FM islands, which rapidly accelerates for $x > x_0 \approx x_p \approx 0.3$, but sustains the basically FM coupling up to $x \rightarrow 1$.

4.1.4.3 Field dependence of the magnetization.

The magnetic field dependence of the magnetization of the $CuCr_{1-x}In_xP_2S$ compounds yields additional insight into their magnetic order. Fig. 4.1.4.3.1 shows FC out-of-plane magnetization curves of the samples with $0 \leq x \leq 0.8$ taken at T = 5 K in fields -5 T $\leq \mu_0 H \leq$ 5 T. Corrections for diamagnetic contributions, as discussed above, have been employed. For low dilutions, $0 \leq x \leq 0.2$, non-hysteretic straight lines are observed as expected for the AF regime (see Fig. 4.1.4.2.1) below the critical field towards paramagnetic saturation. Powder and single crystal data on the x = 0 compound are corroborated except for any clear signature of a spin-flop anomaly, which was reported to provide a slight change of slope at $\mu_0 H_{SF} \approx 0.18$ T [55]. This would, indeed, be typical of the easy *c*-axis magnetization of near-Heisenberg antiferromagnets like $CuCrP_2S$, where the magnetization components are expected to rotate jump-like into the *ab*-plane at $\mu_0 H_{SF}$. This phenomenon was thoroughly investigated on the related lamellar MPS_3-type antiferromagnet, $MnPS_3$ albeit at fairly high fields, $\mu_0 H_{SF} \approx 4.8$ T [80], which is lowered to 0.07 T for diamagnetically diluted $Mn_{0.55}Zn_{0.45}PS_3$ [81].

In the highly dilute regime, $0.4 \leq x \leq 0.8$, the magnetization curves show saturation tendencies, which are most pronounced for x = 0.5, where spin-glass freezing might be expected as reported, *e.g.,* for Fe_{1-}

$_x$Mg$_x$Cl$_2$ [79]. However, no indication of hysteresis is visible in the data. They turn out to excellently fit Langevin-type functions,

$$M(H) = M_0[\mathbf{coth}(y) - 1/y] \qquad (4.1.4.3.1)$$

where $y = (m\mu_0 H)/(k\ T)$ with the 'paramagnetic' moment *m*. Fig. 4.1.4.3.1 shows the functions as solid lines, while Table 4.1.4.3.1 summarizes the best-fit results.

Table 4.1.4.3.1. Best-fit parameters of data in Fig. 4.1.4.3.1 to *Eq.* (4.1.4.3.1).

x	M_0	m	$N = M_0/m$
0.4	65.7 kA/m	5.6×10^{-23} Am^2 = $6.1\mu_B$	1.2 nm^{-3}
0.5	59.6 kA/m	8.5×10^{-23} Am^2 = $9.2\mu_B$	0.7 nm^{-3}
0.8	24.7 kA/m	6.86×10^{-23} Am^2 = $7.4\mu_B$	0.4 nm^{-3}

While the saturation magnetization M_0 and the moment density *N* scale reasonably well with the Cr^{3+} concentration, 1-*x*, the 'paramagnetic' moments exceed the atomic one, $m(Cr^{3+}) = 4.08\ \mu_B$ [55] by factors up to 2.5. This is a consequence of the FM interactions between nearest-neighbor moments. They become apparent at low *T* and are related to the observed deviations from the Curie-Weiss behavior (Fig. 4.1.4.2.3). However, these small '*superparamagnetic*' clusters are obviously not subject to blocking down to the lowest temperatures as evidenced from the ergodicity of the susceptibility curves shown in Fig. 4.1.4.2.1.

4.1.4.3 Anisotropy of magnetization and susceptibility

The cluster structure delivers the key to another surprising discovery, namely a strong anisotropy of the magnetization shown for

the x = 0.5 compound in Fig. 4.1.4.3.1. Both the isothermal field dependences $M(H)$ at T = 5 K (Fig. 4.1.4.3.1a) and the temperature dependences $M(T)$ shown for $\mu_0 H$ = 0.1 T (Fig. 4.1.4.3.1b) split up under different sample orientations. Noticeable enhancements by up to 40% are found when rotating the field from parallel to perpendicular to the c-axis. At T = 5 K we observe $M_\perp \approx 70$ and 2.5 kA/m *vs.* $M_\parallel \approx 50$ and 1.8 kA/m at $\mu_0 H$ = 5 and 0.1 T, respectively (Fig. 4.1.4.3.1a and b).

At first sight this effect might just be due to different internal fields, $H^{int} = H - NM$, where N is the geometrical demagnetization coefficient. Indeed, from our thin sample geometry, 3×4×0.03 mm^3, with $N_\parallel \approx 1$ and $N_\perp << 1$ one anticipates $H_\parallel^{int} < H_\perp^{int}$, hence, $M_\parallel < M_\perp$.

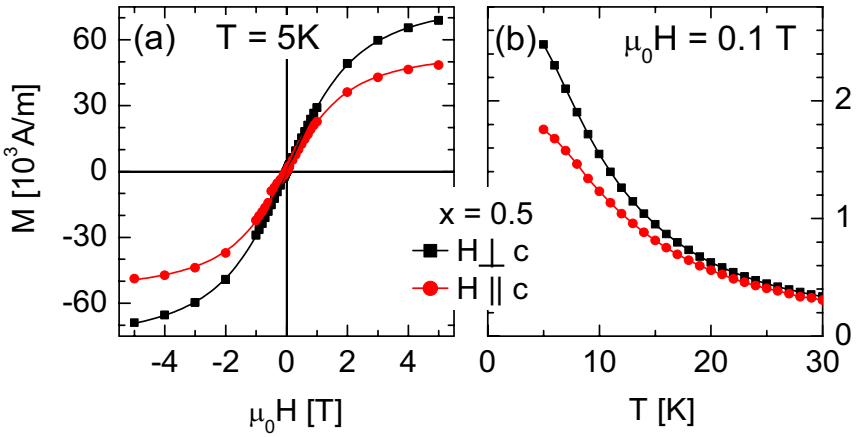

Fig. 4.1.4.3.1. Magnetization M of $CuCr_{0.5}In_{0.5}P_2S_6$ measured parallel (circles) and perpendicularly (squares) to the c axis (a) *vs.* $\mu_0 H$ at T = 5 K (best-fitted by Langevin-type solid lines) and (b) *vs.* T at $\mu_0 H$ = 0.1T (interpolated by solid lines).

However, the demagnetizing fields, $N_\perp M_\perp \approx 0$ and $N_\parallel M_\parallel \approx 50$ and 1.8 kA/m, are no larger than 2% of the applied fields, H = 4 MA/m and 80 kA/m, respectively. These corrections are, hence, more than one order of magnitude too small as to explain the observed splittings. Since the anisotropy occurs in a paramagnetic phase, we can also not argue with AF anisotropy, which predicts $\chi_\perp > \chi_\parallel$ at low T [82]. We should rather consider the intrinsic magnetic anisotropy of the above mentioned

'superparamagnetic' clusters in the layered $CuCrP_2S_6$ structure. Their planar structure stems from large FM in-plane correlation lengths, while the AF out-of-plane correlations are virtually absent. This enables the magnetic dipolar interaction to support in-plane FM and out-of-plane AF alignment in $H_\perp$, while this spontaneous ordering is weakened in $H_\parallel$. However, the dipolar anisotropy cannot explain the considerable difference in the magnetizations at saturation, $M_0^\parallel$=58.5 kA/m and $M_0^\perp$ = 84.2 kA/m, as fitted to the curves in Fig. 4.1.4.3.1a. This strongly hints at a mechanism involving the total moment of the Cr^{3+} ions, which are subject to orbital momentum transfer to the spin-only $^4A_2(d^3)$ ground state. Indeed, in the axial crystal field zero-field splitting of the $^4A_2(d^3)$ ground state of Cr^{3+} is expected, which admixes the $^4T_{2g}$ excited state via spin-orbit interaction [83]. The magnetic moment then varies under different field directions as the gyrotropic tensor components, $g_\perp$ and $g_\parallel$, while the susceptibilities follow $g_\perp{}^2$ and $g_\parallel{}^2$, respectively. However, since $g_\perp$ = 1.991 and $g_\parallel$ = 1.988 [55] the single-ion anisotropies of both M and χ are again mere 2% effects, unable to explain the experimentally found anisotropies.

Since single ion properties are not able to solve this puzzle, the way out of must be hidden in the collective nature of the 'superparamagnetic′ Cr^{3+} clusters. In view of their intrinsic exchange coupling we propose them to form 'molecular magnets′ with a high spin ground states accompanied by large magnetic anisotropy [84] such as observed on the AF molecular ring molecule Cr_8 [85]. The moderately enhanced magnetic moments obtained from Langevin-type fits (Table 4.1.4.3.1) very likely refer to mesoscopic 'superantiferromagnetic′ clusters [86] rather than to small 'superparamagnetic′ ones. More experiments, in particular on time-dependent relaxation of the magnetization involving quantum tunneling at low T, are needed to verify this hypothesis.

It will be interesting to study the concentration dependence of this anisotropy in more detail, in particular at the percolation threshold to the AF phase. Very probably the observation of the converse behavior in the AF phase, $\chi_\perp < \chi_\parallel$ [55], is crucially related to the onset of AF correlations. In this situation the anisotropy will be modified by the spin-flop reaction of the spins to $H_\parallel$, where $\chi_\parallel$ jumps up to the large $\chi_\perp$ and both spin components rotate synchronously into the field direction.

4.1.4.4 Magnetoelectric coupling

Magnetic and electric field-induced components of the magnetization, ***M*** = ***m/V***,

$$\mu_0 M_i = -\partial F / \partial H_i = \mu_0 \mu_{ij} H_j + \alpha_{ij} E_j + \beta_{ijk} E_j H_k + \frac{\gamma_{ijk}}{2} E_j E_k + \delta_{ijkl} H_j E_k E_l \qquad (4.1.4.4.1)$$

related to the respective free energy under Einstein summation [59]

$$F(\mathbf{E},\mathbf{H}) = F_0 - \frac{1}{2}\varepsilon_0 \varepsilon_{ij} E_i E_j - \frac{1}{2}\mu_0 \mu_{ij} H_i H_j - \alpha_{ij} H_i E_j - \frac{\beta_{ijk}}{2} H_i E_j H_k - \frac{\gamma_{ijk}}{2} H_i E_j E_k - \frac{\delta_{ijkl}}{2} H_i H_j E_k E_l \qquad (4.1.4.4.2)$$

were measured using an adapted SQUID susceptometry [77]. Applying external electric and magnetic *ac* and *dc* fields along the monoclinic [001] direction, $E = E_{ac}\cos\omega t + E_{dc}$ and H_{dc}, the real part of the first harmonic *ac* magnetic moment at a frequency $v = \omega/2\pi = 1$ Hz,

$$m'_{ME} = (\alpha_{33} E_{ac} + \beta_{333} E_{ac} H_{dc} + \gamma_{333} E_{ac} E_{dc} + 2\delta_{3333} E_{ac} E_{dc} H_{dc})(V/\mu_o) \qquad (4.1.4.4.3)$$

provides all relevant magnetoelectric (ME) coupling coefficients α_{ij}, β_{ijk}, γ_{ijk}, and δ_{ijkl} under suitable measurement strategies.

First of all, we have tested *linear* ME coupling by measuring m'_{ME} on the weakly dilute AF compound $CuCr_{0.8}In_{0.2}P_2S_6$ (see Fig. 4.1.4.2.1 and 4.1.4.2.2) at $T < T_N$ as a function of E_{ac} alone. The resulting data (not shown) turned out to oscillate around zero within errors, hence, $\alpha \approx 0$. This is disappointing, since the (average) monoclinic space group C2/m [55] is expected to reveal the linear ME effect similarly as in

$MnPS_3$ [87]. We did, however, not yet explore non-diagonal couplings, which are probably more favorable than collinear field configurations.

More encouraging results were found in testing higher order ME coupling as found, *e. g.*, in the disordered multiferroics $Sr_{0.98}Mn_{0.02}TiO_3$ [59] and $PbFe_{0.5}Nb_{0.5}O_3$ [88]. Fig. 4.1.4.4.1 shows the magnetic moment m'_{ME} resulting from the weakly dilute AF compound $CuCr_{80}In_{20}P_2S_6$ after

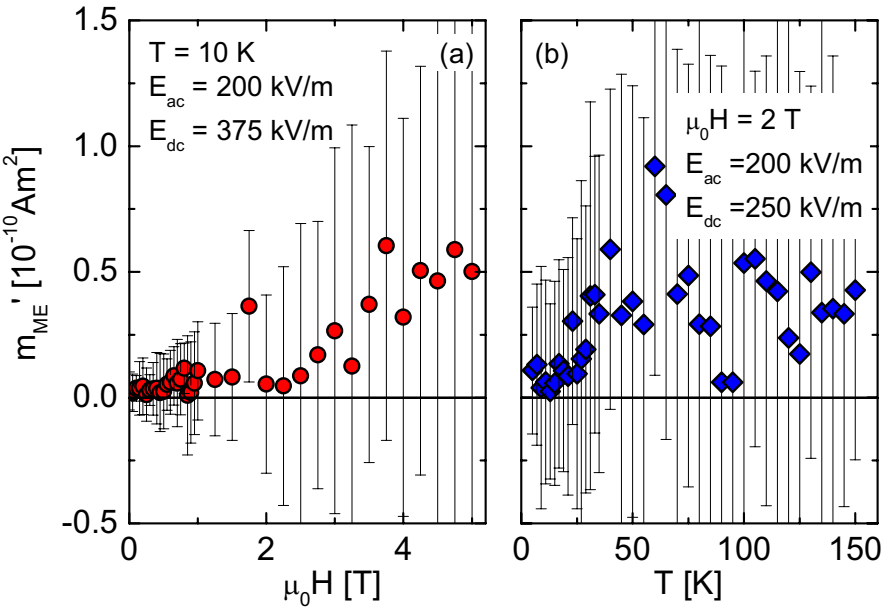

Fig. 4.1.4.4.1. Magnetoelectric moment m'_{ME} of $CuCr_{0.8}In_{0.2}P_2S_6$ excited by E_{ac}= 200 kV/m at v = 1 Hz in constant fields E_{dc} and H_{dc} and measured parallel to the c axis (a) *vs.* $\mu_0 H$ at T = 5 K and (b) *vs.* T at $\mu_0 H$ = 2 T.

ME cooling to below T_N in three applied fields, E_{ac}, E_{dc}, and (a) at variant H_{dc} with constant T = 10 K, or (b) at variant T and constant $\mu_0 H_{dc}$ = 2 T. We notice that very small, but always positive signals appear, although their large error limits oscillate around m'_{ME}= 0. That is why we dismiss a finite value of the second-order magneto-bielectric coefficient γ_{333}, which should give rise to a finite ordinate intercept at H = 0 in Fig. 4.1.4.4.1 a according to *Eq.* (4.1.4.4.3). However, the clear upward trend of $\langle m'_{ME} \rangle$ with increasing magnetic field makes us believe in a

finite *biquadratic* coupling coefficient. The average slope in Fig. 4.1.4.4.1 a suggests $\delta_{3333} = \mu_o \Delta m'_{ME}/(2V\Delta H_{dc} E_{ac} \Delta E_{dc}) \approx 4.4\times10^{-25}$ sm/VA. This value is more than one to two orders of magnitude smaller than those measured in $Sr_{0.98}Mn_{0.02}TiO_3$ [59] and $PbFe_{0.5}Nb_{0.5}O_3$ [88], $\delta_{3333} \approx -9.0\times10^{-24}$ and 2.2×10^{-22} sm/VA, respectively. Even smaller, virtually vanishing values are found for the more dilute paramagnetic compounds such as $CuCr_{0.5}In_{0.5}P_2S_6$ (not shown). The temperature dependence of m'_{ME} in Fig. 4.1.4.4.1 b shows an abrupt increase of noise above T_N = 23 K. This hints at disorder and loss of ME response in the paramagnetic phase.

Conclusions

$CuInP_2S_6$, $Ag_{0.1}Cu_{0.9}InP_2S_6$ and $CuIn_{1+\delta}P_2S_6$ crystals

1. The first-order ferrielectric phase transition of mainly order – disorder type is observed in $CuInP_2S_6$ crystal doped with Ag (10%) or In (10%) at the temperatures 330 K and 285 K, respectively.
2. At low temperatures the dipole glass phase is observed even in nominally pure $CuInP_2S_6$ or in $CuInP_2S_6$ with small addition of paraelectric $AgInP_2S_6$.

Solid solutions of $CuCr_{1-x}In_xP_2S_6$ reveal interesting magnetic properties, which are strongly related to their layered crystal structure:

1. Diamagnetic dilution with In^{3+} of the antiferromagnetic x = 0 compound experiences a low percolation threshold, $x_p \approx 0.3$, toward 'superparamagnetic' disorder without tendencies of blocking or forming spin glass.
2. At low temperatures the 'superparamagnetic' clusters in $x > 0.3$ compounds reveal strong magnetic anisotropy, which suggests them to behave like 'molecular magnets'.

The main results are published in [63], [64], [89],[90]

4.2 DIPOLE GLASS STATE IN MIXTURE OF FERROELECTRIC AND ANTIFERROELECTRIC CRYSTALS

Overview

The copper chromium thiophosphate $CuCrP_2S_6$ crystallizes in a layered two-dimensional structure of the $Cu^{I}M^{III}P_2S_6$ (M = Cr, In) type described above [55], [76], [92], [93]. It is formed by double sheets of sulfur atoms sandwiching the metal cations and P–P groups which occupy the octahedral voids defined by the sulfur atoms. At room temperature, the spread-out copper electronic distribution perpendicular to the layer is satisfactorily modelled by two vertically disposed positions, one distinctly (Cu^1) and the other slightly (Cu^2) shifted from the octahedral centre where the crystal structure has a space group of C2/c [94]. The incomplete occupancy of these sites may be interpreted as a static or dynamic kind of disorder. At 64 K, the Cu positions are confined to those of an antiferroelectric order where the crystal structure

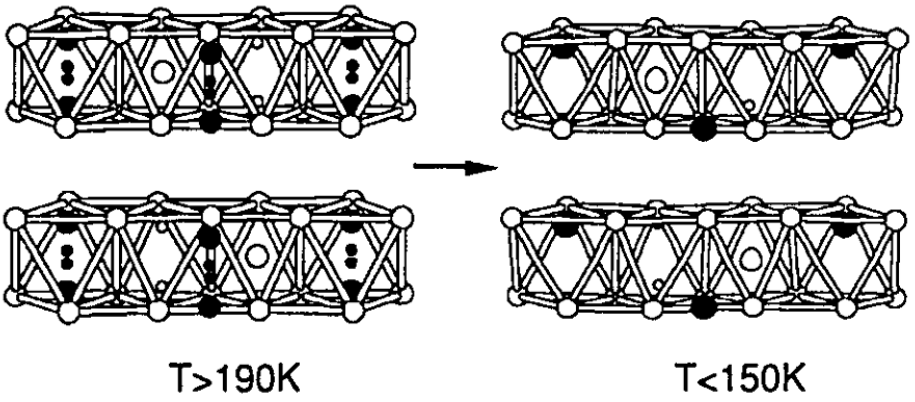

Fig. 4.2.1. Perspective view of two layers of $CuCrP_2S_6$: left in the paraelectric phase and right in the antiferroelectric phase. The sulphur atoms define the framework while the Cu, Cr and P are represented by filled, large empty and small empty circles, respectively [91].

has the space group of Pc [94]. Thus, the mechanism of the dielectric transition is likely to involve hopping of the copper ions among two or

more positions. Two phase transitions have been observed at 155 K and 190 K by dielectric measurement and differential scanning calorimetry (DSC) [91]. The crystal is antiferroelectric below 155 K and paraelectric above 190 K (Fig. 4.2.1). For the intermediate phase between 155 and 190 K, a quasi-antipolar structure has been proposed [91]. Optical absorption measurement has given evidence that the intermediate phase is incommensurate [95]. In the low-temperature region, the magnetic susceptibility has a cusp near 30 K [96], indicating the occurrence of a magnetic phase transition. Neutron powder diffraction has shown antiferromagnetic ordering of the Cr^{3+} spins below 30 K [94],[97].

In present section, we report the dielectric permittivity of $CuCrP_2S_6$ and $CuIn_xCr_{1-x}P_2S_6$ measured at temperature between 25 K and 350 K and discuss the disappearance of ferroelectric ($CuInP_2S_6$) and antiferroelectric ($CuCrP_2S_6$) phase transitions by mixing these crystals in different proportions. The $CuIn_xCr_{1-x}P_2S_6$ crystals have been grown by vapour transport technique [98]. The phase diagram summarizes obtained results. Using double well potential model we calculated the distribution function of relaxation times directly from the dielectric measurements and found relation between the macroscopic and microscopic parameters.

4.2.1 Phase transitions in $CuCrP_2S_6$ and $CuIn_{0.1}Cr_{0.9}P_2S_6$ crystals

The phase transition in $CuCrP_2S_6$ is accompanied by a step-like dielectric anomaly (Fig. 4.2.1.1). The width of the step is approximately 5 K. Taking the temperature, corresponding to the peak point of the step (at the real part of dielectric permittivity) as the temperature of phase transition, it was found that $T_c \approx 170$ K. It should be mentioned that the dielectric loss in $CuCrP_2S_6$ does not show any remarkable anomalous behavior in the vicinity of the phase transition as well as in antiferroelectric phase at lower temperatures.

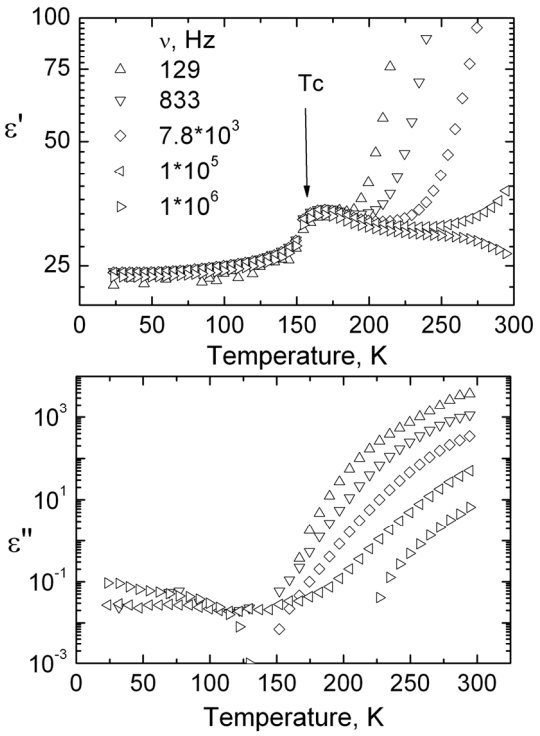

Fig. 4.2.1.1 Temperature dependence of complex dielectric permittivity of $CuCrP_2S_6$.

As can be seen from Fig. 4.2.1.1, at temperatures T > 200 K the dielectric permittivity shows sharp increase with temperature demonstrating pronounced frequency dependence. Obviously hopping conductivity causes this dielectric behavior. In the $CuIn_{0.1}Cr_{0.9}P_2S_6$ mixed crystal, the dielectric behavior is similar to that observed in $CuCrP_2S_6$ except for a broader step in the $\varepsilon'(T)$ dependence. Here it is 20 K. The peak point of the step lies approximately at 167 K (Fig. 4.2.1.2). There is a noticeable shift of the antiferroelectric phase transition temperature due to the substitution of In by Cr in the mixed $CuIn_xCr_{1-x}P_2S_6$ antiferroelectrics. While analyzing the sample from low temperatures, the ε' rises slowly between 30 K and 125 K for $CuIn_{0.1}Cr_{0.9}P_2S_6$ and 150 K for $CuCrP_2S_6$, after which it increases abruptly and then slightly, while at 167 K for $CuIn_{0.1}Cr_{0.9}P_2S_6$ and 170 K for $CuCrP_2S_6$ it starts decreasing. As we can see there ε' maximum is not so well expressed as in $CuInP_2S_6$, therefore such an anomaly is typical for antiferroelectics (please see also Overview) [91]. The T width of this dielectric anomaly and the slope changes just below 167 K ($CuIn_{0.1}Cr_{0.9}P_2S_6$) and 170 K

($CuCrP_2S_6$) agree with a hypothesis of a slowly evolving short-range dipole order. Knowing that the copper dipole configuration is antipolar at T<150 K [50], we infer from the relatively continues decrease of ε' at 125 K ($CuIn_{0.1}Cr_{0.9}P_2S_6$) and 150 K ($CuInCrP_2S_6$) that intermediate phase is quasi – antipolar (or incommensurate). It was found that $\varepsilon'(T)$ follows the Curie –Weiss law (4.2.1.2). The ratio of C_p/C_{af}>>2 indicate about the first order phase transition in both crystals.

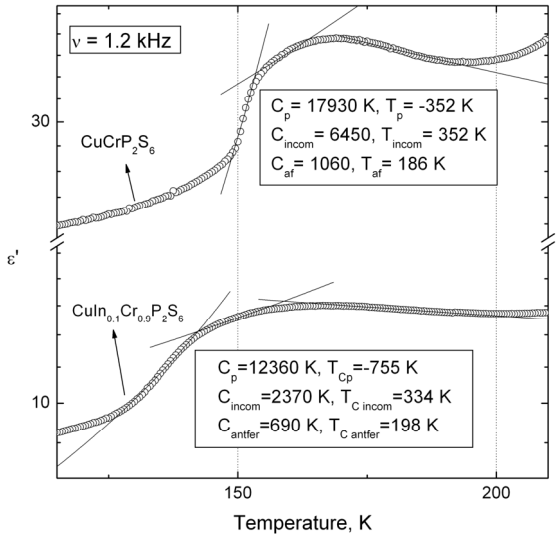

Fig. 4.2.1.2. Temperature dependence of real part of dielectric permittivity of $CuIn_{0.1}Cr_{0.9}P_2S_6$ and $CuCrP_2S_6$. Solid lines are fitted according to the Curie – Weiss law.

The conductivity phenomena can be also investigated in terms of electrical modulus *M*(ω)*. From the movement of the *M"* peak (Fig. 4.2.1.3) we could calculate the activation energy according to the Arhenius law (4.1.1.3) which is 0.385 eV for $CuCrP_2S_6$ and 0.364 eV for $CuIn_{0.1}Cr_{0.9}P_2S_6$, while for $CuInP_2S_6$ in paraelectric phase is 0.672 eV.

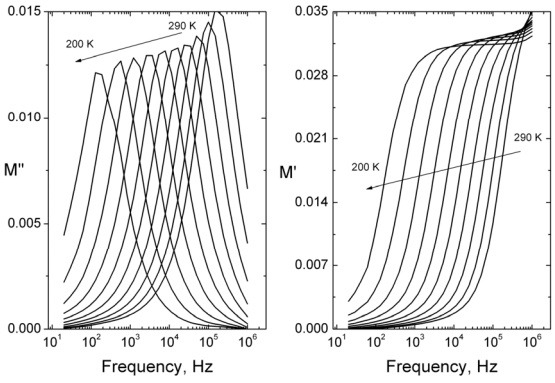

Fig. 4.2.1.3. Frequency dependence of complex electrical modulus of $CuCrP_2S_6$.

4.2.2 Inhomogeneous ferrielectrics

The temperature dependence of real and imaginary parts of complex dielectric permittivity ε^* at various frequencies ν of $CuIn_{0.7}Cr_{0.3}P_2S_6$ and $CuIn_{0.8}Cr_{0.2}P_2S_6$ crystals are presented in Fig. 4.2.2.1. We can see three different regions of dielectric dispersion. At temperatures $T > 220$ K and frequencies $\nu < 1$ MHz dielectric dispersion is mainly caused by the high conductivity. Similar high conductivity was already observed in both $CuCrP_2S_6$ and $CuInP_2S_6$ crystals and was suggested hopping mechanism for Cu^+ ions transport [49],[68]. The dielectric dispersion caused by the relaxation soft mode is observed in the vicinity of the ferroelectric phase transition temperature $T_c \approx 256$ K for $CuIn_{0.7}Cr_{0.3}P_2S_6$ and $T_c \approx 247$ K for $CuIn_{0.8}Cr_{0.2}P_2S_6$ and

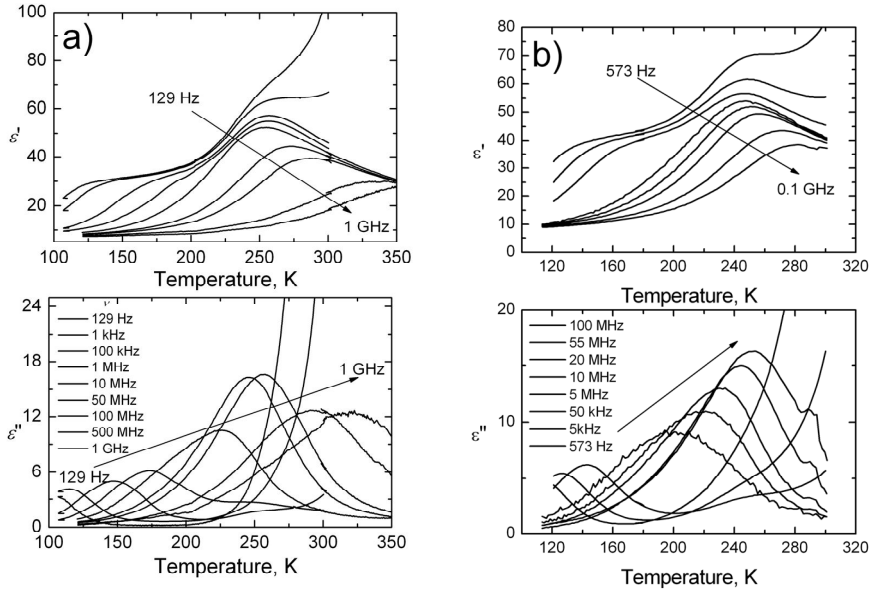

Fig. 4.2.2.1. Temperature dependence of complex dielectric permittivity of a) $CuIn_{0.7}Cr_{0.3}CrP_2S_6$ and b) $CuIn_{0.8}Cr_{0.2}CrP_2S_6$

at higher frequencies (ν > 1 MHz). The dispersion at low temperatures (T <170 K) is characteristic for the freezing into dipolar glass state. It is likely that substitutions in chromium sublattice make more complicated

potential relief in which copper ions move. As a consequence, a part of the copper ions does not participate in the cooperative dynamics involved in the ferroelectric ordering. Therefore it is obvious that defects induced by substitutions partially destroy the long-range polar order.

Unusual (for ferroelectrics) temperature behavior of dielectric dispersion is observed for presented crystals. At higher temperatures ($T>>T_c$) the dielectric dispersion is clearly symmetric and observed only at higher frequencies (above 1 MHz). On cooling it strongly posses to lower frequencies and become more asymmetric (Fig. 4.2.2.2).

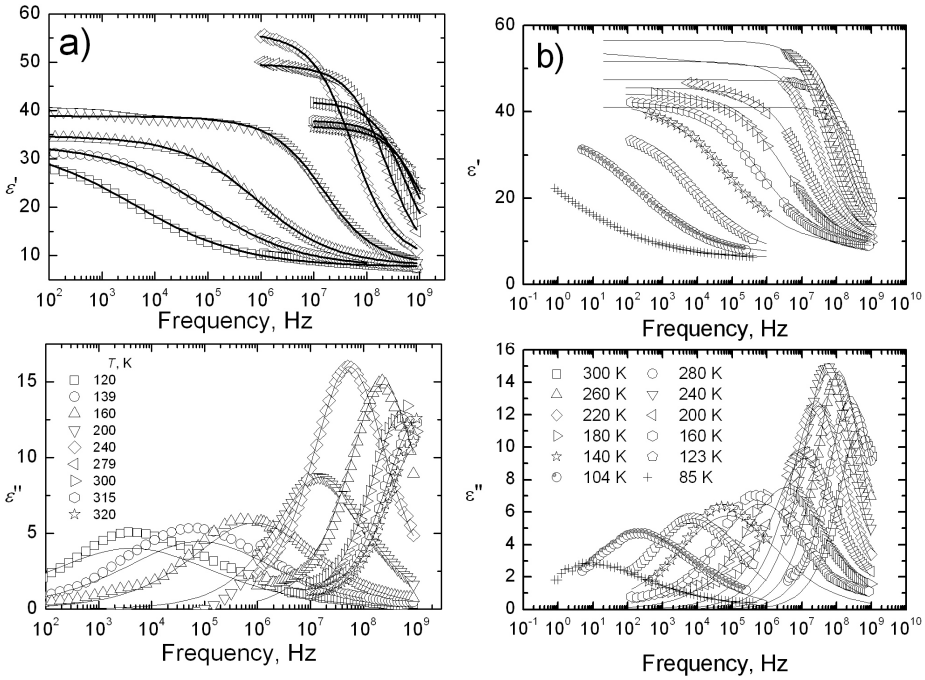

Fig. 4.2.2.2. Frequency dependence of complex dielectric permittivity of a) $CuIn_{0.7}Cr_{0.3}CrP_2S_6$ and b) $CuIn_{0.8}Cr_{0.2}CrP_2S_6$. Solid lines are the best fits according to the Cole – Cole formula (4.1.2.1)

The temperature dependences of the Cole-Cole parameters: α, $\Delta\varepsilon$, ε_∞ and τ we can see in Fig. 4.2.2.3. The parameter α strongly decreases with the increasing temperature and just at the high temperatures ($T >$ 320 K) the dielectric dispersion of studied crystal is Debye like. At low temperatures this parameter reaches anomalous high value (for

ferroelectric) $\alpha_{max} \approx 0.6$. The dielectric permittivity ε_∞ is almost temperature-independent and its average value is $<\varepsilon_\infty> = 8.19$ for $CuIn_{0.8}Cr_{0.2}CrP_2S_6$. The peak of the dielectric strength $\Delta\varepsilon$ close to $T = 256$ K for $CuIn_{0.7}Cr_{0.3}P_2S_6$ indicate a ferroelectric phase transition. The parameter $\Delta\varepsilon$ in the vicinity of the ferroelectric phase transition temperature follows the Curie-Weiss law (4.1.2.2). To find out its order we have calculated the Curie-Weiss constants in the paraelectric and ferroelectric phases respectively: $C_p \approx 4940$ K and $C_f \approx 2580$ K. From the proportion of these constants (1.92) it is clear that $CuIn_{0.7}Cr_{0.3}P_2S_6$

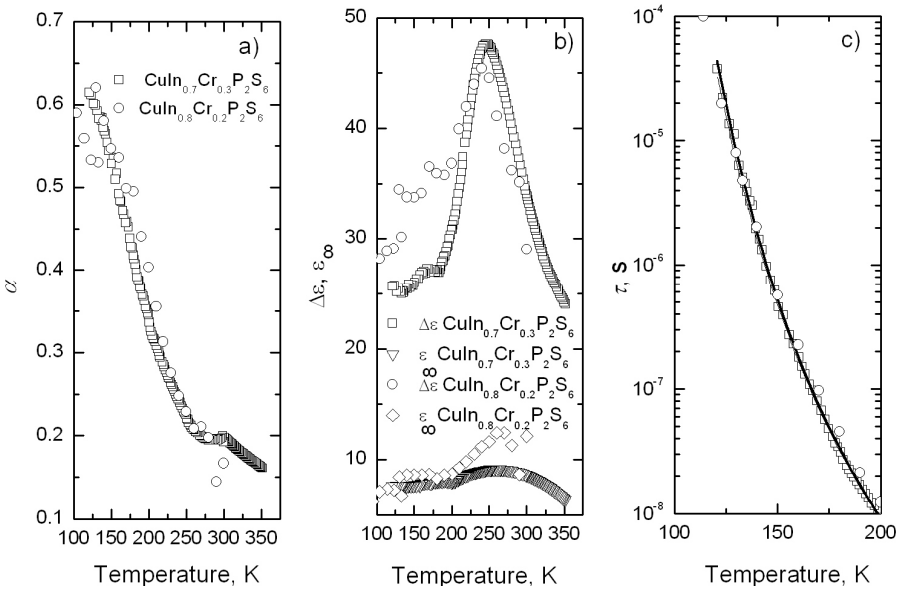

Fig. 4.2.2.3. Temperature dependence of the Cole – Cole parameters of $CuIn_{0.7}Cr_{0.3}P_2S_6$ and $CuIn_{0.8}Cr_{0.2}P_2S_6$ crystals.

crystal undergoes the second order phase transition. The ratio $C_{p,f}/T_C$ is of order 10, therefore the observed phase transition is mainly "order-disorder" type [68]. The Cole-Cole mean relaxation time τ increases with decreasing temperature, no any anomaly of the relaxation time is observed in the vicinity of ferroelectric phase transition. The temperature dependence of the relaxation times at low temperatures follows the Vogel-Fulcher law.

In order to get more precise information about the relaxation-time distribution function, we applied a special approach which description can be found in Chapter 3. The distributions of relaxation times of the investigated ferrielectrics $CuIn_{0.7}Cr_{0.3}P_2S_6$ and $CuIn_{0.8}Cr_{0.2}P_2S_6$ are presented in Fig. 4.2.2.4. One can recognize the relaxation-time distribution function significantly broadens at low temperatures, as it is typical for dipolar glasses. At the phase transition temperature, we have expressed maximum of $f(\tau)$, which is only in ferroelectric phase.

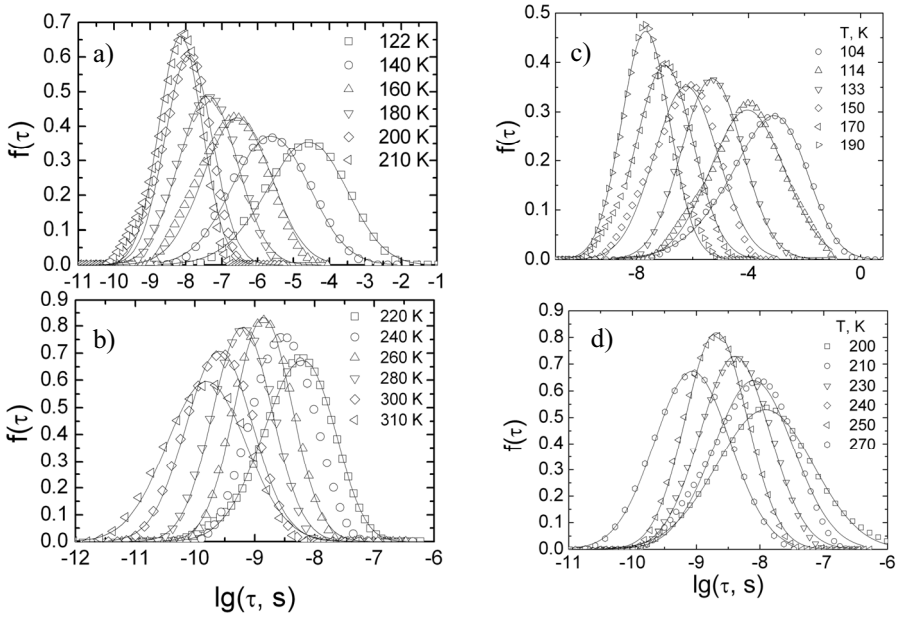

Fig. 4.2.2.4. Distribution of relaxation times of mixed ferroelectric $CuIn_xCr_{1-x}P_2S_6$ crystals: a) $CuIn_{0.7}Cr_{0.3}P_2S_6$, b) $CuIn_{0.7}Cr_{0.3}P_2S_6$ c) $CuIn_{0.8}Cr_{0.2}P_2S_6$ d) $CuIn_{0.8}Cr_{0.2}P_2S_6$ obtained from dielectric spectra (points). The solid lines are best fits according to Eq. (3.4.1).

We consider a copper ion moving in an asymmetric double well potential. The movement consists of fast oscillations in one of the minima with occasional thermally activated jumps between the minima. The jump probability is governed by the Boltzmann probability of overcoming the potential barrier between the minima. Relaxation time in such a system is given by:

$$\tau = \tau_0 \frac{\exp[E_b / k_B (T - T_0)]}{2\cosh(A / 2k_B T)} \quad . \tag{4.2.2.1}$$

with $\tau_0 = \frac{1}{2\pi\nu_\infty}$, where ν_∞ is the attempt frequency. The parameter *A* accounts for the asymmetry of the local potential produced by the mean-field influence of all the other dipoles. Thus, the local polarization of copper ions:

$$p = \tanh(A / 2k_B T) \ . \tag{4.2.2.2}$$

and the distribution function $\varpi(p)$ of the local polarizations:

$$\varpi(p) = \frac{2k_B T}{\sqrt{2\pi}\sigma_A (1 - p^2)} \exp\left[- \frac{(a \tanh[p] - a \tanh[\bar{p}])^2}{2\sigma_A (2k_B T)^2} \right]. \tag{4.2.2.3}$$

We further consider that the asymmetry *A* and the potential barrier E_b of the local potential are randomly distributed around their mean values A_0 and E_{b0} according to the Gaussian law resulting in the distribution functions:

$$f(E_b) = \frac{1}{\sqrt{2\pi}\sigma_{Eb}} \exp(-\frac{(E_b - E_{b0})^2}{2\sigma_{Eb}^2}) . \tag{4.2.2.4}$$

with

$$f(A) = \frac{1}{\sqrt{2\pi}\sigma_A} \exp(-\frac{(A - A_0)^2}{2\sigma_A^2}) . \tag{4.2.2.5}$$

where σ_{Eb} and σ_A are the standard deviations of E_b and *A*, respectively, from their mean values. Fits with the experimentally

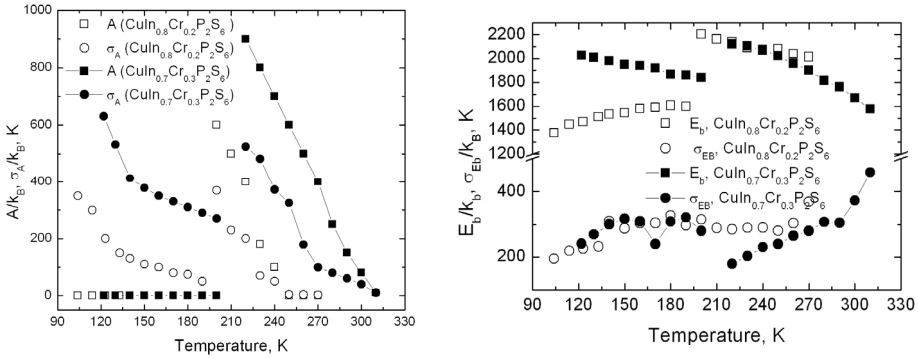

Fig. 4.2.2.5. Temperature dependence of the mean values E_b, *A* and standard deviations σ_{Eb}, σ_A of mixed $CuIn_{0.7}Cr_{0.3}P_2S_6$ and $CuIn_{0.8}Cr_{0.2}P_2S_6$ crystals.

obtained relaxation-time distributions were performed simultaneously for ten different temperatures using the same parameter set: τ_0= 1ps and T_0= 40 K for $CuIn_{0.8}Cr_{0.2}P_2S_6$, τ_0= 1.5 ps and T_0=13 K for $CuIn_{0.7}Cr_{0.3}P_2S_6$. The results are presented in Fig. 4.2.2.4 as solid lines.

The average local potential asymmetry A, average potential barrier E_b and the standard deviations σ_A and σ_{Eb} are temperature

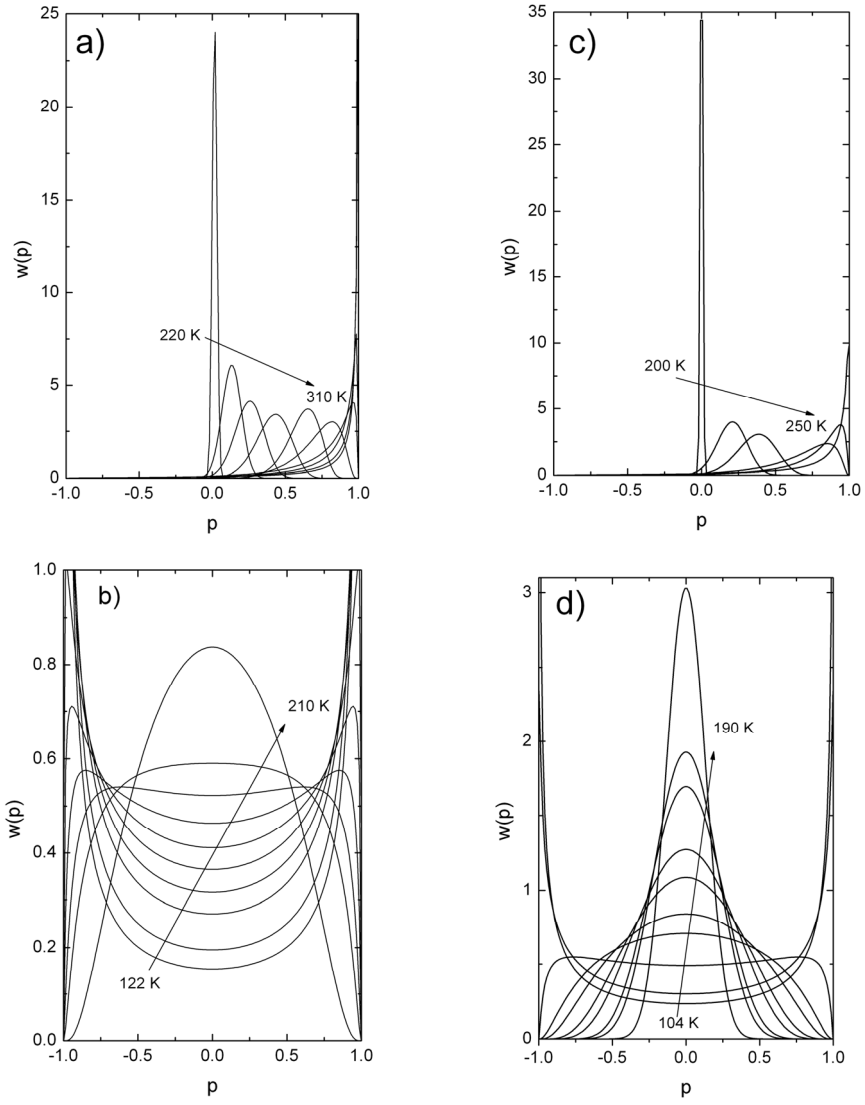

Fig. 4.2.2.6. Distribution of local polarizations $w(p)$ of mixed $CuIn_xCr_{1-x}P_2S_6$ crystals: a) $CuIn_{0.7}Cr_{0.3}P_2S_6$, b) $CuIn_{0.8}Cr_{0.2}P_2S_6$, c) $CuIn_{0.7}Cr_{0.3}P_2S_6$ d) $CuIn_{0.8}Cr_{0.2}P_2S_6$ at several temperatures.

dependent as demonstrated in Fig. 4.2.2.5. The average asymmetry *A* strongly increases on cooling in ferroelectric phase for both crystals. For frozen cooper ions the average asymmetry A is strictly zero. The average potential barrier's height E_b is almost temperature independent. The potential barrier's height and asymmetry distribution is very broad.

A broad distribution of local polarization is observed in both investigated ferrielectrics (Fig. 4.2.2.6). Such broad distribution is typical for inhomogeneous ferroelectrics. It indicates that not all cooper ions are ordered in ferrielectric phase. This fact was confirmed also by X ray investigations of pure $CuInP_2S_6$ [99]. By further cooling non-ordered copper ions form glassy phase and finally become frozen. Knowing the distribution function *w*(*p*), both the average (macroscopic) polarization

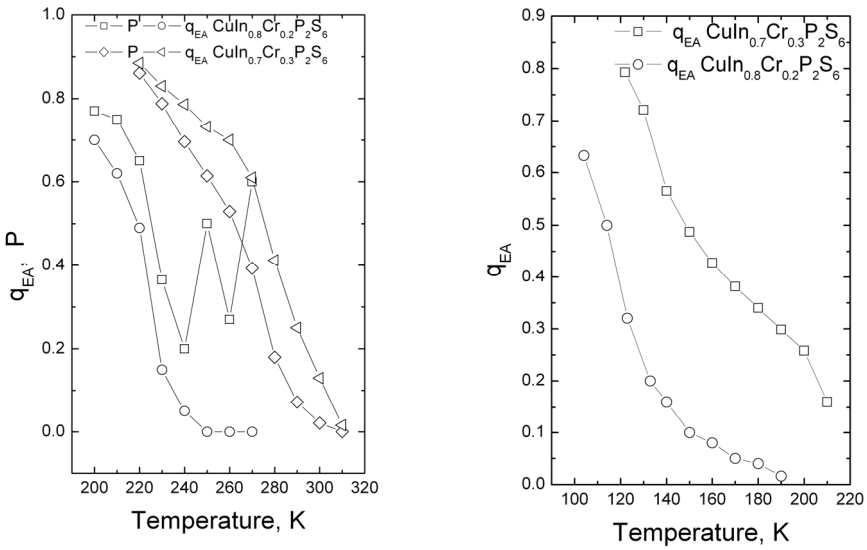

Fig. 4.2.2.7 Temperature dependence of spontaneous polarization *P* and Edwards-Anderson parameter of mixed $CuIn_{0.8}Cr_{0.2}P_2S_6$, and $CuIn_{0.7}Cr_{0.3}P_2S_6$ crystals.

$$\overline{p} = \int_{-1}^{1} p w(p) dp \qquad (4.2.2.6)$$

and the Edwards-Anderson glass order parameter

$$q_{EA} = \int_{-1}^{1} p^2 w(p) dp \qquad (4.2.2.6)$$

can be calculated. The calculated average polarization values are presented in Fig. 4.2.2.7. The temperature behavior of the average polarization is typical for the second order ferroelectric phase transition.

4.2.3 Dipole glass state in mixed $CuIn_xCr_{1-x}P_2S_6$ crystals.

The temperature dependence of the dielectric properties in the $CuIn_xCr_{1-x}P_2S_6$ mixed crystals with x = 0.5 and x = 0.4 is presented in Fig. 4.2.3.1 The shoulder-like *ε'(T)* anomaly shifts toward the higher temperatures with the increasing frequency. The dielectric losses demonstrate a typical relaxation as well. As seen from these data, there

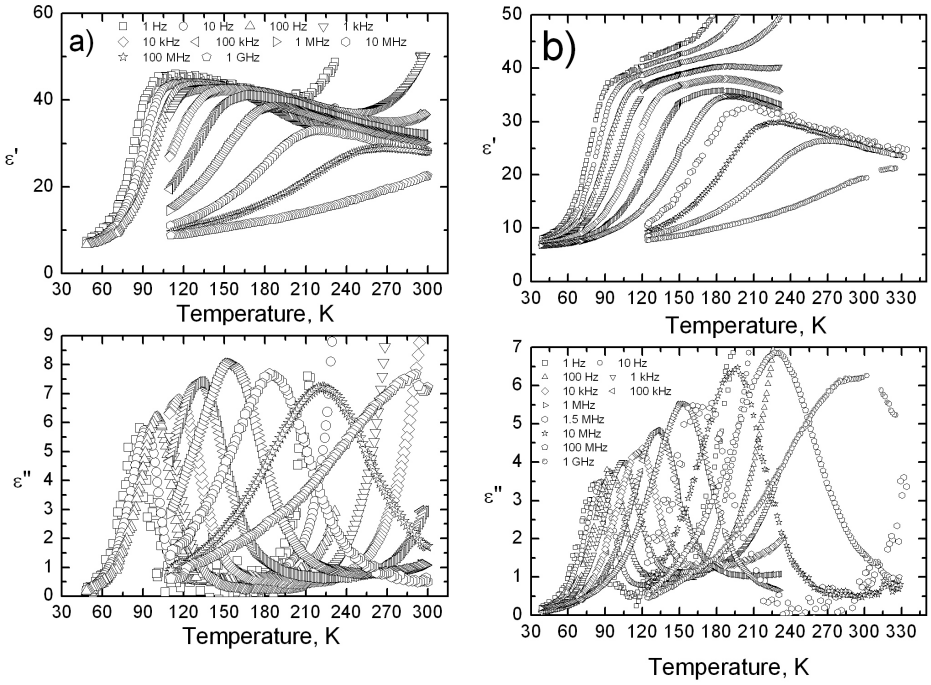

Fig. 4.2.3.1. Temperature dependence of complex dielectric permittivity of a) $CuIn_{0.5}Cr_{0.5}CrP_2S_6$ and b) $CuIn_{0.4}Cr_{0.6}CrP_2S_6$.

is no ferroelectric ordering in these mixed crystals. The dielectric dispersion at low temperatures (T <170 K) is caused by transition into the dipole glass phase. At higher temperatures the dielectric dispersion is clearly symmetric and observed only at higher frequencies. On

cooling it strongly posses to lower frequencies and become more asymmetric. The dielectric dispersion was described with the empirical Cole-Cole formula. The temperature dependence of the parameters is plotted in Fig. 4.2.3.2. Parameter α strongly decreases with increasing temperature and just at high temperatures the dielectric dispersion of the studied crystal is Debye like. At low temperatures this parameter reaches high value $\alpha_{max} \approx 0.7$. The dielectric permittivity ε_∞ is almost temperature-independent and its average value is $\varepsilon_\infty = 10$. The dielectric strength $\Delta\varepsilon$ decreases with the temperature and there is no any expressed maxima in the measured temperature region. The Cole-

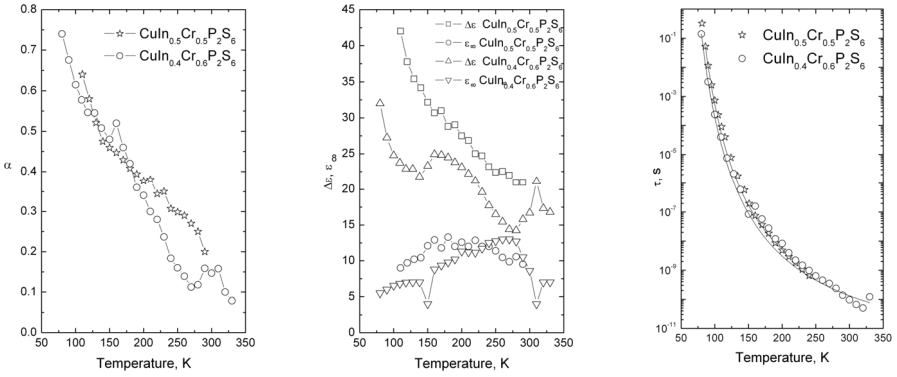

Fig. 4.2.3.2. Temperature dependence of the Cole – Cole parameters of $CuIn_{0.5}Cr_{0.5}P_2S_6$ and $CuIn_{0.4}Cr_{0.6}P_2S_6$ crystals

Cole mean relaxation time τ increase with decreasing temperature. Temperature dependence of relaxation times at low temperatures follows the Vogel-Fulcher law, which parameters are written in the Table 4.2.3.1.

Table 4.2.3.1 Parameters got from Vogel –Fulcher law		
	$CuIn_{0.5}Cr_{0.5}P_2S_6$	$CuIn_{0.4}Cr_{0.6}P_2S_6$
T_0, K	23	20
E/k, K (eV)	1554 (0.134)	1575 (0.136)
τ_0, s	$7.67*10^{-13}$	$4.7*10^{-13}$

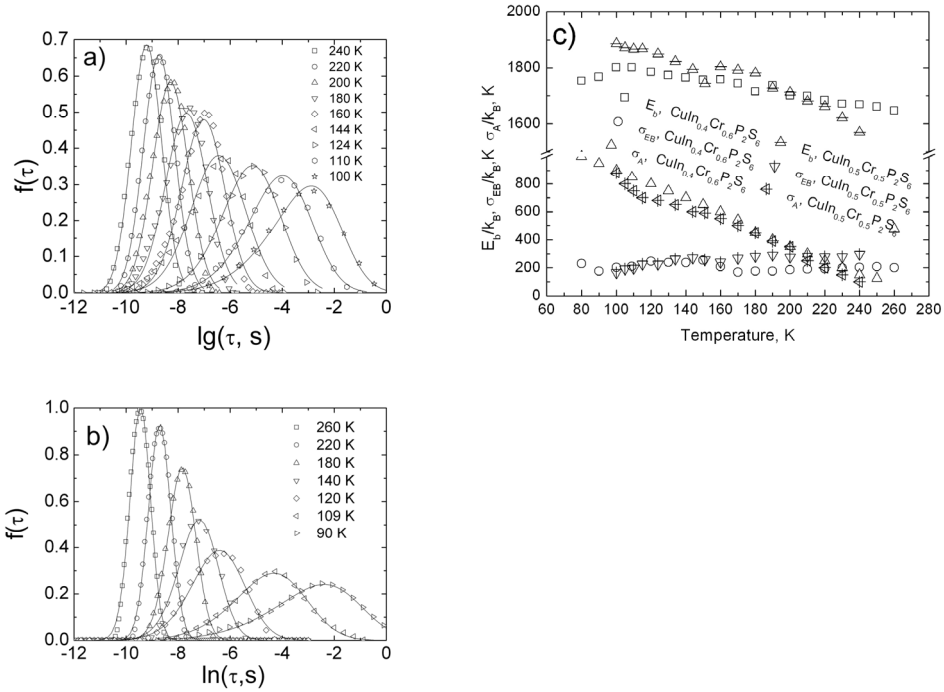

Fig. 4.2.3.3. Distribution of relaxation times of mixed ferroelectric $CuIn_xCr_{1-x}P_2S_6$ crystals: a) $CuIn_{0.5}Cr_{0.5}P_2S_6$, b) $CuIn_{0.4}Cr_{0.6}P_2S_6$. c) Temperature dependence of the mean values E_b, A and standard deviations σ_{Eb}, σ_A of mixed $CuIn_{0.5}Cr_{0.5}P_2S_6$ and $CuIn_{0.4}Cr_{0.6}P_2S_6$ crystals

Broad and very asymmetric distributions of relaxation times are observed in the both investigated dipolar glasses (Fig. 4.2.3.3). To get more insight nature of such distributions, they are fitted by the double well potential model described above. For the frozen copper ions the average potential barrier height is almost temperature independent. The potential barrier height and asymmetry distribution is very broad especially at low temperatures. From double well potential parameters the local polarization distribution has been calculated (Fig. 4.2.3.4). The temperature behavior of the local polarization distribution is very similar to other dipole glasses, like RADP or BP/BPI [100]. It denotes, that the dielectric dispersion in the $CuIn_xCr_{1-x}P_2S_6$ dipole glasses can be described by Random Bond – Random Field (RBRF) model [101]. The

Edvards-Anderson order parameter has been calculated from the local polarization distribution. The order parameter is almost linear function of temperature and not indicates any anomaly. Macroscopic polarization is zero, as it should be for disordered structures.

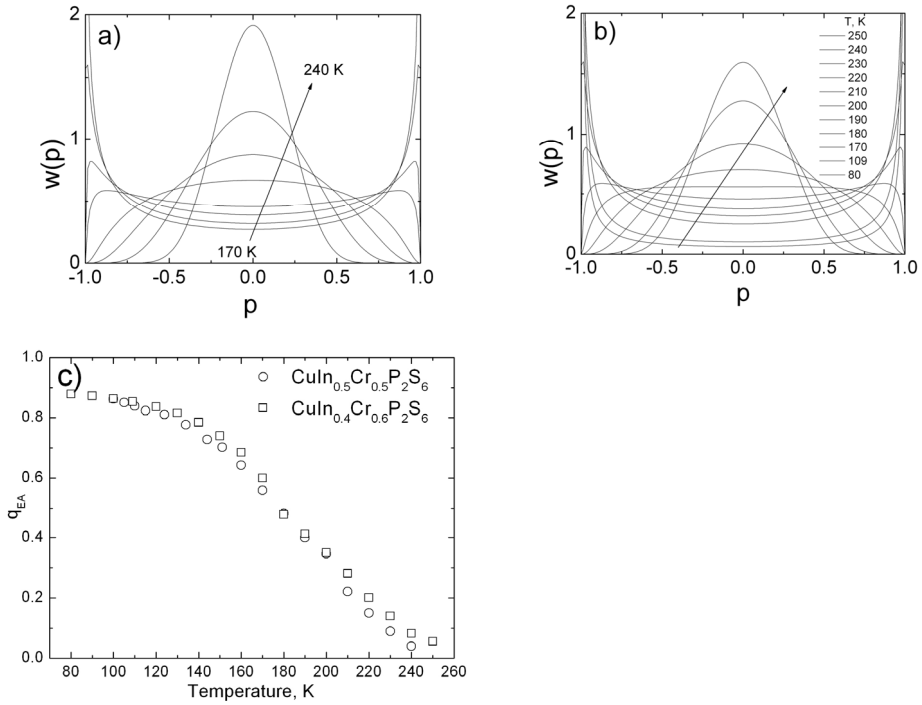

Fig. 4.2.3.4. Distribution of the local polarizations $w(p)$ of mixed $CuIn_xCr_{1-x}P_2S_6$ crystals: a) $CuIn_{0.5}Cr_{0.5}P_2S_6$, b) $CuIn_{0.4}Cr_{0.6}P_2S_6$ at several temperatures. Points are guide for eyes. c) Temperature dependence of Edwards-Anderson parameter of mixed $CuIn_{0.5}Cr_{0.5}P_2S_6$, and $CuIn_{0.4}Cr_{0.6}P_2S_6$ crystals.

We can conclude, that the extraction of continuous relaxation times distribution of the Debye fundamental processes directly from the broadband dielectric spectra allows better understanding dynamic phenomena in mixed $CuIn_xCr_{1-x}P_2S_6$ crystals.

4.2.4 Phase diagram of the mixed $CuIn_xCr_{1-x}P_2S_6$ crystals.

The phase diagram for $CuIn_xCr_{1-x}P_2S_6$ mixed crystal obtained from our dielectric results is shown in Fig. 4.2.4.1. The ferroelectric ordering coexistence with dipole glass phase in $CuIn_xCr_{1-x}P_2S_6$ is present at $0.7 \leq x$. On the other side of the phase diagram for $x \leq 0.9$ the antiferroelectric phase transition occurs. By decreasing x concentration, the antiferroelectric phase transition temperature increases. In the intermediate concentration range for $0.4 \leq x \leq 0.6$, the dipolar glass phase is observed.

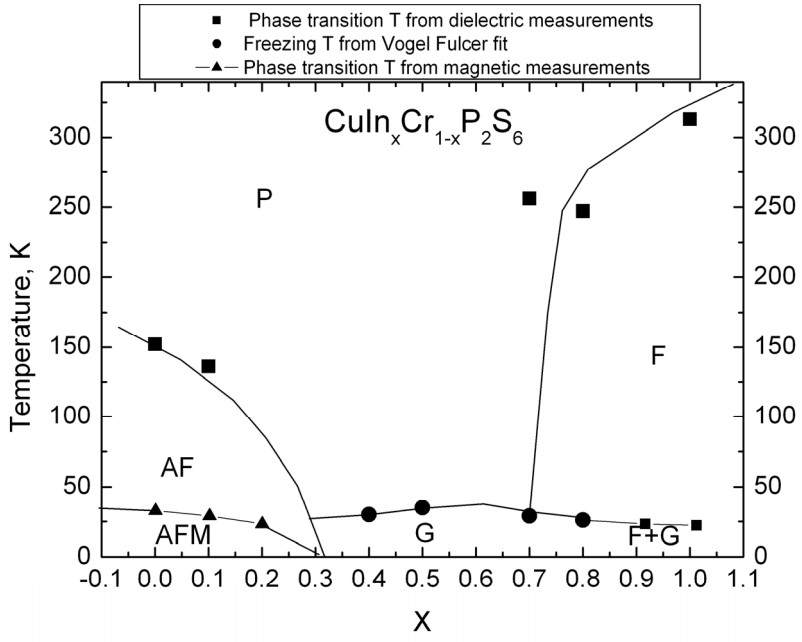

Fig. 4.2.4.1 Phase diagram of $CuIn_xCr_{1-x}P_2S_6$ crystals. AF – antiferroelectric phase; G – glass phase; F+G – ferroelectric + glass phase; AFM – antiferomagnetic phase; P – paraelectric phase.

Conclusions

1. A dipole glass disorder without any ferroelectric or antiferroelectric order is observed in the $CuIn_xCr_{1-x}P_2S_6$ crystals for indium concentrations 0.4 - 0.5.

2. The long-range ferroelectric order coexists with the glassy disorder in the $CuIn_xCr_{1-x}P_2S_6$ crystals for indium concentrations 0.7 - 1.
3. A phase transition into the antiferroelectric phase occurs at $0 \leq x \leq 0.1$ and here no glassy relaxation is observed. The antiferroelectric phase transition temperature shifts to lower temperatures by doping $CuCrP_2S_6$ with 10 % of indium, however the phase transition type remains of the first-order as in pure $CuCrP_2S_6$.
4. The distribution functions of relaxation times of the mixed $CuIn_xCr_{1-x}P_2S_6$ crystals calculated from the experimental dielectric spectra at different temperatures have been successfully described with the asymmetric double potential well model. From these results we calculate the local polarization distributions and temperature dependence of the macroscopic polarization and the Edwards – Anderson parameter.
5. For the ferroelectric $CuIn_xCr_{1-x}P_2S_6$ the temperature dependence of macroscopic polarization shows a second-order phase transition.
6. For the dipolar glasses $CuIn_xCr_{1-x}P_2S_6$ RBRF model is valid.

The results are published in [102].

4.3. Conductivity spectroscopy of new $AgInP_2(S_x,Se_{1-x})_6$ crystals

Overview

In spite of many research efforts, the mechanism of fast ionic conduction in solids is not understood completely yet because of the difficulty in separating the contribution of the ion concentration and mobility from the measured conductivity. Many factors which affect ionic conductivity, i. e. defect concentrations [103], unit cell free volume [104], the size and charge of the dopant and mobile ions [105], their mobility, association and ordering of points defects [106], grain boundary diffusion and segregation of secondary phase [107]. Many studies of ionic conductivity have been reported for oxides, but less for non-oxide materials.

The layered structure MPX_3 (M = metal; X = S, Se) has been the subject of great interest because of the potential use in high – energy density lithium batteries [47]. In the case of sulphides, the divalent metal M(II) could effectively be replaced by a couple of mono and trivalent metals $\left(\frac{1}{2}M(I)+\frac{1}{2}M(III)\right)$, where *M(III)*=Cr, In and *M(I)*= Cu or Ag. Structure containing trivalent metal In and monovalent Cu has been investigated by many groups. It is already known that $CuInP_2Se_6$ and $CuInP_2S_6$ crystals belong to layered structures of $AM^1P_2X_6$ (A, M^1 – Cu, Ag, In, Cr; X – S, Se) [46]. More details about $CuInP_2S_6$ are in 4.1 paragraph.

The selenium analogue $CuInP_2Se_6$ is a very interesting member of this class of materials. A single-crystal X-ray diffraction study showed that the high- and low-temperature structures of $CuInP_2Se_6$ (trigonal space group P-31c and P31c, respectively) are very similar to those of $CuInP_2S_6$ in the paraelectric and ferrielectric phases, with the Cu^I off-centering shift being smaller in the former than in the latter [108]. The broadband dielectric investigations of $CuInP_2Se_6$ crystals showed nearly

a second order ferroelectric phase transition at T_c=226 K [109]. These results are in good accordance with recently performed calorimetric investigations [110]. In these crystals, the dielectric anomaly is accompanied by abrupt decreasing of conductivity, the paraelectric phase is also superionic. The addition phase transition from paraelectric phase to intermediate phase at T=236 K was revealed in ultrasonic experiment [111]. As it follows from these piezoelectric measurements the intermediate phase is polar and probably it is also incommensurate.

Other representative of layered structures is $AgInP_2S_6$ crystal, whose symmetry is trigonal, space group $P\bar{3}1c$ and lattice constants $a = 8.182\,\overset{0}{A}$, $c = 12.957\,\overset{0}{A}$, $V = 428.8\,\overset{0}{A}^3$ [112] and $AgInP_2Se_6$ which has the same symmetry and space group as $AgInP_2S_6$ crystal [112]. The lattice parameters: a = 6.191 (3) Á, c = 12 95 (7) Á. The optical band gap E_g for $AgInP_2S_6$ and $AgInP_2Se_6$ are 2.43 eV and 1.82 eV respectively [113].

It is reasonable to ask the following questions: Is the polar order (at low temperatures) typical for all crystals of $M^IM^{III}P_2X_6$ family? What is behaviour of conductivity of $M^IM^{III}P_2X_6$ crystals by substituting of some ions? The aim of the present work is exactly focused on these issues. We have investigated the dielectric properties and the conductivity of newly synthesized $AgInP_2S_6$ crystals in the wide temperature range (110 K –350 K). Single crystals (Ø=14-16, h=2 mm) of the $AgInP_2S_6$, $AgInP_2Se_6$ were grown by Bridgman technique in Uzhgorod university.

Results

The temperature dependence of complex dielectric permittivity $\varepsilon^*=\varepsilon'-i\varepsilon''$ of $AgInP_2S_6$ crystal is presented in Fig. 4.3.1. At higher temperatures $\varepsilon^*=\varepsilon'-i\varepsilon''$ strongly increase on heating, this increasing is similar to $CuInP_2S_6$ [108] and $CuInP_2Se_6$ [108] crystals is caused by high conductivity. Differently from the $CuInP_2S_6$ and $CuInP_2Se_6$, in the presented crystals there is no anomaly indicating polar phase transition down to lowest temperatures.

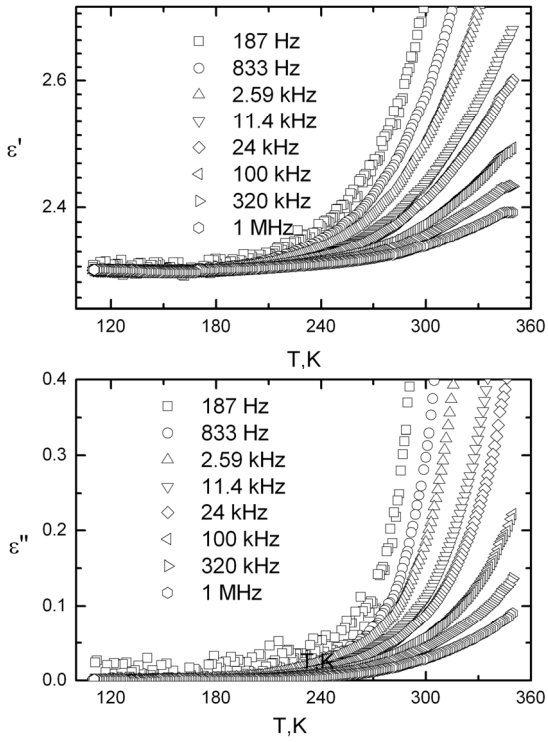

Fig. 4.3.1. Temperature dependence of the real and the imaginary parts of dielectric permittivity of $AgInP_2S_6$ crystals.

Similar behaviour of dielectric permittivity is observed in all crystals $AgInP_2(S_x,Se_{1-x})_6$, where x = 0, 0.25, 0.5, 0.75, 1. Instead of structural phase transition, quiet high ionic conductivity is observed in mixed crystals. With such a high value of conductivity, the blocking contact effect can play an important role. To distinguish the volume conductivity from contact effect we calculated complex specific resistance Z^*:

$$Z' = \frac{\varepsilon''^2}{\varepsilon'^2 + \varepsilon''^2}\frac{1}{\varepsilon_0\omega}. \qquad (4.3.1\ a)$$

$$Z'' = \frac{\varepsilon'^2}{\varepsilon'^2 + \varepsilon''^2}\frac{1}{\varepsilon_0\omega}. \qquad (4.3.1\ b)$$

where $\omega = 2\pi\nu$, ν is the measurement frequency. The half circle at higher frequencies and lower values of Z^* are caused by the volume conductivity of crystal, and the large values Z^* are already influenced by contacts (Fig. 4.3.2).

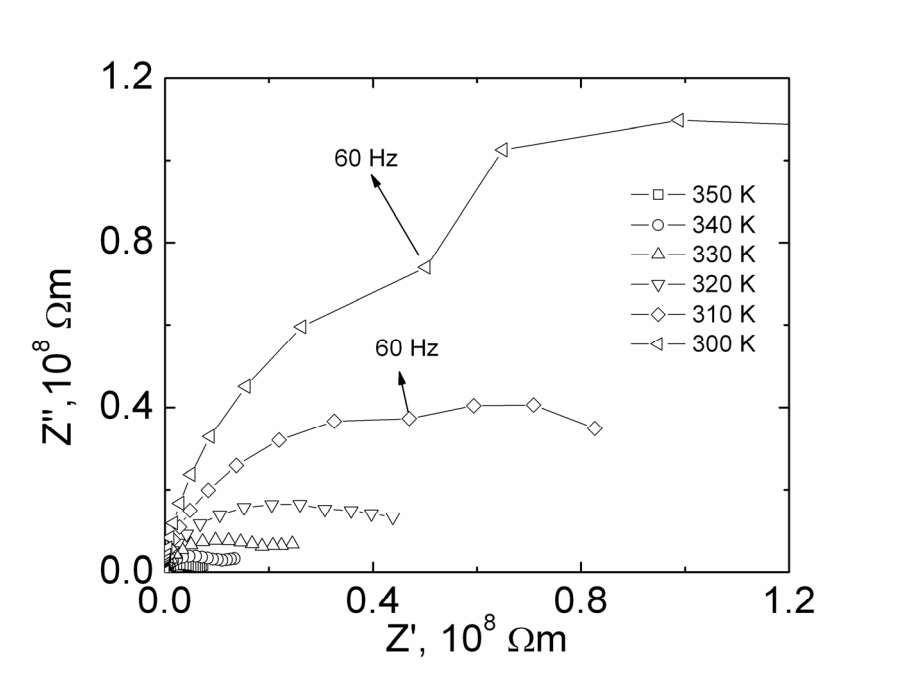

Fig. 4.3.2. Imaginary part of impedance versus the real part of impedance of $AgInP_2S_6$ crystal for different temperatures.

The contact influence is playing an important role at higher temperatures and lower frequencies. So, it is extremely important to extract bulk or volume conductivity from the experimental data. The electrical conductivity σ has been calculated according to the formula (4.1.1.1). The obtained results are presented in Fig.4.3.3. In analogy with $CuInP_2S_6$ [108] and $CuInP_2Se_6$ [114] crystals we can expect that conductivity of mixed $AgInP_2(S_x,Se_{1-x})_6$ crystals can also be ionic (Ag^+ ions).

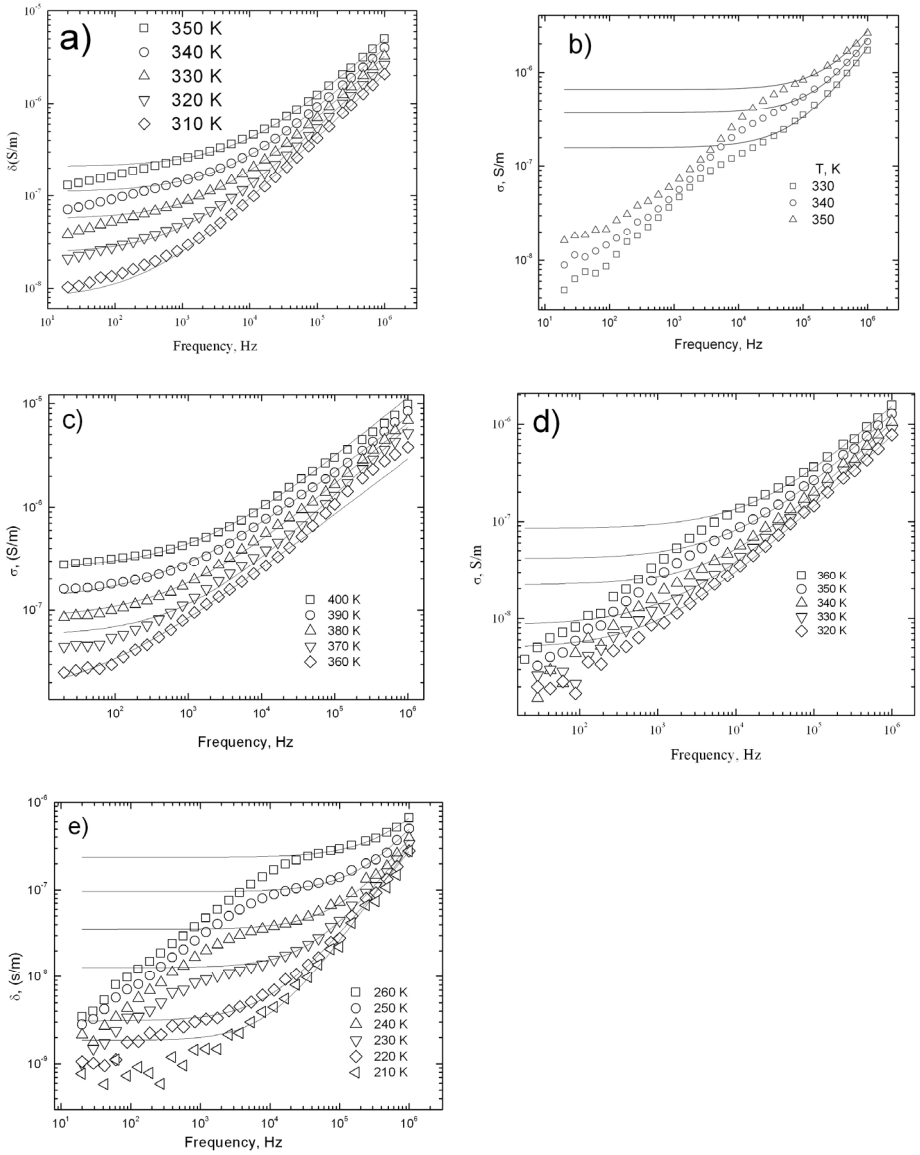

Fig. 4.3.3. Frequency dependence of σ for mixed $AgInP_2(S_x,Se_{1-x})_6$ crystals, where x: 1 a), 0.75 b), 0.5 c), 0.25 d), 0 e). Solid line is theoretically calculated according to the formula $\sigma=\sigma_{DC}+A\omega^s$. Points are experimental data;

Nevertheless, this hypothesis must be confirmed by other experiments. At low frequencies, random distribution of the ionic charge carriers via activated hopping gives rise to a frequency-independent conductivity (dc conductivity). At higher frequencies, conductivity exhibits dispersion, increasing roughly in a power law fashion and eventually becoming almost linear at even higher frequencies. An additional low-frequency dispersion region due to electrode effects characterizes the high-temperature conductivity spectra of the Ag ion conducting materials.

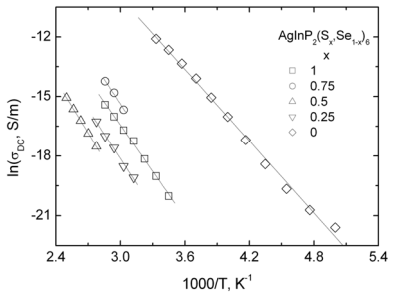

Fig. 4.3.4. 1/*T* dependence of σ_{DC} of mixed $AgInP_2(S_x,Se_{1-x})_6$ crystal.

The frequency behaviour of σ has been fitted according to the Almond-West equation (4.1.1.2) [114]. Temperature dependence of $\ln(\sigma_{DC})$ for mixed $AgInP_2(S_x,Se_{1-x})_6$ crystals is presented in Fig. 4.3.4. From these dependencies we have calculated activation energy E_A and σ_0 of the conductivity according to the Arrhenius law (4.1.1.3). Calculated parameters are written in Table 4.3.1.

Table 4.3.1 Activation energy got from Arenius fit

Compound	$\sigma_0, S/m$	E_A/k, eV
$AgInP_2S_6$	879	0.667
$AgInP_2(S_{0.75},Se_{0.25})_6$	13359	0.716
$AgInP_2(S_{0.5},Se_{0.5})_6$	1366	0.768
$AgInP_2(S_{0.25},Se_{0.75})_6$	727	0.710
$AgInP_2Se_6$	3130	0.519

The obtained activation energy for $AgInP_2S_6$ is very similar for activation energy of conductivity of $CuInP_2S_6$ (E_A/k = 7357 K) [108] and it is substantially higher as activation energy of conductivity of $CuInP_2Se_6$ (E_A/k = 3653 K) [114].

Two formalisms such as electric conductivity and electric modulus [115] have been employed to study the ion dynamics in solids under ac electric field. However, there is a debate on which of these formalisms provides better insights into the phenomena of ion dynamics [116]. Both

formalisms are compared in this work. The complex electric modulus spectra represent a measure of distribution of ion energies or

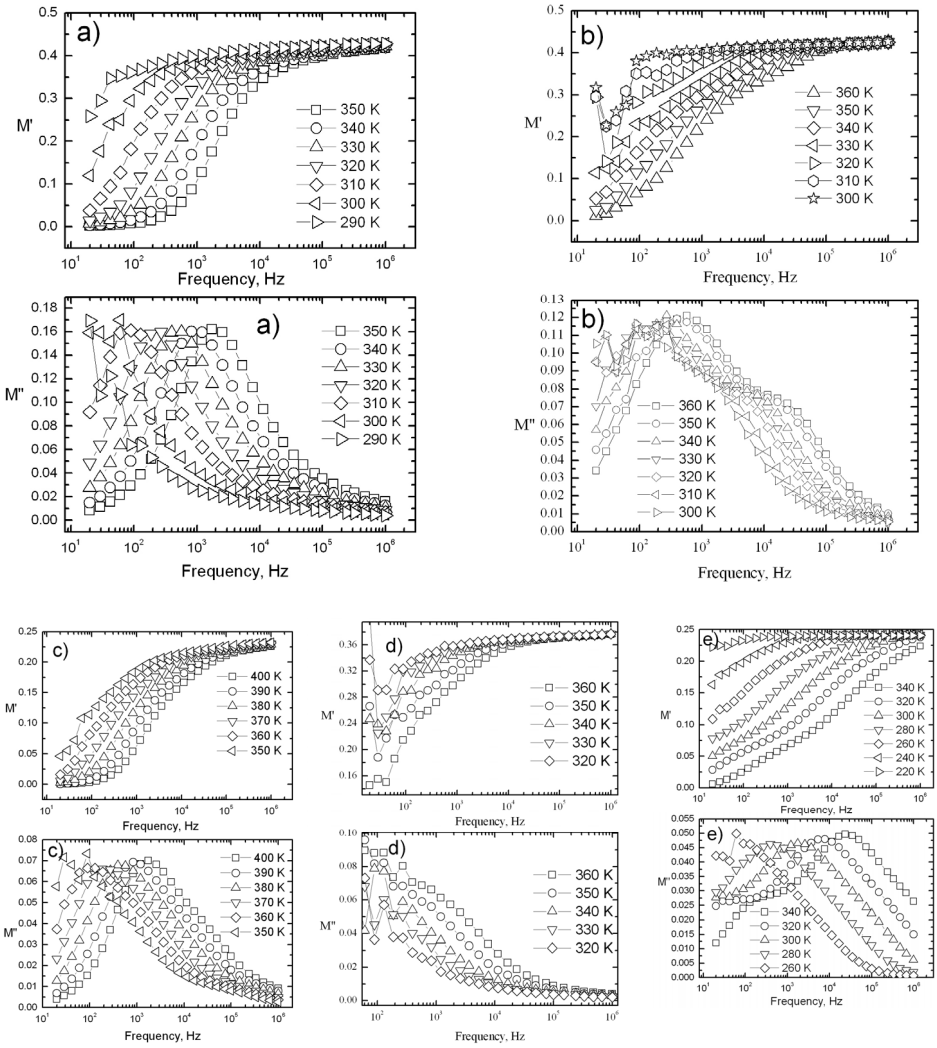

Fig. 4.3.5. Plots of the isothermal frequency spectra of *M′* and *M″* of mixed $AgInP_2(S_x,Se_{1-x})_6$ crystals where x: 1 a), 0.75 b), 0.5 c), 0.25 d), 0 e).

configurations in the disordered structure and also describe the electrical relaxation of ionic solids as a microscopic property of these materials. Electric modulus M^* can easily be calculated from complex dielectric permittivity (4.4) and (4.5). The function $\varphi(t)$ gives the time evolution of the electric field within the materials. Obtained frequency-

dependencies $M^*(\nu)$ are presented in Fig. 4.3.5. The real modulus M' shows dispersion as the frequency increased and tends to saturate at M_∞ at higher frequencies. The imaginary modulus M'' exhibits a maximum M''_{max} centered at dispersion region of M'. The frequency spectra of imaginary modulus M'' of some crystals exhibit two maxima. With such a high value of conductivity, the blocking contact effect can play an important role. The part of the frequency spectra at higher frequencies and higher values of M'' are caused by the volume conductivity of crystal, and the lower values M'' at lower frequencies are already influenced by contacts (Fig. 4.3.3). The contact influence is playing an important role at higher temperatures and lower frequencies. So, it is extremely important to extract bulk or volume conductivity from the experimental data.

Conclusions

We reported a first characterization of newly synthesized $AgInP_2(S_x,Se_{1-x})_6$ crystals, by means of dielectric and conductivity spectroscopy. No anomaly in the temperature dependence of complex dielectric permittivity of $AgInP_2(S_x,Se_{1-x})_6$ crystal indicating a polar phase transition down to lowest temperature (110 K). The dielectric properties of investigated crystals are mainly caused by high ionic conductivity.
The main results are published in [117], [118].

4.4 Phase transitions in $CuBiP_2Se_6$ crystals

Overview

$CuBiP_2Se_6$ exhibits a temperature dependent antiferoelectric ordering of the Cu^+ and Bi^{3+} ions in the lattice [116]. X-ray investigations have showed an intermediate and a fully ordered structure at 173 K and 97 K, respectively [91]. However, till now is a lack of some important information about the phase transition in $CuBiP_2Se_6$, such as phase transition temperature, phase transition type and others. In a similar $CuCrP_2S_6$ system the antiferroelectric phase occurs via an intermediate phase [91]. The electric conductivity of $CuInP_2S_6$ and $CuInP_2Se_6$ was already investigated [89],[49],[62]. It was claimed that the electric conductivity in these compounds in the paraelectric phase is mainly ionic, with the activation energy E=0.64 eV for $CuInP_2S_6$ and E=0.32 eV for $CuInP_2Se_6$ [62],[119]. The electric conductivity of $CuBiP_2Se_6$ was investigated only above the room temperature and the activation energy of 0.14 eV was established [116]

In this paragraph, we present the first investigation of the dielectric properties of $CuBiP_2Se_6$. We demonstrate that the antiferroelectric phase transition is accompanied with freezing into dipolar glass phase at low temperatures.

Experiment procedure

The sample was prepared by melting the elements in the stoichiometric proportion in a quartz ampoule and crystallized by slow cooling. For the dielectric spectroscopy, single crystals were used. All measurements were performed in the direction perpendicular to the layers (along the *c* - direction). The complex dielectric permittivity $\varepsilon^* = \varepsilon' - i\varepsilon''$ was measured by a capacitance bridge HP4284A in the frequency range 20 Hz - 1 MHz. Firstly, measurements were performed on cooling down to lowest temperature, then the sample were heated up to the room temperature

(unpoled sample). After this the measurements were repeated with switched DC electric field (poled sample).

Results and discussion

The temperature dependence of the real and imaginary parts of the dielectric permittivity ε' and ε'' of $CuBiP_2Se_6$ is presented in Figure 4.4.1.1. The measured temperature region can be divided in three intervals: 1) at higher temperatures, dielectric dispersion occurs due to the high electrical conductivity, 2) a frequency independent anomaly of ε' at 136 K indicates an antiferroelectric phase transition, 3) at temperatures lower than 40 K the dielectric dispersion effect can be observed.

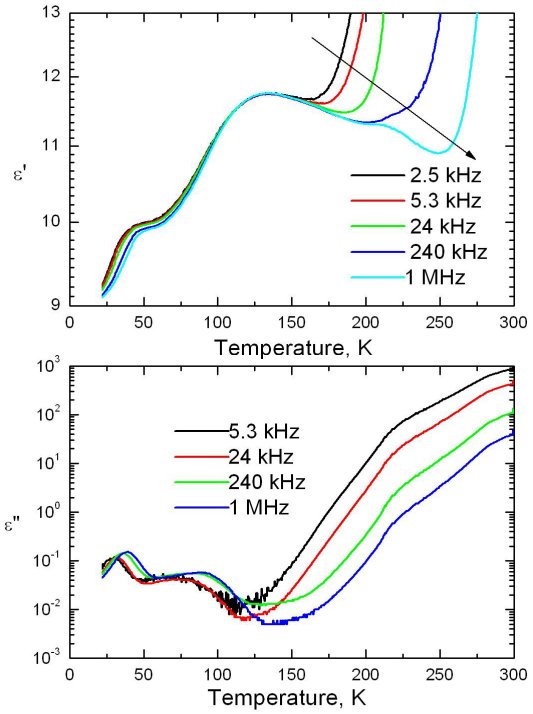

Fig. 4.4.1.1. Temperature dependence of complex dielectric permittivity of $CuBiP_2Se_6$ crystals.

4.4.1 Electric conductivity of $CuBiP_2Se_6$

The electric conductivity σ has been calculated according to the equation (4.1.1.1). The obtained results are presented in Figure 4.4.1.2. The frequency behaviour of σ has been fitted according to (4.1.1.2). Such fit describes good dynamic properties of conductivity of presented crystal, only at higher frequencies (above 100 kHz) and at low temperatures (below 150 K) the discrepancies appear due the dielectric relaxation, its origin is discussed below.

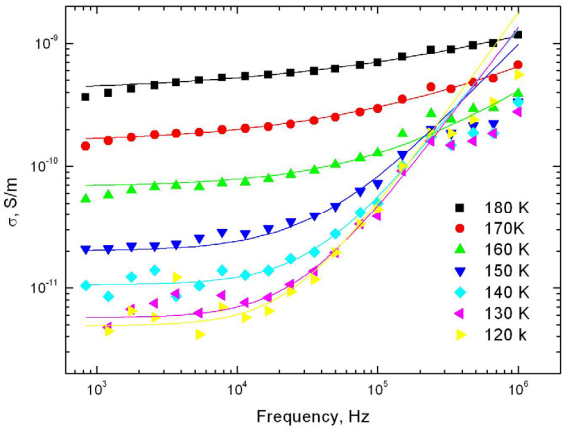

Fig. 4.4.1.2 Frequency dependence of conductivity σ for $CuBiP_2Se_6$ crystals.

The conductivity is related to the electrical modulus M^*, by the following expression (4.1.1.4). Figure 4.4.1.3 shows the isothermal frequency spectra of M' and M''. At higher temperatures (above 210 K) the low-frequency value of M' is zero and represents a lack of the restoring force for the electric field-induced mobile copper ions. As frequency increases, each ion moves a shorter and shorter distance until finally the electric field changes so rapidly that the ions only oscillate within the confinements of their potential energy wells. As a result, M' increases to a maximum asymptotic value $M(\infty) = 1/\varepsilon(\infty)$. The spectra of M'' shows a slightly asymmetric peak centred in the dispersion region of M'. For frequencies to the left of the M'' peak ($\omega\tau < 1$), most ions are mobile over long distances and are able to decay the applied electric field. For frequencies to the right of the M'' peak

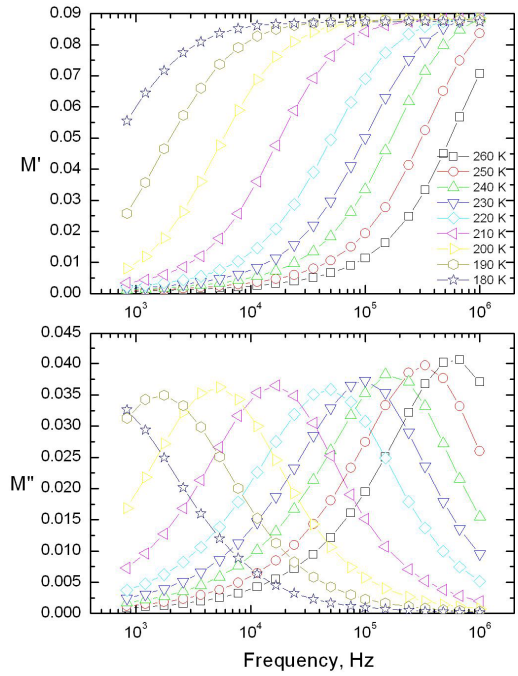

Fig. 4.4.1.3. Plots of the isothermal frequency spectra of M' and M'' of $CuBiP_2Se_6$ crystals.

($\omega\tau > 1$), most ions are spatially confined in their potential wells and are unable to decay the applied electric field.

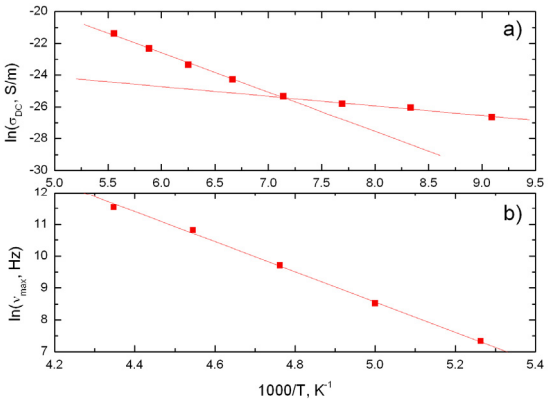

Fig. 4.4.1.4. 1/*T* dependence of σ_{DC} (a) and v_{max} (b) for $CuBiP_2Se_6$ crystals.

The region where the peak occurs ($\omega\tau = 1$) is indicative of the transition from long-range to short-range ion mobility and the peak frequency corresponds to the average electric field (or conductivity) relaxation frequency $1/\tau$. The broadening in the modulus spectra indicates a cooperative motion of mobile ions, especially in the higher-frequency range. From obtained values of σ_{DC} at different temperatures, it was possible to calculate activation energy E_A and σ_0 of the conductivity according to the Arrhenius law (4.1.1.3) (Fig. 4.4.1.4 a). The obtained values are: in paraelectric phase E_A/k = 2473 K (0.21 eV), σ_0 = $4.2*10^{-4}$ S/m and in antiferoelectric phase E_A/k = 605 K (0.05 eV), σ_0 =$7.8*10^{-10}$ S/m. Such values of activation energy clearly differ from larger gap semiconductive $CuBiP_2Se_6$, where in the paraelectric phase E_g=1.2eV [49]. Therefore free electrons contribution to the conductivity should by excluded. The main contribution to the electrical conductivity appears due to copper ions migration through the lattice in $CuInP_2S_6$ [49] and $CuInP_2Se_6$ [116] and as well as in $CuBiP_2Se_6$. In Fig. 4.4.1.4 b) the peaks position of *M″* was plotted versus the temperature. The dependence was fitted also with the Arrhenius law (4.1.1.3). The obtained parameters are $v_{max\infty}$=96 THz, E_B=4728 K (0.4 eV).

4.4.2 Antiferroelectric phase transition.

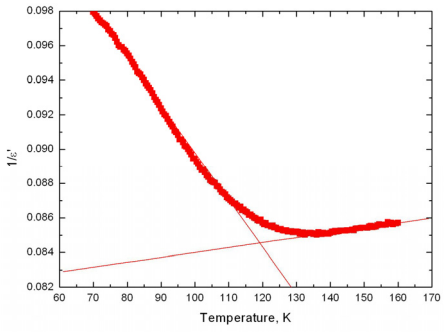

Fig. 4.4.2.1. Curie-Weiss fit of the real part of complex dielectric permittivity for $CuBiP_2Se_6$ crystals.

No dielectric dispersion is observed about antiferroelectric phase transition temperature (136 K), therefore the dielectric permittivity at 2 kHz correspond to the static one (Fig. 4.4.1.1). The Curie-Weiss law (4.1.2.2) has been used for the analysis of the dielectric anomaly close to the antiferroelectric phase transition temperature. In the paraelectric regime, the Curie-Weiss law is found to be valid for 120 < T < 160 K (Fig. 4.4.2.1.). The deviation from Curie-Weiss behavior observed at T > 160 K may be attributed to the occurrence of electric conductivity at the higher temperatures; the simultaneous rise of the ε'' curve above T > 160 K also confirms that. Obtained parameters are C_p=35202 K, T_{cp}=-2857 K, C_{pan}=3543 K and T_{can}=417 K. According to the Kittel phenomenological theory for the second order antiferroelectric phase transition it is valid relation (2.5.1.10) and (2.5.1.11) (please see Chapter 2.5.1)

The relations (2.5.1.10) and (2.5.1.11) easily transforms into (4.1.2.2) by substitution $\lambda=1/C_p$, T_0-$g/\lambda=T_C$. Because $C_p/C_{pan}>2$, the observed phase transition is of first order. Moreover, the value of the dielectric permittivity about antiferroelectric phase transition temperature is low (about 12) (Fig. 4.4.1.1), typically such a low value of dielectric permittivity have a phononic origin, therefore the phase transition is “displacive” type and it is driven by a resonant soft mode. The microscopic mechanism of the phase transition is antiparallel displacement in copper and bismuth sublattice [116].

4.4.3 Freezing phenomena

Temperature dependence of the dielectric loss exhibits a distinct peak that is shifted towards higher temperatures with increase in the measured frequency (Fig. 4.4.1.1). Such dielectric dispersion (Fig. 4.4.3.1) is typical for dipolar glasses [120] and (or) for domain freezing [89]. The similar dielectric dispersion also occurs in $CuInP_2S_6$ and $Ag_{0.1}Cu_{0.9}InP_2S_6$ at low temperatures [121]. The complex dielectric dispersion is strongly asymmetric at low temperatures in $CuBiP_2Se_6$ (Fig. 4.4.3.1). From the dielectric spectra the distribution of relaxation times $f(\tau)$ have been calculated by solving Fredholm equations (3.4.1 a) and (3.4.1 b). The regularization parameter has been selected according to recommendations published in [122]. Obtained distribution of relaxation times $f(\tau)$ are presented in Fig. 4.4.3.2.

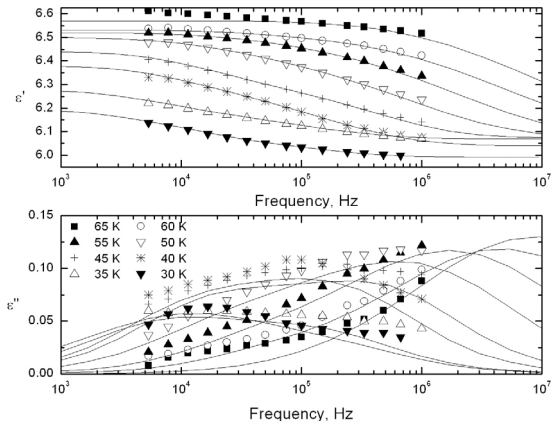

Fig. 4.4.3.1. Frequency dependence of complex dielectric permittivity of $CuBiP_2Se_6$ crystals measured at different temperatures. Solid lines are the best fit according to (4.1.1.3).

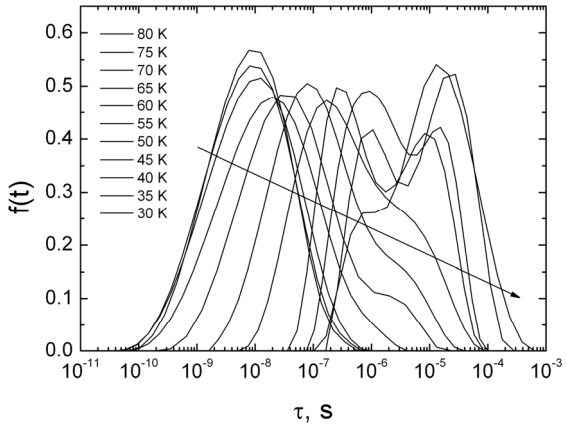

Fig. 4.4.3.2. Distribution of relaxation times of $CuBiP_2Se_6$ crystals.

Symmetric and narrow distribution of

relaxation times is observed at higher temperatures. On cooling the *f(τ)* function becomes asymmetrically shaped and a second maximum appears. In order to explain the nature of two maxima of distribution of relaxation times the measurements were performed under DC bias field (*E*=3.1 kV/cm). The distributions of relaxations times *f(τ)* at 60 K of poled and unpoled sample are presented in Fig. 4.4.3.3. The part of long relaxation time distribution is strongly affected by external DC electric field. The dynamic of ferroelectric or antiferroelectric domains usually is strongly affected by external electric field [123].

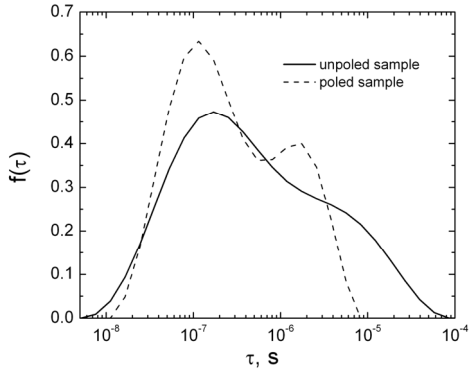

Fig. 4.4.3.3. Distribution of relaxation times of unpoled and poled $CuBiP_2Se_6$ crystals at T=60 K.

Therefore this part of distribution of relaxation times is obviously caused by antiferroelectric domain dynamics. However, the short relaxation time distribution part is less affected by external DC electric field. Usually, the dielectric dispersion of dipole glasses is very weakly affected by external DC electric field [116]. Therefore, this part of distribution of relaxation times can be partially caused by the dipolar glass. The longest limits of the *f(τ)* function τ_{max} (level 0.1 of the maximum *f(τ)* was chosen for definition of the limits) and most probable relaxation τ_{mp} were calculated at various temperatures (Fig. 4.4.3.4). The most probable and longest relaxation times increase on cooling according to the Vogel-Fulcher law (4.1.3.2). Obtained parameters are summarized in Table 4.4.3.1. The activation energy is lower for the poled than for the unpoled sample. The freezing temperature of the longest relaxation time of poled sample is also lower than for the unpoled sample. The activation energy and freezing temperature of

most probable time of unpoled sample is lower then for pure $CuInP_2S_6$ and $Ag_{0.1}Cu_{0.9}InP_2S_6$[89].

Table 4.4.3.1. Parameters of Vogel-Fulcher law of the longest and the most probable relaxation time of unpoled and poled $CuBiP_2Se_6$ crystals.

obtained for	τ_0, ps	T_0, K	E_f/k, K (eV)
τ_{max}, unpoled crystals	0.25	16	1264 (0.109)
τ_{mp}, unpoled crystals	46.1	2	418 (0.036)
τ_{max}, poled crystals	11	13	818 (0.07)
τ_{mp}, poled crystals	344	9	233 (0.02)

What is the nature of low-temperature phase in $CuBiP_2Se_6$? The broad dielectric dispersion (Fig. 4.4.1.1) and distributions of relaxation times (Fig. 4.4.3.2 – 4.4.3.3) suggests existence of antiferroelectric domains in $CuBiP_2Se_6$ crystals. However, additionally some contribution to the dielectric dispersion is clearly expressed in the distribution of relaxation times (Fig. 4.4.3.2 and Fig. 4.4.3.3), therefore small disordered clusters (dipole glass phase) can coexist with large antiferroelectric domains.

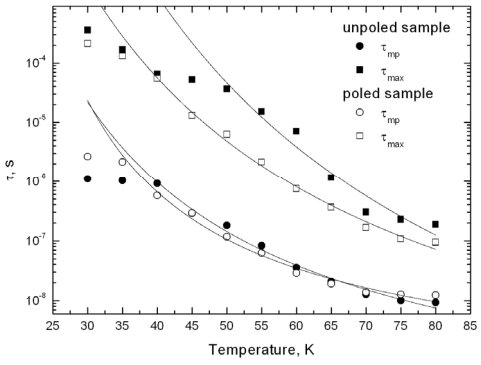

Fig. 4.4.3.4 Longest and most probable relaxation time of unpoled and poled $CuBiP_2Se_6$ crystals.

Usually the dipole glass phase appears in mixed ferroelectric-antiferroelectric crystals and it is related with a frustrated ion ordering. The frustrated ions ordering appears due to the disorder and competitive (ferroelectric and antiferroelectric) interactions. Antiferroelectric interactions were observed in $CuBiP_2Se_6$ only between copper and bismuth ions [116]. The interactions between copper ions, similar to $CuInP_2S_6$ and $CuInP_2Se_6$, can be ferroelectric. However, the strong antiferroelectric interactions between copper and bismuth ions cover more weak ferroelectric interactions between copper

ions. Additionally, some degree of disorder (15%) was observed in copper sublattice down to lowest temperatures [89]. So we must conclude that the frustrated ions ordering can appear in copper sublattice in $CuBiP_2Se_6$. The low-temperature phase in $CuBiP_2Se_6$ can be very similar to the dipole glass phase in ferrielectrics $CuInP_2S_6$ and $Ag_{0.1}Cu_{0.9}InP_2S_6$ [89]. The difference is only in the dominant interactions, in $CuInP_2S_6$ the dominant interaction is ferroelectric while in $CuBiP_2Se_6$ the main interaction is antiferroelectric.

In sulphur analog ($CuBiP_2S_6$ crystals) there are no any phase transitions clearly expressed in dielectric permittivity data [124]. At higher temperatures the dielectric properties are strongly influenced by high electric conductivity. The DC conductivity and conductivity relaxation time exhibit an anomaly close to the phase transition temperature T_c=220 K. Activation energies of both parameters are very similar, this suggests that the conductivity mechanism is single Cu ions hopping, and phase transition is of a superionic type. Close to the phase transition temperature the dielectric relaxation appears, and its origin is discussed in [124].

Conclusions

At the temperature T_c=136 K crystal undergoes a first order antiferroelectric phase transition of displacive type. The antiferroelectric phase transition is related with the antiparallel displacement in copper and bismuth sublattice. However, not all copper ions are ordered below the antiferroelectric phase transition temperature. The non-ordered copper ions freeze at very low temperatures.

The main results are published in [63], [124].

4.5 Dielectric investigations of phase transitions in $Cu_6PS_5(I_x,Br_{1-x})$ mixed crystals

Overview

Cu_6PS_5X (X = Br, I) crystals belong to the family of tetrahedrally close-packed structures termed the argyrodytes [125]. At room temperature they have a common cubic high temperature structure with $F\bar{4}3m$ space group, the typical feature of which is an anion framework of interpenetrating centered icosahedra [126],[127]. Both of them are characterized by a high concentration of disordered vacancies [125]. The crystals are very interesting because they undergo superionic and other structural phase transitions and have semiconductor and piezoelectric properties [126],[128]. Besides, they are of interest as nonlinear optical materials as well as piezoelectric materials for transducers [129],[130]. The synthesis of solid solutions of this family should vary their properties in a broad range. Cu_6PS_5Br undergoes a first-order superionic phase transition near 166–180 K and a second-order ferroelastic phase transition at about 268 K [130]. Below the ferroelastic phase transition temperature Cu_6PS_5Br crystals belong to monoclinic syngony (space group Cc), and the superionic phase transition reveals the features of an isostructural transformation [131]. In general, X-ray diffraction, electrical conductivity NMR, Raman scattering and optical absorption techniques agree that Cu sites within the Cu_6PS_5X cubic lattice are only partially occupied at room temperature and that the copper cation is highly mobile in these compounds. The electrical properties of Cu_6PS_5Br were investigated in [129]. The Cu_6PS_5I crystals according to [127] undergo a superionic transition in the temperature range (144 – 175 K) and ferroeleastic one (270 - 274 K). The conductivity measurements at room temperature were presented in [131], where authors showed that conduction is purely ionic with electronic contribution less than 1%. Other conductivity measurements showed strong anomaly with broad and continuous

change in activation energy in the region of 270 K, which was observed on Arrhenius plot and much weaker one around 194 K [132]. It was reported in [133] that different preparation procedures in single-crystal growth of Cu_6PS_5I lead to static structural disorder due to the deviation of the copper content from stoichiometry. This has an influence on the temperature of superionic phase transitions in Cu_6PS_5I.

The aim of this paragraph is to investigate dielectric properties (20 Hz – 1 MHz) of $Cu_6PS_5(I_x,Br_{1-x})$ crystals in wide temperature range and to obtain a phase diagram.

Experimental

The single crystals of $Cu_6PS_5(I_x,Br_{1-x})$ were grown by the method of chemical transport reactions. The crystals were grown from a mixture enriched by $CuBr+Cu_2S$. The temperature at the hot end of the vessel was kept at 650^0 C, and at the cool one 550^0 C. More details about the sample preparation are given in [134]. At room temperature, the crystals belong to the cubic $F\bar{4}3m$ point group of symmetry. The comparatively large crystals of 3×3×4 mm dimensions were used for dielectric experiments. The complex dielectric permittivity $\varepsilon^*=\varepsilon'-i\varepsilon''$ was measured by a capacitance bridge HP4284A in the frequency range 20 Hz – 1 MHz and by closed cycle cryostat. The amplitude of the AC signal was 1 V. Silver paste was used for contacts. All measurements were done on cooling with the rate 1 K/min, starting from 420 K and going down to 25 K. Frequency spectra were measured at the constant temperature.

Results and discussion

Temperature dependencies of complex ε*=ε'-iε" dielectric permittivity of mixed $Cu_6PS_5(I_x,Br_{1-x})$ crystals are very similar to the corresponding dependencies of pure Cu_6PS_5Br and Cu_6PS_5I crystals [135]. For example, the temperature dependency of complex dielectric permittivity of mixed $Cu_6PS_5(I_{0.25}Br_{0.75})$ crystal is presented in Fig. 4.5.1

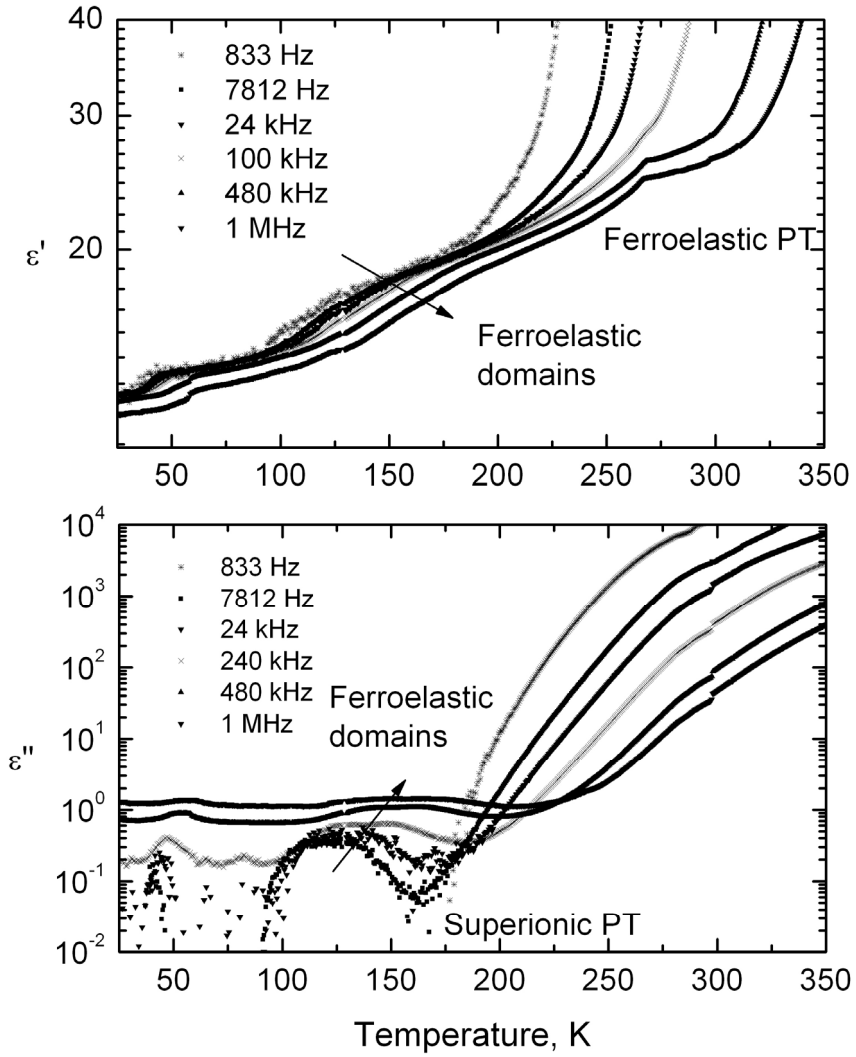

Fig. 4.5.1. Temperature dependence of the real and imaginary parts of dielectric permittivity of $Cu_6PS_5(I_{0.25}Br_{0.75})$ crystal at different frequencies.

From the dependency one can see, that the crystal, similar to pure Cu_6PS_5Br and Cu_6PS_5I crystals, undergoes two phase transitions in 120 – 300 K temperature region. At higher temperatures the ferroelastic phase transition is well expressed at 266 K. At lower temperatures (T=170 K) an anomaly in imaginary part of dielectric permittivity ε'' indicate the superionic phase transition, which quiet well coincide with

ultrasonic investigations [131]. The phase transition temperatures of mixed $Cu_6PS_5(I_x,Br_{1-x})$ crystals are written in Table 4.5.1. The results show, that the anionic substitution has a little influence to elastic transition temperature (it slightly decreases), while the temperature of superionic phase transition increases considerably (of about 20 K, in 75 % Br concentration sample).

Table 4.5.1 The phase transition temperatures of mixed $Cu_6PS_5(I_x,Br_{1-x})$ crystals.

	Ferroelastic phase transition temperature, K	Superionic phase transition temperature, K
Cu_6PS_5I	273 K (270 K [136], 269 K [136])	156 K (165-175 K [130], 144-169 K [136])
$Cu_6PS_5(I_{0.75},Br_{0.25})$	270 K	154 K
$Cu_6PS_5(I_{0.5},Br_{0.5})$	271 K	161 K
$Cu_6PS_5(I_{0.25},Br_{0.75})$	266 K	170 K
Cu_6PS_5Br	266 K (268 K [137][136])	166 K (166 – 180 K [137] [114])

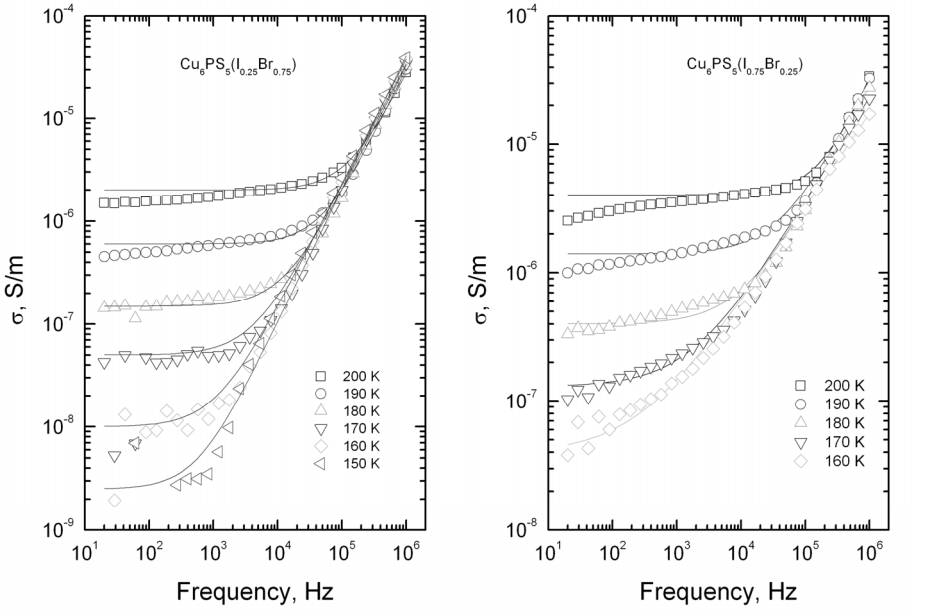

Fig. 4.5.2. Frequency dependence of σ for $Cu_6PS_5(I_{0.25}Br_{0.75})$ and $Cu_6PS_5(I_{0.75}Br_{0.25})$ crystals. Solid line is theoretically calculated according to the formula $\sigma=\sigma_{DC}+A\omega^s$. Points are experimental data.

For more detailed analysis, we calculate the real part of electrical conductivity from the dielectric meaurements. The obtained results for several bromine concentration x are presented in Fig.4.5.2 At low frequencies, random distribution of the ionic charge carriers via activated hopping gives rise to a frequency independent conductivity (DC conductivity). At higher frequencies, conductivity exhibits dispersion, increasing roughly in a power law fashion and eventually becoming almost linear at even higher frequencies. The high-temperature conductivity spectra of the Cu ion conducting materials are characterized by an additional low-frequency dispersion region due to electrode effects. The frequency behaviour of σ has been fitted according to the Almond-West type power law (4.2) with single exponent [121]. Temperature dependence of ln(σ_{DC}) and activation energy for different bromine concentration *x* are presented in Fig. 4.5.3

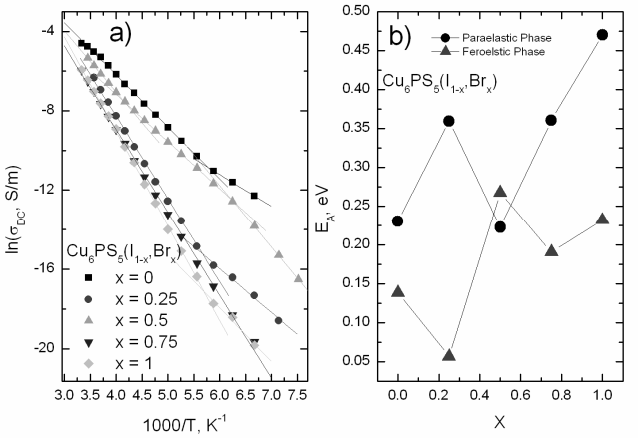

Fig. 4.5.3. a) Temperature dependence of ln(σ_{DC}) and b) activation energy for different bromine concentration *x*.

From the temperature dependence of ln(σ_{DC}) it was possible to calculate activation energy E_A of the conductivity according to the Arrhenius law (4.1.1.3). Calculated parameter dependency of bromine concentration is presented in Fig. 4.5.3 b). Activation energy for Cu_6PS_5I crystal is less as in bromide analog. This confirms that the potential relief for copper ions in Cu_6PS_5I is shallower than for its bromide analog. In the paraelectric phase the concentration dependency of the activation energy E_A have a minimum

at x=0.5, while in the ferroelastic phase at x=0.25.

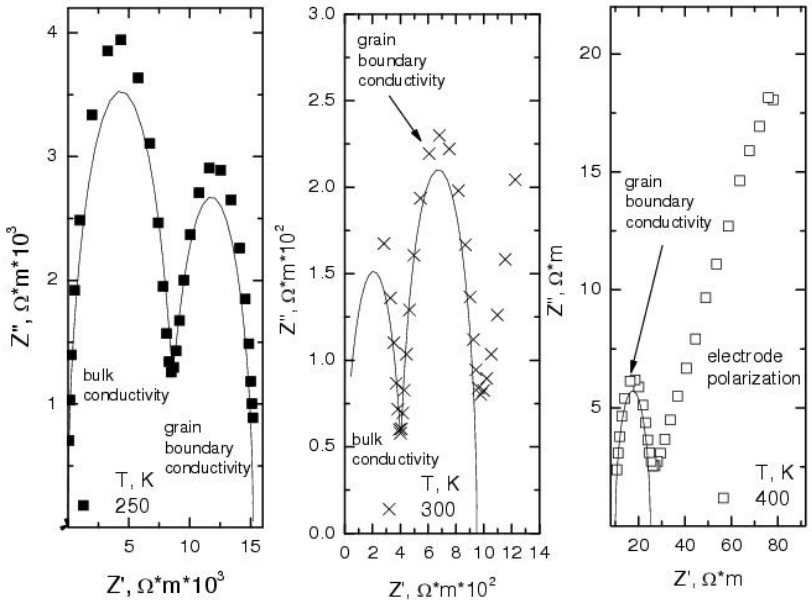

Fig. 4.5.4. Cole-Cole plot of the complex specific resistance of Cu_6PS_5Br. Solid lines are the best fit according to (4.5.2).

Due to the conductivity phenomena, the blocking contact effect may play an important role in the dielectric spectra. To separate the volume polarization and electrode polarization due to ionic and electronic conductivity, the specific resistance representation of the measured results was used for analysis. The frequency-dependence of the complex specific resistance was obtained from the dielectric spectra according to formula (4.3.1). The dependence of imaginary part of the specific resistance versus the real part on cooling is presented in Fig. 4.5.4. From the dependence it is possible to identify: electrode polarization and two different contributions to the electrical conductivity. At low temperatures these contributions can be associated with bulk conductivity at high frequency and grain boundary conductivity at lower frequencies (Fig. 4.5.4). The contributions are broad enough and cannot be adequate described by single RC.

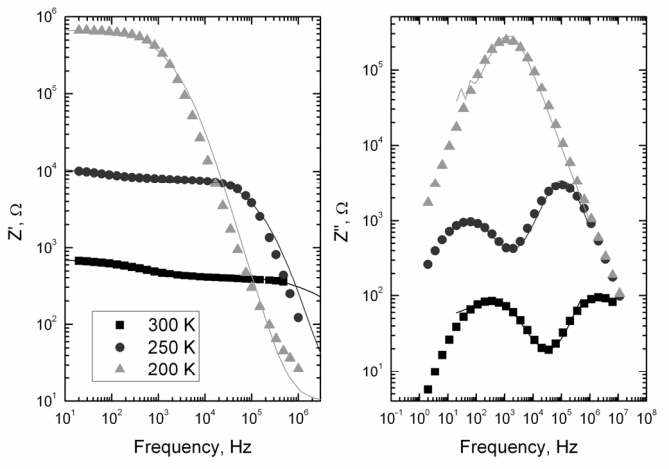

Fig. 4.5.5. The frequency-dependence of the real and the imaginary part of the complex specific resistance at different temperatures for $Cu_6PS_5(I_{0.25}Br_{0.75})$ crystal. Solid lines are the best fit according to (4.22).

The frequency-dependence of the real and the imaginary part of the complex specific resistance on cooling of $Cu_6PS_5(I_{0.25}Br_{0.75})$ are presented in Fig. 4.5.5. The distribution of relaxation times has been calculated directly from the complex specific resistance spectra in the temperature region from 150 K to 300 K according to a formula

$$Z^*(\nu) = Z_\infty + \Delta Z \int_{-\infty}^{\infty} \frac{f(\tau) d \lg \tau}{1 + i\omega\tau} \qquad (4.5.2)$$

and method described in [137]. The calculated distributed times of $Cu_6PS_5(I_{0.25}Br_{0.75})$ crystals are presented in Fig. 4.5.6 a). At 200 K

Table 4.5.2. The actyvation energy of mixed $Cu_6PS_5(I_x,Br_{1-x})$ crystals got from the Arrhenius law.

	Short relaxation	**Long relaxation**
Cu_6PS_5I	2708 K (0.233 eV)	
$Cu_6PS_5(I_{0.75},Br_{0.25})$	4516 K (0.389 eV)	1873 K (0.161 eV)
$Cu_6PS_5(I_{0.5},Br_{0.5})$	2434 K (0.209 eV)	2036 K (0.175 eV)
$Cu_6PS_5(I_{0.25},Br_{0.75})$	4443 K (0.383 eV)	2746 K (0.237 eV)
Cu_6PS_5Br	4945 K (0.426 eV)	3846 K (0.331 eV)

temperature distribution function has one symmetrical peak, which moves to shorter relaxation times with increasing temperature. At higher

temperatures function $f(\tau)$ has two symmetric peaks, which correspond to the two different processes. The temperature dependence of the maxima of relaxation times distribution is shown in Fig. 4.5.6 b) The mean relaxation times diverges according to the Arrhenius law.

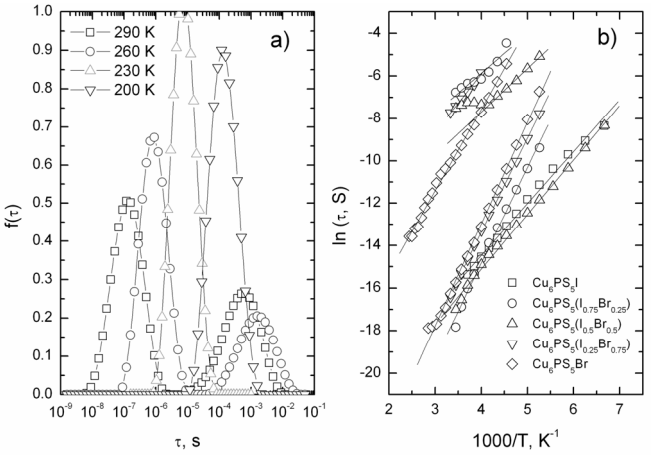

Fig.4.5.6. a) Distribution of the relaxation times $f(\tau)$ of $Cu_6PS_5(I_{0.25}Br_{0.75})$ crystal at different temperatures. b) Temperature-dependence of the relaxation time peaks in $f(\tau)$ for $Cu_6PS_5(I_{1-x}Br_x)$ crystals.

The calculated values are written in the Table 4.5.2. The values of activation energy of short relaxation times is very similar to the DC conductivity activation energy (Fig. 4.5.3). Therefore, DC conductivity below room temperature mainly is caused by bulk process.

Conclusions

1. In mixed $Cu_6PS_5(I_x,Br_{1-x})$ crystals at high temperatures ferroelastic and at low temperatures superionic phase transitions are observed. The ferroelastic phase transition temperature of mixed $Cu_6PS_5(I_x,Br_{1-x})$ crystals shifts to lower temperatures (273 K – 268 K) with increasing bromine concentration, while superionic PT temperature increases (156 K – 166 K).
2. In paraelectric phase activation energy calculated from the DC conductivity have a minimum when x=0.5 and in ferroeleastic phase the minimum is at x=0.25.

3. The distribution of relaxation times calculated from the impedance spectra let us to separate the conductivity in bulk and in grain boundaries.

The main results are presented in [133].

4.6 The dielectric spectroscopy of $Pb_5Ge_3O_{11}$ crystals doped with Cu^+ impurities

Overview

Lead germanate, $Pb_5Ge_3O_{11}$, is an uniaxial ferroelectric which shows a first – order phase transition at T_c=451 K and ambient pressure [138],[139]. X – ray [140],[141] and neutron [139] studies reveal a chain – like structure in the *z*-direction with single and double germinate tetrahedral alternately disposed with axes of symmetry parallel to *z*, and lead atoms forming a layer structure of regular spacing perpendicular to *z*. Large single crystals of lead germanate may be grown so, that good samples of different orientation are readily available for studies of scattering or domain – wall mobility. Above T_c, the crystal is paraelectric with $C_{3h}^1(P\bar{6})$ hexagonal symmetry and the lattice constants $a = 10.26\,\overset{0}{A}$ and $c = 10.69\,\overset{0}{A}$ [140]. Below T_c, the crystal is ferroelectric with trigonal symmetry $C_3^1(P3)$, and axis of polarization parallel to *z*; the crystal looses mirror symmetry normal to the *z* axis [142]. The static dielectric permittivity ε is observed to have an anomaly at T_c and to obey a Curie – Weiss law in its temperature dependence above and below T_c [143]. Raman experiments [139] show a mode that softens. X-ray and neutron scattering has also provided information on the movements of the equilibrium positions of the atoms in the unit cells [140],[139]. Transforming from the paraelectric phase involves small torsions of the germanate tetrahedra and shifts of the lead atoms. The largest movement at 293 K of an oxygen atom is $0.36\,\overset{0}{A}$ along *z*, while the largest lead and germanium displacements are about $0.15\,\overset{0}{A}$ along *z*. All displacements are less than 5% of the lattice constants. These experiments also confirm that the transition is displacive [144].

Lead germanate can be used in ceramics form for high – capacitance condensers or in crystalline form in transducers, where use

is made of its piezoelectric behaviour. It is employed in optical memory devices because it shows pronounced hysteresis and optical activity [144]; lead germanate has fast switching times t_s in the microsecond range and needs a relatively weak coercive field E_c (≤14kV/cm at 50 Hz) [142]. PGO crystal obey the Curie – Weiss law above T_c [145],[143]

$$\varepsilon_{33}^{-1} \propto T - T_B, \; T_B < T_C. \tag{4.6.1}$$

and that the soft – mode frequency $\varpi_0(T)$ closely follows the form [146]

$$\varpi_0^2(T)/\varpi_0^2(0) = (T_A - T)/T_A, \; T_A > T_C \tag{4.6.2}$$

below T_C. For the second – order phase transition, one has T_A=T_B=T_C. Light and neutron – scattering experiments reveal a prominent central – peak feature well below T_C [147], in addition to an anomalous central peak near the critical temperature [148],[149]. The low-temperature central peak has been attributed to the presence of domain walls [150] though its origin and form have not been properly explained. This peak has a width Γ which is below current experimental resolution (which is denoted by $\Delta\omega$).

Pure PGO crystal has been investigated by many groups [151-153]. Quite interesting results are received by doping this crystal with copper ions. The results of Cu^{2+} ESR spectra studies in PGO crystals were reported later [154],[141]. The measurements of the orientation and temperature dependencies of ESR spectra show that Cu^{2+} centers replace Pb^{2+} ions in positions with trigonal symmetry [155]. The anisotropy and motional averaging of ESR spectra are interpreted as the result of the off-center localization and thermally activated dynamics of Cu^{2+} centers [153]. Shifting Cu^{2+} in (ab) plane, perpendicular to polar c-axis, should obviously lead to appearance of the local dipole moments. In this case the dielectric properties of PGO doped with Cu^{2+} would demonstrate the characteristic peculiarities of the temperature and frequency behavior [153].

Experimental

Dielectric permittivity measurements of PGO crytals doped with copper were done in wide frequency (20 Hz to 3 GHz) and temperature (120 K to 470 K) range. Crystals of 3x3x3 mm dimension were used for measurements at low frequencies (20 Hz- 1 MHz). Stick like form crystals were prepared for the measurements at high frequencies. Silver paste was used for contacting. All measurements were performed on cooling with a rate of 1K/min.

Results

The dielectric measurements were done along polar axis c. The temperature dependence of complex dielectric permittivity ε^* of PGO at high temperatures is presented in Fig.4.6.1. The dielectric anomaly in this crystal is associated with ferroelectric phase transition, which is observed at 441 K. The dielectric dispersion covers all measured frequency range, from 20 Hz to 3 GHz. Close to the ferroelectric phase transition temperature real part of complex dielectric permittivity reduces for 6 times going from low to high

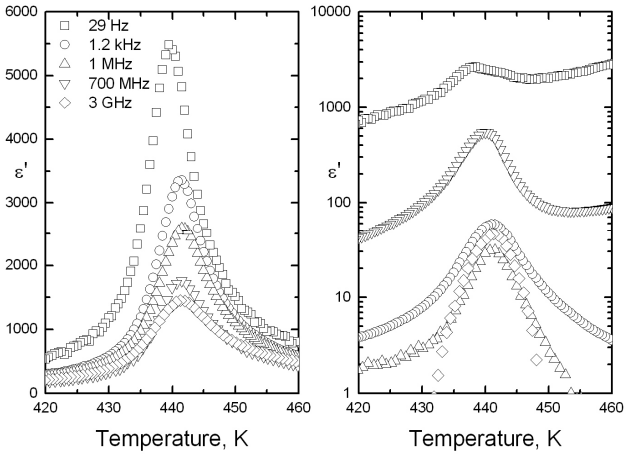

Fig. 4.6.1. Temperature dependence of real and imaginary part of dielectric permittivity of PGO crystal.

frequencies. This result indicates egzistence of relaxational soft mode in PGO and that the ferroelectric phase transition is of “order-disorder” type. The resonant soft mode was also observed in PGO crystals [152]. Therefore, the ferroelectric phase transition in PGO is mixed “order-disorder” and displacive.

For more detailed dielectric analysis PGO crystal was doped with 0.1 % and 0.5 % of Cu^{2+} ions. With increasing Cu^{2+} concentration T_C noticeably shifts to low temperatures and *ε(T)* anomaly becomes smeared. Figure 4.6.2 illustrates the influence of Cu^{2+} impurities on ferroelectric anomaly *ε′(T)* in PGO crystal. The influence of impurities to T_c is explained by the idea that copper ions are the “rigid” defects which stabilize high symmetry configuration of the lattice surroundings at cooling below the phase transition point of defectless structure. The *1/ε′(T)* was fitted according to the Curie-Weiss law (4.1.2.2). The proportion of Curie-Weiss constants is 1.23 for PGO, 1.64 for PGO (Cu 0.1%) and 2.33 for PGO (Cu 0.5%), and it indicates nearly the second order phase transition. The ratio $C_{p,f}/T_C$ is in order 60, this observed phase transition is higher

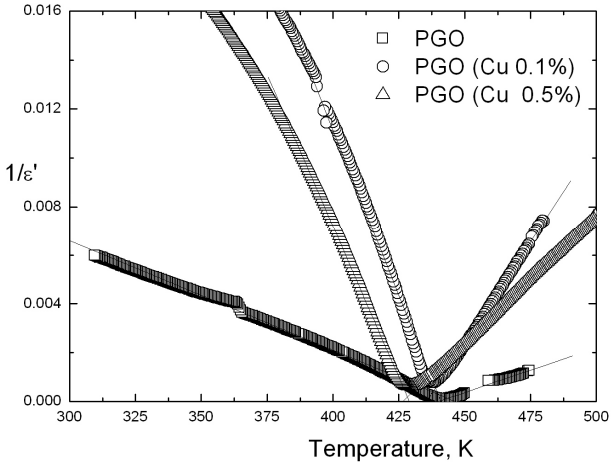

Fig.4.6.2. Temperature dependence of inverse dielectric permittivity at 1 MHz frequency.

for typical “order-disorder” phase transitions. This also confirms that the phase transition in PGO is mixed displacive [156] and order-disorder.

The dielectric permittivity at low temperatures

At lower temperatures the dielectric anomaly is associated with domain walls motion and dipolar glass properties. Displacements of Cu^{2+} from the lattice point should induce electric dipole moments

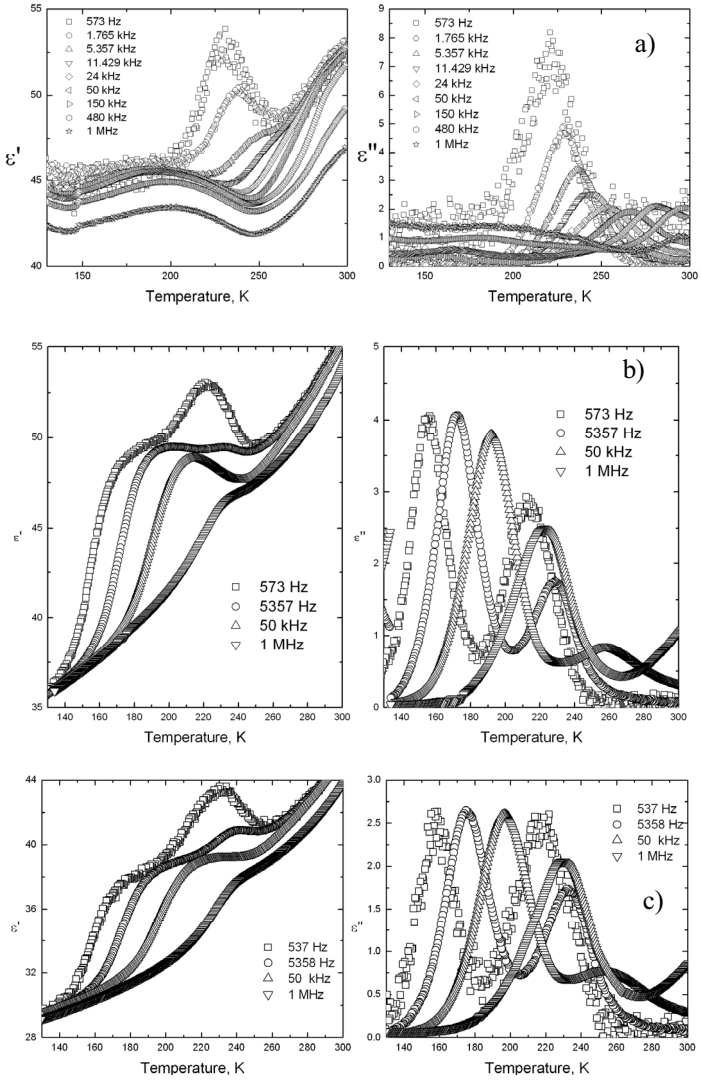

Fig. 4.6.3. Temperature dependence of complex dielectric permittivity of: a) PGO, b) PGO (Cu^{2+} 0.1%) and c) PGO (Cu^{2+} 0.5%)

perpendicular to polar axis. Then hopping between off-center positions accompanied by dipoles re-orientations should contribute to the dielectric properties of PGO doped with Cu^{2+}. Real and imaginary part of dielectric permittivity was studied on PGO samples doped with 0.1 % and 0.5 % Cu^{2+} impurities. Temperature dependencies of ε^* studied in the interval 25 ÷ 300 K are shown in Fig. 4.6.3.

It has to be mentioned that description of the experimental data needs to take into account two different relaxation processes. Corresponding contributions are visible in Fig. 4.6.3 as distortion of the high-temperature wing of *ε"(T)* basic peak and small maximum at 240 K. *ε"(T)* maximum at 240 K is observed in doped and pure PGO crystals as well. Presumably low-frequency dielectric relaxation along the *c*-axis is resulted by domain walls motion [89].

For the more detailed analysis we calculated the distribution of relaxation times function according to the method described in chapter

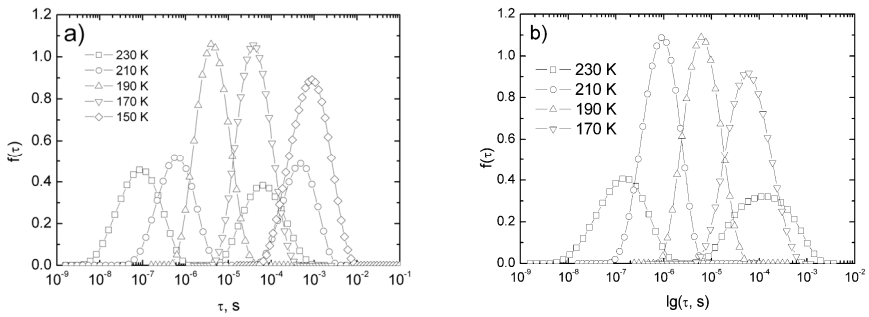

Fig. 4.6.5. Distribution of relaxation times for: a) PGO (Cu 0.1 %) and b) PGO (Cu 0.5 %).

3.2. For the pure PGO there is expressed just one maximum, which moves to longer relaxation times with decreasing temperature. When we apply external electric field of 2 kV/cm, the long-time edge of the relaxation times function moves to longer times. It indicates that the domains grow with increasing external electric field. When PGO is doped with 0.1 % and 0.5 % of Cu^{2+} ions, the distribution of relaxation times function spread in two peaks (Fig. 4.6.5).

Table. 4.6.2. Activation energy calculated from the Vogel-Fulcher law fitting parameters τ from Cole – Cole model.						
Crystal	τ_{01}, s	τ_{02}, s	E_1/k, K (eV)	E_2/k, K (eV)	T_{01},K	T_{02},K
PGO(E = 0 kV/cm)	$1.63*10^{-12}$	-	2594 (0.224)	-	89	-
PGO(E = 2 kV/cm)	$3.07*10^{-14}$	-	3624 (0.312)	-	71	-
PGO (Cu 0.1%)	$7.8*10^{-14}$	$6.3*10^{-14}$	2939 (0.253)	4010(0.346)	23	34
PGO (Cu 0.5 %)	$3.04*10^{-14}$	$2.6*10^{-16}$	3387 (0.292)	5191(0.447)	10	37

One peak corresponds to the classical hopping of Cu^{2+} over the barriers and other one is caused by the relaxation of domains [154]. The movement of the peak of distribution function was fitted with Vogel - Fulcher law (Fig. 4.6.6), where calculated parameters are written in the table 4.6.2. From these results we can conclude, that dielectric measurements let us to distinguish two different relaxation processes, with different activation energy. The activation energy got from the dielectric measurements for the PGO crystal quite well coincides with ESR measurements [154]. Therefore it is noticed, that domains relaxation requires smaller activation energy, than random dipole freezing phenomena. Increasing copper concentration both activation energies increases and freezing temperature decreases. It shows that just a small amount of impurities significantly changes many physical parameters.

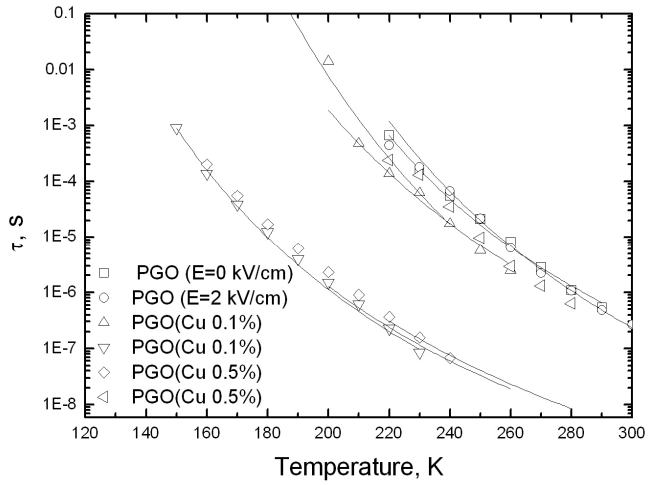

Fig. 4.6.6. Temperature dependence of relaxation times.

Conclusions

1. The ferroelectric phase transition in PGO crystals is mixed “order-disoder” and displacive.
2. Small amount of copper ions noticeably changes the phase transition temperature - with increasing copper concentration second order phase transition temperature moves to lower temperatures.
3. At low temperatures the dielectric dispersion in PGO crystals doped with Cu ions is caused by domain wall dynamics and dipole glass freezing. It is determined that the domain relaxation requires lower energy then for the random freezing dipoles.

6. REFERENCE LIST

[1] D. Brewster, *J. Sci*, vol. 208, no. 1, 1824.
[2] J. Gaugain, *C.R. Acad. Sci. Paris*, vol. 1264, no. 42, 1856.
[3] V. K. Wadhawan, Netherlands: Gordon and Breach Science Pulbishers, 2000.
[4] J. and P. Curie, *C.R. Acad. Sci. Paris*, vol. 294, no. 91, 1890.
[5] G. Heartling, *J. Am. Ceram. Soc.*, vol. 82, p. 797, 1999.
[6] J. Valsek, *Phys. Rev.*, vol. 15, p. 537, 1920.
[7] G. Busch & P. Scherrer, Naturwissenschaft, 23, p. 737, 1938.
[8] S. Francis, *Inorganic syntheses*, vol. 14, p. 142, 1973.
[9] B. T. Matthias and J. P. Remeika, *Phys. Rev.*, vol. 76, p. 1886, 1949.
[10] G. Shirane, S. Hoshino, K. Suzuki, Phys. Rev.,80, p. 1105, 1950.
[11] J. F. Nye '*Physical properties of crystals*', Clarendon Press, Oxford, 1964.
[12] L. Brilouin, *Wave Propagation in Periodic Structures*. New York: Dover Publications, 1953.
[13] P. Debye, *Polar molecules*. New York: Dover Publications, 1954.
[14] P. Debye, *Ver. Deut. Phys. Gesell.*, vol. 15, no. 777, 1913.
[15] W. Kanzik, H. R. Hart, and S. Roberts, *Phys. Rev. Lett.*, vol. 13, pp. 543-545, 1964.
[16] P. P. Peressini, J. P. Harrison, and R. O. Pohl, *Phys. Rev.*, vol. 180, pp. 926-930, 1969.
[17] A. T. Fiory, *Phys. Rev. B*, vol. 4, pp. 614-627, 1971.
[18] K. Binder and A. P. Young, *Reviews of Modern Physics*, vol. 58, no. 4, p. 801, Oct. 1986.
[19] B. E. Vugmeister, M. D. Glinchuk, and A. P. Pecheny, *Ferroelectrics*, vol. 64, no. 1, p. 1, 1985.
[20] M. Saint-Paul and J. I. G. Gilchrist, *J. Phys. C* 19, p. 2091, 1986.
[21] C. N. Guy, *Journal of Physics F: Metal Physics*, vol. 12, no. 7, pp. 1453-1465, 1982.
[22] R. Pirc, B. Tadic , and R. Blinc, *Phys. Rev. B* 36, p.8607, 1987.
[23] F. Lüty and J. Ortiz-Lopez, *Phys. Rev. Lett.* vol. 50, p. 1289, 1983.
[24] J. Banys, J. Macutkevic, S. Lapinskas, C. Klimm, G. Völkel, and A. Klöpperpieper, *Physical Review B*, vol. 73, no. 14, p. 144202, Apr. 2006.
[25] T. Panchenko, M. Volnyanskii, V. Monya, and V. Duda, *Sov. Phys. Solid State*, vol. 19, p. 1311, 1977.
[26] C. Kittel, *Introduction to Solid State Physics, 4th ed. (Wiley,New York, 1971)*
[27] E. Fatuzzo and W. Merz, *Ferroelectricity (North – Holland, Amsterdam, 1967).*
[28] R. Cowley, J. Axe, and M. Iizumi, *Phys. Rev. Lett.*, vol. 36, p. 806, 1976.
[29] K. Germann, *Phys. Status Solidi A*, vol. 38, p. 81, 1976.

[30] A. Brant, *Isledovanie dielektrikov na sverchvysokich castotach*. Moskva: Fizmatgiz, 1963.
[31] M. Fiebig, *J. Phys. D*, vol. 38, p. R123, 2005.
[32] W. Eerenstein, N. D. Mathur, and J. F. Scott, *Nature*, vol. 442, no. 7104, pp. 759-765, 2006.
[33] X. Chen, A. Hochstrat, P. Borisov, and W. Kleemann, *Applied Physics Letters*, vol. 89, no. 20, p. 202508, 2006.
[34] C. Binek, A. Hochstrat, X. Chen, P. Borisov, W. Kleemann, and B. Doudin, *J. Appl. Phys.*, vol. 97, p. 10C514, 2005.
[35] V. Laukhin et al., *Physical Review Letters*, vol. 97, no. 22, p. 227201, Nov. 2006.
[36] N. Spalding and M. Fiebig, *Science*, vol. 309, p. 391, 2005.
[37] D. Astrov, *Sov. Phys. JETP*, vol. 11, p. 780, 1960.
[38] H. Schafer, E. Sternin, R. Stannarius, M. Arndt, and F. Kremer, *Phys. Rev. Lett.*, vol. 76, p. 2177, 1996.
[39] B. G. Kim, J. J. Kim, and H. M. Jang, *Ferroelectrics*, vol. 240, p. 249, 2000.
[40] R. Pelster, T. Kruse, H. G. Krauthaeuser, G. Nimtz, and P. Pissis, *Phys. Rev. B*, vol. 57, p. 8763, 1998.
[41] A. V. Tichonov, *Dokl. Akad. Nauk SSSR* vol. 153,N3, 1963.
[42] C. L. Lawson and R. J. Hanson, Solving Least Squares Problems (SIAM, Philadelphia, 1995).
[43] S. W. Provencher, *Comput. Phys. Commun*. vol. 27, p. 213, 1982.
[44] J. Banys, S. Lapinskas, A. Kajokas, A. Matulis, C. Klimm, G.Völkel, and A. Klöpperpieper, *Phys. Rev. B,* vol. 66, p. 144113, 2002.
[45] V. Maisonneuve, V. B. Cajipe, A. Simon, R. Von Der Muhll, and J. Ravez, *Physical Review B*, vol. 56, no. 17, p. 10860, Nov. 1997.
[46] V. Maisonneuve, M. Evain, C. Payen, V. B. Cajipe, and P. Molinie, J. Alloys Compd. vol. 218, p. 157, 1995
[47] V. Maisonneuve, V. B. Cajipe, A. Simon, R. Von der Muhll,and J. Ravez, *Phys. Rev. B,* vol. 56, p. 10860, 1997.
[48] A. Simon, J. Ravez, V. Maisonneuve, C. Payen, and V. B. Cajipe, *Chem. Mater.* vol. 6, p. 1575, 1994.
[49] J. Banys, J.Macutkevic, V. Samulionis, A. Brilingas, and Yu. Vysochanskii, *Phase Transitions* vol. 77, p. 345, 2004.
[50] V. Maisonneuve, J. M. Reau, M. Dong, V. B. Cajipe, C. Payen, and J. Ravez, *Ferroelectrics*, vol. 196, p. 257, 1997.
[51] Yu. M. Vysochanskii, V. A. Stepanovich, A. A. Molnar, V. B. Cajipe, and X. Bourdon, *Phys. Rev. B*, vol. 58, p. 9119, 1998.
[52] A. Gutgalis, J. Banys, J. Macutkevic, and Yu. Vysochanskii, *Ferroelectrics* vol. 353, p. 91, 2007.
[53] J. Macutkevic, J. Banys, R. Grigalaitis, and Y. Vysochanskii, *Physical Review B*, vol. 78, no. 6, p. 064101, 2008.

[54] Yu. Vysochanskii, R. Yevych, L. Beley, V. Stepanovich, V. Mytrovcij, O. Mykajlo, A. Molnar, and M. Gurzan, *Ferroelectrics* vol. 284, p. 161, 2003.
[55] P. Colombet, A. Leblanc, M. Danot, and J. Roulxel, *J. Solid State Chem*, vol. 41, p. 174, 1982.
[56] D. Bertrand, A. R. Fert, M. C. Schmidt, F. Bensamka, and S. Legrand, *J. Phys. C: Solid State Phys.*, vol. 15, p. L883, 1982.
[57] J. Mattsson, J. Kushauer, D. Bertrand, J. Ferré, P. Meyer, J. Pommier, and W. Kleemann, *J. Magn. Magn. Mat.*, vol. 152, p. 129, 1996.
[58] M. M. Maior, S. F. Motrja, M. I. Gurzan, I. P. Pritz, and Y. M. Vysochanskii, *Ferroelectrics*, vol. 376, no. 1, p. 9, 2008.
[59] V. V. Shvartsman, S. Bedanta, P. Borisov, W. Kleemann, A. Tkach, and P. M. Vilarinho, *Physical Review Letters*, vol. 101, no. 16, p. 165704, Oct. 2008.
[60] W. Kleemann et al., *The European Physical Journal B*, vol. 71, no. 3, pp. 407-410, 2009.
[61] W. Klingen, G. Eulenberger, and H. Hahn, *Ibid.*, vol. 97, p. 401, 1973.
[62] J. Macutkevic, J. Banys, and Yu. Vysochanskii, *Phys. Status Solidi A*, vol. 206, p. 167, 2009.
[63] A. Dziaugys, J. Banys, J. Macutkevic, R. Sobiestijanskas, and Y. Vysochanskii, *Phys. Status Solidi A*, vol. 207, pp. 1960-1967, 2010.
[64] A. Dziaugys, J. Banys, and Y. Vysochanskii, *Zeitschrift für Kristallographie*, vol. 226, no. 2, pp. 171-176, 2011.
[65] I. P. Studenyak, V. V.Mitrovcij, Gy. S. Kovacs,M. I. Gurzan, O. A. Mikajlo, Yu. M. Vysochanskii, and V. B. Cajipe, *Phys. Status Solidi B, vol.* 236, p. 678, 2003.
[66] X. Bourdon, A. R. Grimmer, and V. B. Cajipe, *Chem. Mater.* vol. 11, p. 2680, 1999.
[67] J. Banys, J. Macutkevic, R. Grigalaitis, and Y. Vysochanskii, *Solid State Ionic*, vol. 179, p. 79, 2008.
[68] J. Grigas, *Microwave dielectric spectroscopy of ferroelectrics and related materials*. Amsterdam: Gordon and Breach Science Pulbishers, 1996.
[69] J. Banys, R. Grigalaitis, J. Macutkevic, A. Brilingas, V. Samulionis, J. Grigas, and Yu. Vysochanskii, *Ferroelectrics* vol. 318, p. 163 2005.
[70] F. L. Howell, N. J. Pinto, and V. H. Schmidt, *Physical Review B*, vol. 46, no. 21, p. 13762, Dec. 1992.
[71] J. Banys, J. Macutkevic, C. Klimm, and G. Volkel, *Phase Transitions* vol. 81, p. 303, 2008.
[72] J. Banys, J. Macutkevic, R. Grigalaitis and Yu. Vysocianskii, *Solid State Ionics* vol.179, p. 79, 2008.
[73] I. Suzuki and K. Okada, *J. Phys. Soc. Jpn*. vol. 45, p. 1302,1978.

[74] R. Blinc, J. Dolinsek, R. Pirc, B. Tadic, B. Zalar, R. Kind, and O. Liechti, *Phys. Rev. Lett*. vol. 63, p. 2248, 1989.
[75] R. Kind, R. Blinc, J. Dolinsek, N. Korner, B. Zalar, P. Cevc, N. S. Dalal, and J. DeLooze, *Phys. Rev. B* vol. 43, p. 2511, 1991.
[76] V. Maisonneuve, V. B. Cajipe, A. Simon, R. Von Der Muhll, and J. Ravez, *Phys. Rev. B*, vol. 56, p. 10860, 1997.
[77] P. Borisov, A. Hochstrate, V. V. Shvartsman, and W. Kleemann, *Rev. Sci. Instrum.*, vol. 78, p. 106105, 2007.
[78] J. A. Mydosh, *Mydosh, J. A. (1993). Spin glasses - an experimental introduction (first edition),* Oxford: Taylor&Francis, 1993.
[79] D. Bertrand, F. Bensamka, A. R. Fert, F. Gelard, J. P. Redoules, and S. Legrand, *J. Phys. C: Solid State Phys.*, vol. 17, p. 1725, 1984.
[80] D. J. Goossens, A. J. Struder, S. J. Kennedy, and T. J. Hicks, *J. Phys.: Condens. Matter*, vol. 12, p. 4233, 2000.
[81] A. M. Mulders, J. C. P. Klaasse, D. J. Goossens, J. Chadwick, and T. J. Hicks, *J. Phys.: Condens. Matter*, vol. 14, p. 8697, 2002.
[82] S. Blundell, *S. Blundell, Magnetism in Condensed Matter, Chap. 5,* Oxford Univ. Press, 2001.
[83] R. L. Carlin, R. D. Willett, D. Gatteschi, and O. Kahn, *Magneto-structural correlations in exchange-coupled systems*, vol. 140, pp. 127-155, 1984.
[84] L. Bogani and W. Wernsdorfer, *Nat. Mater.*, vol. 7, pp. 179-186, 2008.
[85] D. Gatteschi, R. Sessoli, and J. Villain, *Molecular Nano Magnets*. Oxford: Oxford Univ. Press, 2006.
[86] L. Neel, *Acad. Sci. Paris, C. R.*, vol. 252, pp. 4075-4080, 1961.
[87] E. Ressouche, M. Loire, V. Simonet, R. Ballou, A. Stunault, and A. Wildes, *Phys. Rev. B*, vol. 82, pp. 100408(R)-1 - 100408(R)-4, 2010.
[88] W. Kleemann, V. V. Shvartsman, P. Borisov, and A. Kania, *Phys. Rev. Lett.*, vol. 105, pp. 257202-1 - 257202-4, 2010.
[89] A. Dziaugys, J. Banys, J. Macutkevic, and R. Sobiestijanskas, Yu. Vysochanskii, *Phys. Status Solidi A*, vol. 8, p. 1960, 2010.
[90] A. Dziaugys, J. Banys, V. Samulionis, and Y. Vysochanskii, *Ultragarsas*, vol. 63, p. 3, 2008.
[91] "V.B. Cajipe, J. Ravez, V. Maisonneuve, A. Simon, C. Payen, R. von der Muhll, J.E. Fisher, *Ferroelectrics*, vol. 185, p. 135, 1996.
[92] V.B. Cajipe, J. Ravez, V. Maisonneuve, A. Simon, C. Payen, R. von der Muhll, J.E. Fisher, *Ferroelectrics*, vol. 185, p. 135, 1996.
[93] V. Maisonneuve, C. Payen, and V. B. Cajipe, *J. Solid State Chem*, vol. 116, p. 208, 1995.
[94] V. Maisonneuve, V. B. Cajipe, and C. Payen, *Chem. Mater.*, vol. 5, p. 758, 1993.

[95] I. Studenyak, O.A. Mykajlo, Yu. Vysochanskii, V.B. Cajipe, J. *Phys.: Condens. Matter* vol. 15, p. 6373, 2003.
[96] X. Bourdon, V. Maisonneuve, V.B. Cajipe, C. Payen, J.E. Fisher, *J. Alloys Compd.* vol. 283, p.122, 1999.
[97] M. M. Maior, L. M. Belej, M. I. Gurzan, and Y. M. Vysochanskii, *Ferroelectrics*, vol. 349, no. 1, p. 71, 2007.
[98] C. Kittel, *Phys. Rev.*, vol. 82, p. 729, 1951.
[99] J. Banys, C. Klimm, G. Volkel, H. Bauch, A. Klopperpieper, *Phys. Rev. B* vol. 50, p. 16751 – 16753, 1994.
[100] J. Banys, P. J. Kundrotas, C. Klimm, A. Klöpperpieper, and G. Völkel, *Physical Review B*, vol. 61, no. 5, p. 3159, Feb. 2000.
[101] R. Pirc, B. Tadicacute, and R. Blinc, *Physical Review B*, vol. 36, no. 16, p. 8607, Dec. 1987.
[102] A. Dziaugys, J. Banys, V. Samulionis, J. Macutkevic, Yu. Vysochanskii, V. Shvartsman, W. Kleemann*, Ferroelectrics / Book , ISBN 978-953-307-455-9,* Intech, 2011.
[103] T. Yao, Y. Uchimoto, M. Kinuhata, T. Inagaki, and H. Yoshida, *Solid State Ionics*, vol. 132, p. 189, 2000.
[104] H. Hayashi, H. Inaba, N. G. Lan., M. Dokiya, and H. Tagawa, *Solid State Ionics*, vol. 122, p. 1, 1999.
[105] S. Dikmen, P. Shuk, and M. Greenblatt, *Solid State Ionics*, vol. 126, p. 89, 1999.
[106] J. Huan, L. Jiang, L. Zhe, Z. Xin, H. Tianmin, and S. Wenhui, *Solid State Ionics*, vol. 126, p. 277, 1999.
[107] R. Brec, G. Ouvrard, A. Louisy, and J. Rouxel, *Solid state ionics* vol. 11, p. 179, 1983.
[108] J. Banys, J. Macutkevic, and Y. Vysochanskii, *Phys. Status Solidi A*, vol. 206, p. 167, 2009.
[109] K. Moriya, N. Kariya, I. Pritz, Y. Vysochanskii, A. Inaba, and T. Matsuo, *Ferroelectrics*, vol. 346, p. 143, 2007.
[110] V. Samulionis and J. Banys, *Journal of European Ceramic Society*, vol. 25, p. 2543, 2005.
[111] Z. Ouili, A. Leblanc, and P. Colombet, *J. Solid State Chem*, vol. 66, p. 86, 1987.
[112] R. Pfeiff and R. Kneip, *Journal of Alloys and Compounds*, vol. 186, p. 111, 1992.
[113] S. F. Motrya, V. V. Tovt, I. P. Prits, M. V. Potoriy, and P. M. Milyan, *Науковий вісник УжНУ. Серія «Хімія»*, vol. 23, pp. 29-31, 2010.
[114] A. K. Jonscher, *Dielectric relaxation in solids*. London: Chelsea Dielectric Press, 1983.
[115] I. M. Hodge, K. L. Ngai, and C. T. Moynihan, *J. Non-Cryst. Solids*, vol. 351, p. 104, 2005.
[116] M. Gave, D. Bilc, S. D. Mahanti, J. D. Breshears, and M. Kanatzidis, *Inorg. Chem.*, vol. 44, p. 5293, 2005.

[117] A. Dziaugys, J. Banys, J. Macutkevic, and Y. Vysochanskii, *Integrated Ferroelectrics*, vol. 103, pp. 52-59, 2009.
[118] A. Dziaugys, J. Banys, J. Macutkevic, and Y. Vysochanskii, *Ferroelectrics*, vol. 391, pp. 151-157, 2009.
[119] A. Galdamez, V. Manriquez, J. Kasaneva, and R. Avila, *Materials Research Bulletin*, vol. 38, p. 1063, 2003.
[120] Y. N. Huang, X. Li, Y. Ding, Y. N. Wang, N. M. Shen, Z. F. Zhang, C. S. Fang, S. H. Zhuo, P. C. W. Fung, *Phys. Rev. B*, vol. 55, p. 16159, 1997.
[121] J. Macutkevic, J. Banys, and A. Matulis, *Nonlinear analysis: modeling and control*, vol. 9, p. 75, 2004.
[122] S. Hong, J. Woo, H. Shin, J. U. Jeon, Y. E. Pak, E. L. Colla, N. Setter, E. Kim, and K. No, *Journal of Apllied Physics*, vol. 89, p. 1377, 2001.
[123] J. Banys, C. Klimm, G. Volkel, H. Bauch, and A. Klopperpieper, *Phys. Rev. B*, vol. 50, p. 16751, 1994.
[124] A. Dziaugys, J. Banys, J. Macutkevic, V. Samulionis, and Y. Vysochanskii, *physica status solidi (c)*, vol. 6, no. 12, pp. 2734-2736, 2009.
[125] W. F. Kuhs, R. Nitsche, and K. Scheunemann, *Materials Research Bulletin*, vol. 11, p. 1115, 1976.
[126] W. F. Kuhs, R. Nitsche, and K. Scheunemann, *Acta Crystallogr.*, vol. 34, p. 64, 1978.
[127] W. F. Kuhs, R. Nitsche, and K. Scheunemann, *Materials Research Bulletin*, vol. 14, p. 241, 1979.
[128] A. Haznar, A. Pietraszko, and I. Studenyak, *Solid State Ionics*, vol. 119, p. 31, 1999.
[129] M. Kranjcec, I. Studenyak, V. V. Bilanchuk, and V. V. Panko, *J. Phys. Chem. Solids*, vol. 65, p. 1015, 1977.
[130] A. Gagor, A. Pietraszko, and D. Kaynts, *J. Solid State Chem*, vol. 178, p. 3366, 2005.
[131] R. B. Beeken, J. J. Garbe, and N. R. Petersen, *Journal of Physics and Chemistry of Solids*, vol. 64, p. 1261, 2003.
[132] I. Studenyak, M. Kranjcec, G. Kovacs, V. V. Panko, and O. Mykajlo, *Materials Science and engineering*, vol. 97, p. 34, 2003.
[133] A. Dziaugys, J. Banys, V. Samulionis, and I. Studenyak, *Integrated Ferroelectrics*, vol. 109, p. 18, 2009.
[134] I. Studenyak, M. Kranjcec, A. Slivka, and P. Guranich, *Journal of Physics and Chemistry of Solids*, vol. 60, p. 1897, 1999.
[135] V. Samulionis, J. Banys, I. Studenyak, and V. V. Panko, *Ferroelectrics*, vol. 379, p. 62, 2009.
[136] I. Studenyak, G. Kovac, A. Orliukas, and Y. Kovacs, *Akad. Nauk. Ser. Fiz*, vol. 56, p. 86, 1992.
[137] Studenyak I., Stefanovich V., Kranjcec M., Desnica D., Azhnyuk Y., Kovacs G.S., Panko V. *Solid State Ionics*, vol. 95, p. 221, 1997.

[138] H. Iwasaki, K. Sugii, T. Yamada, and N. Niizeki, *Appl. Phys. Lett.*, vol. 18, p. 444, 1971.
[139] Y. Iwata, N. Koyano, and I. Shibuya, *J. Phys. Soc. Jpn*, vol. 35, p. 1269, 1973.
[140] Y. Iwata, H. Koizumi, N. Koyano, I. Shibuya, and N. Niizeki, *J. Phys. Soc. Jpn*, vol. 35, p. 314, 1973.
[141] M. Kay, R. Newnham, and R. Wolfe, *Ferroelectrics*, vol. 9, p. 1, 1975.
[142] S. Nanamatsu, H. Sugiyama, and K. Doi, *J. Phys. Soc. Jpn*, vol. 31, p. 616, 1971.
[143] J. Ryan and K. Hisano, *J. Phys. C*, vol. 6, p. 566, 1973.
[144] S. Cummins and T. Luke, *Proc. IEEE*, vol. 61, p. 1039, 1973.
[145] E. Fatuzzo, G. Harbeke, W. J. Merz, R. Nitzsche, H. Roetschi and W. Ruppel, *Phys. Rev*. vol. 127, p. 2036, 1962.
[146] C. H. Perry and D. K. Agrawal, *Solid State Commun.*, vol. 8, p. 225, 1970.
[147] P. S. Peercy, *Ferroelectrics* vol. 16, p. 193, 1977.
[148] S. Shapiro, J. Axe, G. Shirane, and T. Riste, *Phys. Rev. B*, vol. 6, p. 4332, 1972.
[149] T. Riste, *Anharmonic Lattices, Structural Transitions and Melting,* Noordhoff, 1974.
[150] O. Shuichiro, A. Koji, and I. Hiroshi, *Jpn J Appl Phys Part 1*, vol. 44, no. 9, pp. 6644-6647, 2005.
[151] S. C. Sabharwal and S. N. Jha, Sangeeta, *Bulletin of Materials Science*, vol. 33, no. 4, pp. 395-400, 2010.
[152] J.-H. Kim, J.-B. Kim, K.-S. Lee, B.-C. Choi, J.-N. Kim, and S.-D. Lee, *Solid State Communications*, vol. 86, no. 4, pp. 257-260, Apr. 1993.
[153] M. P. Trubitsyn and V. G. Pozdeev, *Physics of the Solid State*, vol. 42, no. 12, pp. 2254-2257, 2000.
[154] M. P. Trubitsyn, S. Waplak, and A. S. Ermakov, *Physics of the Solid State*, vol. 42, no. 7, pp. 1341-1347, 2000.
[155] I. B. Bersuker, *Bersuker IB, 1971. Structure and properties of coordination compounds. Khimia Leningrad 312.* 1971.
[156] A. Kudzin, M. Volnianskii, V. Duda, M. P. Trubitsyn, and A. S. Ermakov, *Ukr. Journ. Phys. Optics*, vol. 1, p. 53, 2001.